



**NTNU – Trondheim**  
Norwegian University of  
Science and Technology

# SiC supported Co catalysts for the Fischer-Tropsch synthesis

**Sindre Håvik**

Chemical Engineering and Biotechnology

Submission date: June 2012

Supervisor: Anders Holmen, IKP

Co-supervisor: Bjørn Christian Enger, IKP  
Andreas Lillebø, IKP

Norwegian University of Science and Technology  
Department of Chemical Engineering



# Declaration

I hereby declare that this thesis is an independent work according to the exam regulations of the Norwegian University of Science and Technology.

Trondheim, June 15<sup>th</sup> 2012

---

Sindre Håvik



# Abstract

With rising crude oil prices and outlook of declining crude oil production, conversion of natural gas into liquid fuels is gaining worldwide interest. Fischer-Tropsch synthesis is an important tool in achieving this conversion of natural gas, producing long-chained hydrocarbon products. These may be further processed into automotive fuel and other demanded products.

Ever since Fischer-Tropsch synthesis was invented in the 1920's, much effort has been put into development and improvement of all aspects regarding the process. Although cobalt has been found to be the most viable catalyst for natural gas conversion today, much resources are put in to optimize the catalyst with regards to promoters and support materials.

Usual support materials for cobalt catalyzed Fischer-Tropsch synthesis are  $\text{Al}_2\text{O}_3$ ,  $\text{SiO}_2$  and  $\text{TiO}_2$ . This thesis has investigated SiC as support material.

Seven different SiC-support samples were obtained from commercial manufacturer SICAT, and impregnated using the incipient wetness impregnation method with 12.5 wt.% cobalt loading. Characterization methods applied were volumetric adsorption, volumetric chemisorption, X-ray diffraction, temperature programmed reduction, electron microscopy and steady-state isotopic transient kinetic analysis. All SiC-supported catalysts tested were reduced at lower temperatures than  $\text{Al}_2\text{O}_3$ -supported Co- and CoRe-catalysts. Volumetric chemisorption showed poor dispersion of cobalt metal (2-3%) on the SiC-supported catalysts.

In total, seven SiC-supported catalysts and one  $\text{Al}_2\text{O}_3$ -supported reference catalyst, were run in an experimental Fisher-Tropsch synthesis rig to obtain activity and selectivity results. The SiC-supported catalysts showed varying activity results, and were all less active than the  $\text{Al}_2\text{O}_3$ -supported reference catalyst. However, at the same CO conversion level, SiC-supported catalysts yielded an increased  $\text{C}_{5+}$  hydrocarbon selectivity compared to the reference catalyst.

The decreased activity, and increased  $\text{C}_{5+}$  selectivity observed for the SiC-supported catalysts, were suspected to be caused by alkali and alkaline earth metal impurities in the support samples. After the first batch of catalysts were tested and found little active, SICAT supplied a second set of purer support samples. However, the results suggested that there were still enough impurities present to cause significant loss of activity compared to the reference catalyst.



# Samandrag

Med stigande oljeprisar og framsyn om fallande råoljeproduksjon samlar omdanning av naturgass til flytande drivstoff interesse verda rundt. Fischer–Tropsch-syntese er eit viktig verktøy i denne omdanningsprosessen på grunn av dei langkjeda hydrokarbona som vert produsert. Desse kan vidare foreldast til drivstoff for bilar eller andre etterspurte produkt.

Heilt sidan Fischer–Tropsch-syntesen vart oppdaga på 1920-talet har mykje innsats vorte lagt ned i å utvikle og forbetre alle aspekt rundt prosessen. Sjølv om kobolt i dag er funnen til å vere den økonomisk mest levedyktige katalysatoren for omdanning av naturgass, vert mykje ressursar satt inn i å optimalisere katalysatoren med omsyn på promotorar og berarmaterialar.

Vanlege berarmaterialar for koboltkatalysert Fischer–Tropsch-syntese er  $\text{Al}_2\text{O}_3$ ,  $\text{SiO}_2$  and  $\text{TiO}_2$ . I denne diplomoppgåva er SiC undersøkt som berarmateriale for kobolt.

Sju forskjellige SiC-berarar vart levert frå produsenten SICAT, og impregnert med 12,5% kobolt. Dei ferdige katalysatorane vart karakterisert ved volumetrisk adsorpsjon, volumetrisk kjemisorpsjon, røntgendiffraksjon, temperaturprogrammert reduksjon, elektronmikroskopi, og „steady-state isotopic transient kinetic analysis”. Alle dei SiC-baserte katalysatorane vart redusert ved lågare temperaturar samanlikna med  $\text{Al}_2\text{O}_3$ -baserte Co- og CoRe-katalysatorar. Kjemisorpsjon av hydrogen viste at dei SiC-baserte katalysatorane hadde dårleg dispersjon av kobolt (2-3%).

Alle sju SiC-baserte katalysatorar, og ein  $\text{Al}_2\text{O}_3$ -basert referansekatalysator, vart testa i ein eksperimentell Fischer–Tropsch-rigg for å undersøkje aktivitets- og selektivitetsresultat. Dei SiC-baserte katalysatorane viste svært varierende resultat, og alle var mindre aktiv enn referansekatalysatoren. Likevel viste resultatata at, ved same omsettingsgrad til CO, hadde dei SiC-baserte katalysatorane høgare selektivitet til  $\text{C}_{5+}$ -hydrokarboner.

Dei låge katalysatoraktivitetane og økte  $\text{C}_{5+}$ -selektivitetane var mistenkt å vera forårsaka av alkalie- og jordalkaliemetall som forureina katalysatorane. Etter at dei første fire katalysatorane var funne å vere lite aktive, sendte SICAT tre nye berarmaterialar. Desse skulle innehalde mindre forureiningar. Tross dette, tyda resultatata på at det endå var nok forureiningar tilstades til å skape eit signifikant tap av katalysatoraktivitet.





# Acknowledgments

This thesis is written as a fulfillment to the two-year master's programme at NTNU, leading to the degree of Master of Science (MSc) in Chemical Engineering.

The work of this thesis was conducted during the second year of the master's programme. Preparation of four SiC-supported cobalt catalysts and the characterization of these were performed during the autumn of 2011, through the *specialization project*. Three more SiC-supported catalysts were prepared and characterized, and all Fischer-Tropsch synthesis experiments were carried out during the spring of 2012.

Firstly, I would like to thank my supervisor, Prof. Anders Holmen, for giving me the chance to work with such an exciting and satisfying task for my master's thesis.

Many thanks to co-supervisor Andreas H. Lillebø. I am very grateful for everything you have taught me, helped me with, and all the interesting discussions we have had (both on and off the subject of catalysis). Thank you for making the writing of the master's thesis a great experience to me.

I would also like to thank Edd A. Blekkan and Bjørn Christian Enger for help and guidance throughout the project. Our discussions of my experimental results are greatly valued.

A big thank you to Jia Yang and John Walmesley, who performed the SSITKA and electron microscopy experiments, respectively. I am very grateful for your contribution and your accommodating nature towards me.

Last, but not least, I would like to thank Jan Ove, Reidun, Jarle and Matz Håvik for supporting me, and always being there for me, throughout my studies.



# Contents

Abstract	i
Samandrag	iii
Acknowledgments	v
Contents	vii
List of figures	xi
List of tables	xiii
List of symbols and abbreviations	xv
<b>1 Introduction</b>	<b>1</b>
1.1 Gas-to-liquids . . . . .	1
1.1.1 Drivers . . . . .	1
1.1.2 History . . . . .	3
1.2 Fischer-Tropsch synthesis . . . . .	4
1.2.1 Reactions . . . . .	4
1.2.2 Catalysts . . . . .	7
1.2.3 Reactors . . . . .	7
1.3 Scope of the work . . . . .	9
<b>2 Literature review</b>	<b>11</b>
2.1 SiC as support material . . . . .	11
2.2 Synthesis of SiC . . . . .	11
2.3 Catalyst preparation . . . . .	12
2.3.1 Impregnation of catalyst . . . . .	12
2.3.2 Calcination . . . . .	12
2.4 Support properties . . . . .	13
2.5 Dispersion and particle size . . . . .	13
2.6 Reduction . . . . .	14
2.7 Fischer-Tropsch synthesis . . . . .	15
2.7.1 Experimental FT synthesis work . . . . .	15
2.7.2 Selectivity . . . . .	17
2.7.3 Turnover frequency . . . . .	19
2.7.4 Effect of water . . . . .	20

2.7.5	Impurities . . . . .	22
2.7.6	Effect of alkali metals . . . . .	23
<b>3</b>	<b>Experimental</b>	<b>27</b>
3.1	Preparation of catalyst . . . . .	27
3.1.1	Support materials . . . . .	28
3.1.2	Catalysts . . . . .	28
3.1.3	Impregnation and calcination . . . . .	28
3.2	Characterizations . . . . .	30
3.2.1	Volumetric adsorption . . . . .	30
3.2.2	Temperature programmed reduction . . . . .	31
3.2.3	Volumetric chemisorption . . . . .	32
3.2.4	X-ray diffraction . . . . .	34
3.2.5	SSITKA . . . . .	35
3.2.6	Electron microscopy . . . . .	35
3.2.7	Elemental analysis . . . . .	35
3.3	Fischer-Tropsch synthesis . . . . .	35
<b>4</b>	<b>Results and discussion</b>	<b>41</b>
4.1	Characterizations . . . . .	41
4.1.1	Electron microscopy . . . . .	41
4.1.2	Volumetric adsorption . . . . .	43
4.1.3	Temperature programmed reduction . . . . .	47
4.1.4	Chemisorption and XRD . . . . .	50
4.2	Fischer-Tropsch synthesis . . . . .	53
4.2.1	First batch . . . . .	54
4.2.2	Second batch . . . . .	57
4.2.3	CO conversion of 50% . . . . .	58
4.2.4	Olefin/paraffin ratio . . . . .	60
4.2.5	CO conversion vs. C <sub>5+</sub> selectivity . . . . .	61
4.2.6	FTS results in the literature . . . . .	62
4.2.7	Mechanism of alkali and alkali earth metals effects . . . . .	62
<b>5</b>	<b>Conclusion</b>	<b>65</b>
<b>6</b>	<b>Future work</b>	<b>67</b>
	<b>Bibliography</b>	<b>68</b>
<b>A</b>	<b>Additional results</b>	<b>75</b>
A.1	SSITKA . . . . .	75
A.2	Elemental analysis . . . . .	76
A.3	Volumetric adsorption . . . . .	76
A.4	Volumetric chemisorption . . . . .	91
<b>B</b>	<b>Example of calculations</b>	<b>95</b>
B.1	Incipient wetness impregnation . . . . .	95
B.2	Volumetric adsorption . . . . .	96

B.3	Volumetric chemisorption . . . . .	98
B.4	X-ray diffraction . . . . .	100
B.5	Fischer-Tropsch synthesis . . . . .	101
<b>C</b>	<b>Poster presentation</b>	<b>105</b>
<b>D</b>	<b>Communication</b>	<b>109</b>
D.1	Information on support material from manufacturer SICAT . . . . .	109
D.2	Molab AS . . . . .	115
<b>E</b>	<b>Risk assessment</b>	<b>117</b>



# List of Figures

1.1	Development in proved reserves from 1990-2010 . . . . .	2
1.2	Natural gas transportation options to markets . . . . .	2
1.3	Historical development of crude oil price . . . . .	3
1.4	The three main steps in the GtL technology . . . . .	4
1.5	Fischer-Tropsch chain growth . . . . .	6
1.6	Possible reactor designs for Fischer-Tropsch synthesis . . . . .	8
2.1	Simplified rendering of the FT synthesis reaction network . . . . .	18
2.2	Distribution of FTS products as a function of the chain growth probability	19
2.3	Effect of dispersion on turnover frequency in various cobalt supported cat- alysts . . . . .	20
2.4	Influence of cobalt particle size on TOF . . . . .	20
2.5	Effect of deactivation by water on Co-Re/Al <sub>2</sub> O <sub>3</sub> catalyst . . . . .	21
2.6	Effect of water addition on SiO <sub>2</sub> - and TiO <sub>2</sub> -supported Co and Co-Re catalysts	21
2.7	Effect of Na concentration in catalysts on the site-time yield . . . . .	22
2.8	Effect of alkali metals on site-time yield and C <sub>5+</sub> selectivity . . . . .	23
3.1	Schematic drawing of the experimental rig used in the FTS experiments. .	40
4.1	TEM images of catalyst C1 . . . . .	42
4.2	STEM images of catalyst C1 . . . . .	43
4.3	BET adsorption and desorption isotherms of S4 and C4 . . . . .	46
4.4	TPR curves of catalysts R1 and R2 . . . . .	47
4.5	TPR curves of catalysts C1-C7 . . . . .	48
4.6	Collected XRD patterns of support materials S1-S4 . . . . .	51
4.7	Collected XRD patterns of catalysts C1-C4 . . . . .	52
4.8	CO conversions of catalysts C1-C7 and R2 . . . . .	54
4.9	C <sub>5+</sub> selectivities of catalysts C1-C7 and R2 . . . . .	55
4.10	Normalized reaction rate plotted against time on stream . . . . .	56
4.11	CO conversion and C <sub>5+</sub> selectivity as a function of time on stream for catalysts C4, C5 and R2 . . . . .	59
4.12	Olefin/paraffin ratio for catalysts C1-C7 and R2 . . . . .	60
4.13	C <sub>5+</sub> selectivity as function of CO conversion . . . . .	61
A.1	Volumetric adsorption results S1/C1 . . . . .	78
A.2	Volumetric adsorption results C1 . . . . .	79
A.3	Volumetric adsorption results S2/C2 . . . . .	80
A.4	Volumetric adsorption results C2 . . . . .	81

A.5	Volumetric adsorption results S3/C3	82
A.6	Volumetric adsorption results C3	83
A.7	Volumetric adsorption results S4/C4	84
A.8	Volumetric adsorption results C4	85
A.9	Volumetric adsorption results S4/C4	86
A.10	Volumetric adsorption results S5/C5	87
A.11	Volumetric adsorption results S6/C6	88
A.12	Volumetric adsorption results S7/C7	89
A.13	Volumetric adsorption results extrudate S1–S3	90
A.14	Adsorption isotherms for catalyst C1	91
A.15	Adsorption isotherms for catalysts C2 and C3	92
A.16	Adsorption isotherms for catalysts C4 and C5	93
A.17	Adsorption isotherms for catalysts C6 and C7	94
B.1	BET surface area plot for C1	97
B.2	Adsorption isotherms for catalyst C1	98



# List of Tables

1.1	Major overall reactions in Fischer-Tropsch synthesis . . . . .	5
1.2	Typical product mixture from running FT synthesis at low temperature with cobalt catalyst . . . . .	5
2.1	Summary of FTS experimental results in the literature . . . . .	17
3.1	Support properties provided by SICAT . . . . .	27
3.2	Properties of SiC- and reference Al <sub>2</sub> O <sub>3</sub> -catalysts . . . . .	28
3.3	Molecular weights of Co and Co(NO <sub>3</sub> ) <sub>2</sub> ·6H <sub>2</sub> O . . . . .	29
3.4	Calibrated response factors to the thermal conductivity detector of the gas chromatograph . . . . .	37
4.1	Experimental results: Volumetric adsorption . . . . .	44
4.2	Experimental results: BET surface area of S4 samples with different pre- treatment . . . . .	46
4.3	Experimental results: Temperature programmed reduction . . . . .	49
4.4	Experimental results: H <sub>2</sub> -chemisorption and XRD . . . . .	50
4.5	Experimental results: Fischer-Tropsch synthesis . . . . .	53
A.1	SSITKA results . . . . .	75
A.2	Elemental analysis of S1 and C1 . . . . .	76
A.3	Complete results from parallel analyses of S4 and C1–C3 . . . . .	77
A.4	Volumetric adsorption results for S1–S3 extrudates . . . . .	77
B.1	Values for calculation of surface area for C1 . . . . .	96
B.2	Values for calculation of dispersion for C1 . . . . .	99



# List of Symbols and Abbreviations

Some of the variables listed below have multiple definitions. However, it should be clear from the context which definition is the correct one.

## Greek symbols

$\alpha$	Chain growth probability	
$\alpha$	Slope of linear function	$\text{g/cm}^3 \text{ STP}$
$\eta$	Intersection of slope of linear function with Y-axis	$\text{g/cm}^3 \text{ STP}$
$\theta$	X-ray attack angel	$^\circ$
$\rho$	Density	$\text{Cm}^3/\text{g}$
$\sigma$	Average surface area occupied by one atom	$\text{cm}^2$
$\sigma$	Standard deviation	
$\chi$	Component mole fraction	$\text{g}$

## Latin symbols

A	GC peak area	
$A_{BET}$	Surface area from BET isotherm	$\text{m}^2/\text{g}$
$A_0$	Occupied surface area of one $\text{N}_2$ molecule	$\text{m}^2$
d	Cobalt oxide particle size	nm
D	Cobalt dispersion	
f	Particle shape factor	
f	Response factor	
F	Adsorption stoichiometry	
$\dot{F}$	Flow rate	$\text{mol/g}_{\text{cat}} \text{ h}$
$k_b$	Boltzmann constant	$\text{J/K}$
m	Mass	$\text{g}$
$M_W$	Molecular weight	$\text{g/mol}$
$N_A$	Avogadro's number	$\text{mol}^{-1}$
$N_0$	Number of molecules adsorbed in the first monolayer	$\text{g}^{-1}$
P	Pressure	mmHg
$P_0$	Equilibrium pressure	mmHg

$P_{STP}$	Pressure at STP conditions	Pa
$r$	Reaction rate	mol/g <sub>cat</sub> h
$r_0$	Initial reaction rate	mol/g <sub>cat</sub> h
$R$	Ratio	
$S$	Selectivity	%
$S_m$	Specific surface area	m <sup>2</sup> /g
$T_{STP}$	Temperature at STP conditions	K
$v_{ads}$	adsorbed amount of H <sub>2</sub>	mol/g STP
$\dot{V}$	Volume flow rate	ml/h
$V_a$	Volume adsorbed	cm <sup>3</sup> /g STP
$V_m^{i.g.}$	Molar volume of ideal gas	ml/mol
$V_{sp}$	Specific volume	cm <sup>3</sup> /g
$V_0$	Volume of adsorbed gas in the first monolayer	cm <sup>3</sup> /g STP
$W_n$	Weight fraction of component with $n$ carbon atoms	
$x_m$	Mass fraction	
$x_i$	Value	
$\bar{x}$	Mean of values	
$X$	Conversion	

## Abbreviations

ASF	Anderson-Schulz-Flory
BET	Brunauer, Emmett and Teller (isotherm)
BJH	Barrett, Joyner and Halenda (isotherm)
BtL	Biomass-to-liquids
C	Catalyst
C <sub>5+</sub>	Hydrocarbons with five or more carbon atoms
CtL	Coal-to-liquids
FID	Flame ionization detector
FT	Fischer-Tropsch
FTS	Fischer-Tropsch synthesis
FWHM	Full width at half maximum
GC	Gas chromatograph
GHSV	Gas hourly space velocity
GtL	Gas-to-liquids
HSA	High surface area
IWI	Incipient wetness impregnation
IWP	Incipient wetness point
LNG	Liquefied natural gas
MFC	Mass flow controller
MSI	Metal-support interaction
O/P	Olefin/paraffin
PC	Pressure controller
S	Support

SSITKA	Steady-state isotopic transient kinetic analysis
STEM	Scanning transmission electron microscopy
STP	Standard temperature and pressure
STY	Site-time yield
TCD	Thermal conductivity detector
TEM	Transmission electron microscopy
TOF	Turnover frequency
TPR	Temperature programmed reduction
TX	Texas
UK	United Kingdom
US	United States (of America)
US\$	United States dollars
VFM	Volume flow meter
WGS	Water-gas-shift
XRD	X-ray diffraction



# Chapter 1

## Introduction

With rising crude oil prices and outlook of declining crude oil production, conversion of natural gas into liquid fuels is gaining worldwide interest. In addition to being an alternative fuel source to crude oil, such a conversion of natural gas can be a way of monetizing on natural gas fields that has no other viable transportation method for the gas resources to a consumer market. The Fischer-Tropsch (FT) synthesis, as a part of the Gas-to-liquids (GtL) process, has showed itself as a fitting tool for these purposes.

### 1.1 Gas-to-liquids

Often mentioned with the collective term XtL, Gas-to-liquids, along with Coal-to-liquids (CtL) and Biomass-to-liquids (BtL), are today the three main processes of producing synthetic liquid fuels. Among them, the GtL route is most viable with respect to economical and political aspects. Other upgrading uses of natural gas are ammonia and methanol synthesis.

#### 1.1.1 Drivers

Today, the production of fuels and chemicals is based heavily on crude oil. Natural gas is primarily utilized for heating in domestic, commercial and industrial settings. In 2010 the proved reserves of crude oil and natural gas were about  $1400 \cdot 10^9$  and  $1200 \cdot 10^9$  barrels oil equivalent, respectively [19]. As the remaining crude oil reserves consist of heavier crude qualities, viz. more difficult and costly production, natural gas is thought to become more important to the fuel and chemicals production in the future. Development of the worlds proved reserves the last 20 years are shown in figure 1.1.

Although crude oil and natural gas reserves are of similar size (barrel oil equivalents), more than half the natural gas reserves are not of interest to be produced. This is due to remotely located natural gas reserves in lack of pipelines, or other necessary infrastructure, to enable transport to a market. Historically, the easily transported crude oil has been produced, while natural gas from the same reservoir has been flared off as an unwanted by-product.

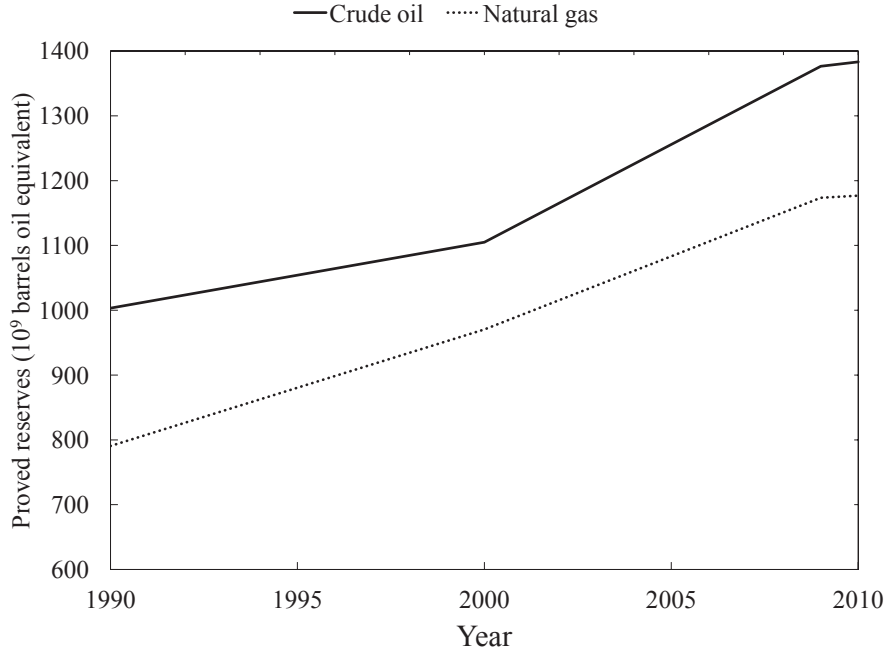


Figure 1.1: Development in proved reserves from 1990-2010 [19, 62].

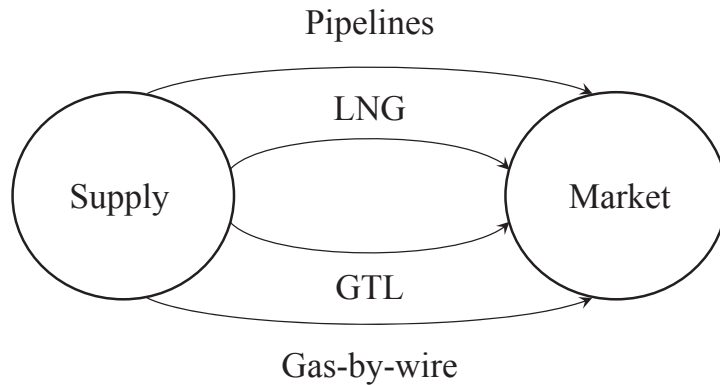


Figure 1.2: Natural gas transportation options to markets [13].

Natural gas was seen as an unwanted by-product in the North Sea for many years. Eventually, the need for natural gas in continental Europe and the UK made it economically feasible to transport this gas in pipelines from Norway to the European market. Where pipelines are not a feasible solution, the GtL technology is one option for bringing the gas to a market. The liquids may be transportation fuels, produced via FT synthesis, or alternative fuels such as methanol and dimethyl ether [13]. Other options for remote resources to be transported to a market are liquefied natural gas (LNG) technology and gas-by-wire technology, see figure 1.2.

Favorable products from FT synthesis include jet and diesel fuels. These are essentially free of particulates, sulfur and nitrogen compounds, especially the diesel fuels are of high



quality. As the FT products are mostly linear hydrocarbons, the diesel fuels produced can have cetane numbers of up to 75. FT products are also favorable compared to methanol and dimethyl ether since motor vehicle engines are not designed for the latter fuels [23, 29].

Fuels derived from natural gas have historically not been able to compete with prices of fuels derived from crude oil. However, technological developments are now making natural gas derived fuels commercially attractive. Current crude oil prices of around US\$100/barrel also boost the incentive for GtL plants. The crude oil prices are expected to stabilize just below US\$100 the coming years. See historical development of crude oil prices in figure 1.3.

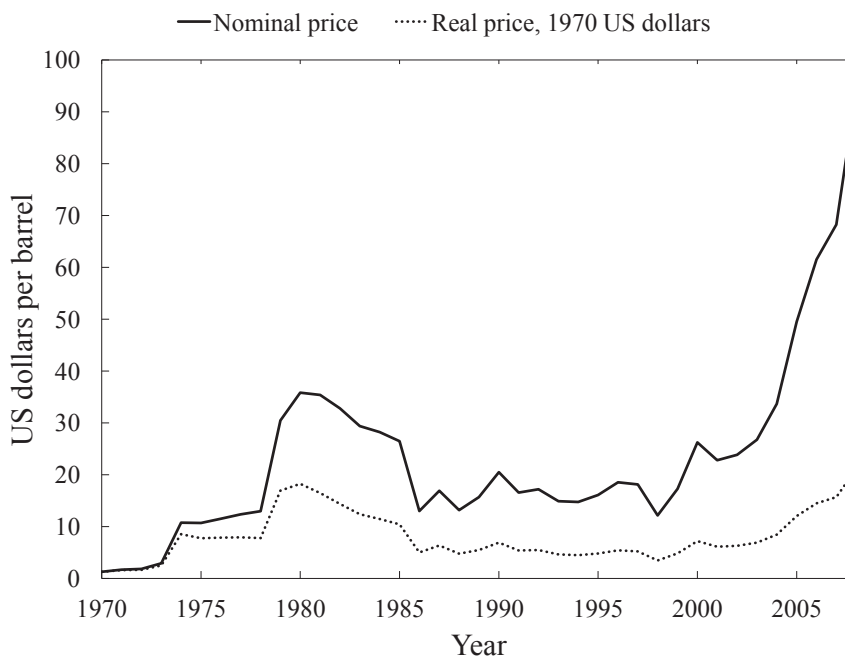


Figure 1.3: Historical development of crude oil price [61].

### 1.1.2 History

Discovery of the FT synthesis has been acknowledged Hans Fischer and Franz Tropsch in the 1920's [32]. The Germans had little access to crude oil during World War II, but were rich in coal. Thus, they used the FT process to meet the demand for diesel fuel from their war campaigns. All nine plants built by the Germans, went out of operation when the war ended. However, interest in the FT process remained due to a worldwide view that the crude oil reserves were limited. During the 1950s one plant was operated in Brownsville, TX, but a steep increase in methane prices forced the plant to close down. In South Africa, one coal based plant was constructed, but never completed due to the discovery of huge oil fields in the Middle East [30].

The present installed GtL worldwide capacity consist of four plants. These are the Shell SMDS plant in Malaysia (14 700 bbl/day), the PetroSA plant in South Africa (25 000 bbl/day), the Qatar Petroleum/Sasol Oryx GtL plant in Qatar (34 000 bbl/day), and the

Shell Pearl GtL plant in Qatar (140 000 bbl/day). The two plants in Qatar are regarded as the new generation of GtL plants and were opened in 2007 and 2011, respectively [36].

The number of GtL plants is small, but interest in the technology is great. Among the many licensors of GtL technology are Blue Star Sustainable Technologies Corp., BP/-Davy process Technology, Chiyoda Corp., ConocoPhillips, Energy International, Exxon-Mobil, Foster Wheeler Energy, Hydrocarbon Technologies, Inc., National petrochemical Co., Raytheon E&C, Rentech, Sasol, Shell, Statoil, Syncrude Technology, Synergy Technologies Corp./ECP, Synfuels International and Syntroleum Corp. [13].

## 1.2 Fischer-Tropsch synthesis

The entire GtL technology consists of three main steps: reforming, FT synthesis and product upgrading, as shown in figure 1.4. Of these three steps, FT synthesis is the process which is of greatest interest to further development and research. This thesis will focus on the FT synthesis step, and more specific on the catalysts that are used in this process.

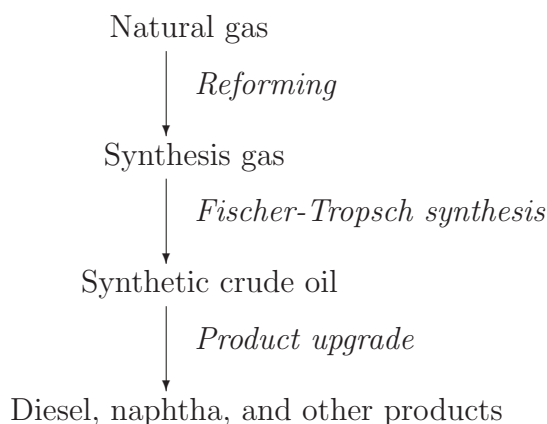


Figure 1.4: The three main steps in the GtL technology [13].

### 1.2.1 Reactions

The FT synthesis can be described as a polymerization mechanism where a  $C_1$ -unit is added step by step to a growing chain [41], see figure 1.5. A set of generalized equations are given in table 1.1. Worth noting is the high exothermicity of the reactions. For each mole of  $-CH_2-$  formed, 165 kJ heat is produced. Thermodynamically, the commercial FT synthesis is favorably run at a temperature range of 463–573 K and pressures between 15–30 bar [12].

Running the FT synthesis at different reaction conditions yields different product mixtures. A typical product mixture from running at low temperature with a cobalt catalyst is given in table 1.2.

Table 1.1: Major overall reactions in Fischer-Tropsch synthesis [12].

Main reactions	
Alkanes	$n\text{CO} + (2n + 1)\text{H}_2 \rightarrow \text{C}_n\text{H}_{2n+2} + n\text{H}_2\text{O}$
Alkenes	$n\text{CO} + 2n\text{H}_2 \rightarrow \text{C}_n\text{H}_{2n} + n\text{H}_2\text{O}$
Water-gas-shift	$\text{CO} + \text{H}_2\text{O} \rightarrow \text{CO}_2 + \text{H}_2$
Side reactions	
Alcohols	$n\text{CO} + 2n\text{H}_2 \rightarrow \text{C}_n\text{H}_{2n+2}\text{O} + (n - 1)\text{H}_2\text{O}$
Boudouard reaction	$2\text{CO} \rightarrow \text{C} + \text{CO}_2$

Table 1.2: Typical product mixture from running FT synthesis at low temperature with cobalt catalyst [13].

Component	Fraction
n-alkanes	75-90%
1-alkenes	5-15%
n-alcohols	5%
Branched alkanes and alkenes	<5%
Aldehydes, ketones and acids	<1%

As mentioned, FT synthesis follows a polymerization reaction which involves the following key steps [1]:

1. Reactant adsorption
2. Chain initiation
3. Chain growth
4. Chain termination
5. Product desorption
6. Readsorption and further reaction

Since the discovery of the FT synthesis in early 1920's, mechanisms of the chain growth reactions have been discussed. A variety of mechanisms have been proposed over the years, and the main difference between them is what monomer is responsible for the chain growth. If focusing on the production of hydrocarbons the discussion is confined to which oxygen-containing intermediates are participating in the reactions. The three mechanisms [41] that have been proposed are:

- *Enol mechanism*
- *CO insertion mechanism*
- *Carbide mechanism*

In the enol mechanism the chain growth monomer, replacing "X" in figure 1.5, is assumed to be an adsorbed methanal molecule. Chain growth in the CO insertion mechanism is assumed to take place through insertion of CO into an adsorbed alkyl species. Both of these mechanisms assume associative adsorption of CO. The carbide mechanism assumes that CO adsorbs dissociatively on the metal surface and proposes adsorbed methylene as the chain growth monomer [24, 41]. Fischer and Tropsch initially proposed the carbide mechanism, which is presently regarded by the majority of researchers to be most likely [90]. Although studies [25, 90] on the CO insertion mechanism are making this theory more popular.

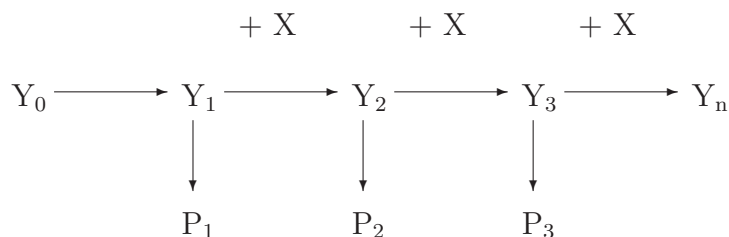


Figure 1.5: Fischer-Tropsch chain growth. Where  $Y_0$  to  $Y_1$  is the initiation step,  $Y_n$  is the growing chain, X is a  $C_1$ -unit and  $P_n$  is products with n carbon atoms [41].

### 1.2.2 Catalysts

Choice of catalyst for the FT synthesis is guided by the origin of the synthesis gas (syngas) used. The catalysts water-gas-shift (WGS) activity (table 1.1) is an important factor regarding the syngas composition. Syngases originating from heavy hydrocarbon sources such as coal, have a low  $H_2/CO$  ratio due to the low hydrogen content of coal. The stoichiometric  $H_2/CO$  ratio for FT synthesis is  $\approx 2.15$  [13]. Thus, in this case it is of interest to have a catalyst with high WGS activity to produce the lacking  $H_2$ . If natural gas is used to produce the syngas, a catalyst with low WGS activity is beneficial since the syngas produced has a  $H_2/CO$  ratio close to stoichiometric for FT synthesis.

It is generally accepted that most group 8, 9 and 10 transition metals have measurable CO hydrogenation activity, where product distribution distinguishes one from the other [1]. Among these, iron, nickel, cobalt and ruthenium are viable candidates with respect to activity. Although, prices of the metals are also an important factor when choosing a catalyst. If the relative price of Fe is set to 1, the price of Ni is 250, Co is 1,000 and Ru is 50,000 [30].

Nickel was the first catalyst used for hydrogenation of CO by Sabatier and Sanders to produce methane [1]. Thus, nickel is not a suitable catalyst for natural gas based FT synthesis since production of methane is unwanted. Ruthenium has been found to be an excellent catalyst for production of FT wax. Due to low availability, resulting in high prices, ruthenium is not a viable option for industrial use.

Remaining candidates are iron and cobalt. Iron catalysts are best suited for syngases with low  $H_2/CO$  ratio. Catalysts based on iron have high WGS activity, and it is the least expensive metal to use. Cobalt catalysts have almost no WGS activity and are best suited for syngases derived from natural gas. Cobalt is relatively expensive compared to iron, but the resources are expected to last for about 300 years [68].

Due to the relatively high cost of cobalt metal it is desirable to disperse it on a porous support material. Silica, alumina, titania or zinc oxide are typical support materials used, or combinations of these oxides [76]. Pore size and mechanical strength are important factors for the catalysts performance. Promotion of cobalt catalysts with other metals is also common, the promoting metals usually being lanthanum, platinum, palladium, rhenium or ruthenium. Promoters are known to lower the temperature needed to activate the catalyst [76] and to increase the catalyst activity by increasing the dispersion of the catalyst metal [16].

### 1.2.3 Reactors

As the FT reactions are highly exothermic, heat transfer and temperature control in the reactor are important to the reactor design. The design of reactors for the FT synthesis has been an ongoing process since the commercial use started prior to World War II. Today there are three leading reactor designs; fluidized-bed reactors, fixed-bed reactors and slurry bubble column reactors [73], see figure 1.6.

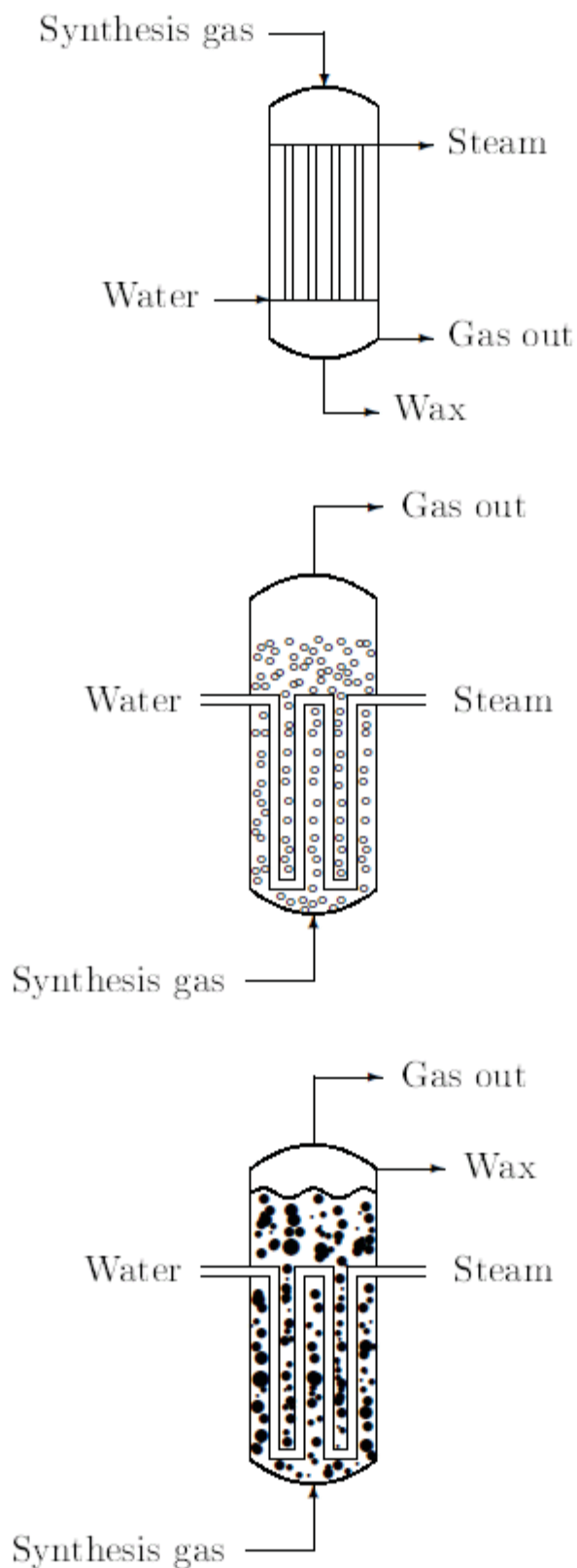


Figure 1.6: Possible reactor designs for Fischer-Tropsch synthesis. From the top: Tubular fixed-bed reactor, fluidized bed reactor and bubble column reactor [13].

## 1.3 Scope of the work

SiC is a novel support material to the Fischer-Tropsch synthesis. There are few publications regarding this use of SiC, yet the results seem promising. The purpose of this thesis is to investigate the attributes of the Co/SiC catalysts system, and possibly to support the published findings.

To achieve this, Co/SiC catalysts will be prepared and characterized. Characterizations to be done are volumetric adsorption, volumetric chemisorption, X-ray diffraction and temperature programmed reduction.

The catalysts will also be tested in an experimental Fischer-Tropsch synthesis rig.





# Chapter 2

## Literature review

This chapter will briefly focus on important aspects reported in the literature. Relevant subjects regarding support material, catalysts and Fischer-Tropsch synthesis will be presented.

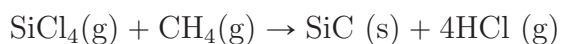
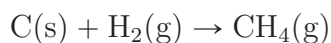
### 2.1 SiC as support material

Utilization of SiC as catalyst support material in general, was for a long time moderate since the commercially available support materials had a low specific surface area, below 1 m<sup>2</sup>/g. Improvements in the synthesizing methods made it possible to obtain SiC support materials with medium surface area (20–100 m<sup>2</sup>/g) and appropriate pore size distributions [66]. Today, commercial SiC supports are available with surface areas up to 35 m<sup>2</sup>/g [72]. Properties that make SiC an interesting support material is its stability at high temperatures, it is not easily sintered, and it has an inert surface that should be non-reactive as reactions occur on the dispersed metal surfaces, even at high temperatures [85].

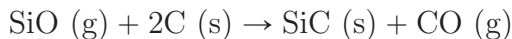
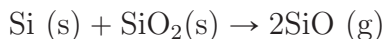
SiC is relatively new to FT synthesis, thus there is a small selection of literature regarding this use of the support material. Nevertheless, literature regarding FT catalysts supported on other materials should be comparable.

### 2.2 Synthesis of SiC

In the mid to late 1990s, a lot of research was done on how to synthesize high surface area SiC [59]. Moene et al. [55, 56] used chemical vapor deposition techniques to synthesize porous SiC with surface areas up to 80 m<sup>2</sup>/g by the following nickel catalyzed reactions:



Another method of synthesizing SiC is the shape memory synthesis by, Ledoux et al. [51, 52]. The method is based on the SiC being formed from an activated carbon skeleton. The synthesis takes place over two reactions: Firstly an equimolar mix of silicon and silicon dioxide react to form silicon monoxide vapors, which in turn reacts with the active carbon forming porous  $\beta$ -SiC. The two reactions are:



SiC formed by this method can have surface areas in the range of 10–100 m<sup>2</sup>/g.

## 2.3 Catalyst preparation

Catalyst preparation consists of two steps, both important to the final characteristics of the catalyst. These are the impregnation- and calcination steps.

### 2.3.1 Impregnation of catalyst

Incipient wetness impregnation is a commonly used technique for the preparation of cobalt supported catalysts [13, 77]. This method was used in the work of this thesis, and it is explained in section 3.1.3. Other preparation methods used are slurry phase impregnation [45], ion adsorption, and homogeneous deposition precipitation [8]. Deionized water or organic compounds are usually used as solvents in impregnation methods [88].

Cobalt precursor–support interactions are important factors in the preparation of catalysts. These are often referred to as metal–support interactions (MSI) in literature [38]. Jacobs et al. [45] studied supported FT catalysts, and found MSI effects in the order  $\text{Al}_2\text{O}_3 > \text{TiO}_2 > \text{SiO}_2$ . Optimum cobalt dispersions are favored by precursor–support combinations with intermediate interaction strength [44].

Strong MSIs favor small cobalt oxide particles and little agglomeration of these during the reduction to metallic cobalt. Yet, the downside is that strong MSIs favor reactions between the active metal phase and the support material too. The former promotes high dispersion of the active metal, while the latter results in loss of the active metal.

### 2.3.2 Calcination

Calcination of the catalyst is done to remove residual nitrates that are left from the preparation of the catalyst. The temperature of the calcination has to be high enough to remove the nitrates sufficiently. Calcination may be done with or without the presence of oxygen (air).

Calcination conditions are significant for the performance of the final catalyst [84, 70]. van de Loosdrecht et al. [84] reported that presence of H<sub>2</sub>O as moisture and NO<sub>x</sub> could lead to sintering of the cobalt metal or a change in the cobalt oxide phase to a less

active one. While Reinalda and Kars [70] on the other hand claimed that elevated levels of  $\text{NO}_x$  present during calcination would have beneficial effects on FT synthesis due to agglomeration of cobalt crystallites.

Borg et al. [14] studied the effect of calcination atmosphere and temperature on  $\gamma\text{-Al}_2\text{O}_3$  supported cobalt catalysts. It was found that increasing the calcination temperature lead to less residual nitrates left on the catalyst after the calcination was done. From an initial nitrogen content of 6.3 wt.% on the uncalcined sample the amount of nitrogen decreased steadily until settling at around 0.2 wt.% for temperatures above 673 K.

Cobalt dispersion was also investigated for catalysts calcined in different atmospheres and at different temperatures. The results showed that for catalysts calcined in air, higher volume flow led to higher dispersion of cobalt. Also, regardless of volume flow, the dispersion decreased with increasing temperatures between 523–673 K. A catalyst calcined in 1:1 air/steam atmosphere showed no change in dispersion with increasing temperature. It was concluded that high air flow rates during calcination led to the highest catalyst activities.

## 2.4 Support properties

Borg et al. [15] studied the effects of support variables on  $\text{Al}_2\text{O}_3$ -supported Co catalysts. It was found that high surface area support materials lost a significant amount of surface area when the cobalt precursor was introduced. However, the shape of the pore size distribution was not affected by the loss of surface area. A weak correlation of increasing cobalt particle size with increasing average pore diameter of the support was found.

Storsæter et al. [79] found a more distinct correlation between particle size and average pore diameter. With increasing average pore diameter of  $\text{Al}_2\text{O}_3 > \text{SiO}_2 > \text{TiO}_2$ , the particle sizes of metallic cobalt increased significantly.

With respect to FT synthesis Borg et al. [15] found that cobalt-time yield and  $\text{C}_{5+}$  selectivity was fairly constant in the catalyst grain size range of 53–225  $\mu\text{m}$ . For larger sized catalyst grains both the activity and selectivity decreased significantly. Also, increasing pore diameters were found to favor the  $\text{C}_{5+}$  selectivity.

## 2.5 Dispersion and particle size

Catalyst dispersion describes the ratio of surface atoms to the total number of atoms for a given metal. Dispersion and average particle size of the active metal are directly related, since smaller particles give increase the ratio of surface atoms. The values can be obtained from volumetric adsorption or X-ray diffraction characterization methods, which both were used in the work of this thesis (see sections 3.2.3 and 3.2.4).

Storsæter et al. [78, 79] studied Co and CoRe catalysts on  $\text{Al}_2\text{O}_3$ -,  $\text{SiO}_2$ - and  $\text{TiO}_2$  supports. It was found that  $\text{Al}_2\text{O}_3$ -support gave the highest Co dispersion, while  $\text{TiO}_2$  support

gave the lowest Co dispersion. Results showed that promotion of Re led to a higher dispersion on the Al<sub>2</sub>O<sub>3</sub>- and SiO<sub>2</sub>-supported catalysts. However, no change was observed in the dispersion of the CoRe/TiO<sub>2</sub> catalyst, compared to the un-promoted catalyst.

A study of Ru catalyst supported on Al<sub>2</sub>O<sub>3</sub> and TiO<sub>2</sub> was performed by Panagiotopoulou et al. [64]. It was found that catalyst particle size and dispersion, depended on the loading of Ru on the supports. The trend was that decreased catalyst loading led to decreased particle size and increased dispersion on the support surfaces.

de la Osa et al. [28] investigated CoCa/SiC catalysts with different Co and Ca loadings. They also found that Co particle sizes decreased with decreasing Co loading. Catalysts promoted with Ca showed even greater decrease of particle sizes than the ones without promotion.

## 2.6 Reduction

Reduction of the catalyst, often performed *in situ*, is needed to activate it prior to the synthesis. Temperature programmed reduction (TPR) is widely used to investigate the reducibility of a catalyst metal on different support materials. Metal–support interactions (section 2.3.1) has an effect on the reducibility in the way that stronger MSI increases the reduction temperature. The reduction of cobalt oxide is believed to take place in two steps [14]:



de la Osa et al. [26] investigated cobalt supported on Al<sub>2</sub>O<sub>3</sub>, bentonite, TiO<sub>2</sub> and SiC. It was found that the Co/bentonite- and Co/TiO<sub>2</sub>-catalysts temperature controlled reduction (TPR) results showed a single wide reduction peak, indicating a direct reduction from Co<sub>3</sub>O<sub>4</sub> to Co<sup>0</sup>. While the Co/Al<sub>2</sub>O<sub>3</sub>- and Co/SiC-catalysts showed two reduction peaks, indicating that the reduction was taking place over two steps; Co<sub>3</sub>O<sub>4</sub> to CoO and then CoO to Co<sup>0</sup>.

A study on Co/SiC, Co/Al<sub>2</sub>O<sub>3</sub> and Co/Al<sub>2</sub>O<sub>3</sub>-SiC foam catalysts was performed by Lacroix et al. [50]. The TPR results showed that in accordance with the literature Al<sub>2</sub>O<sub>3</sub> was reduced in two steps, one reduction peak at around 643 K and a large, wider second reduction peak centered at 873 K. Interestingly, the Co/SiC catalyst was reduced completely at a very low temperature, 653 K, just slightly above the reduction temperature of the first step of the Co/Al<sub>2</sub>O<sub>3</sub> catalyst.

The same two step reduction as with Co/Al<sub>2</sub>O<sub>3</sub> was also visible with the Co/Al<sub>2</sub>O<sub>3</sub>-SiC catalyst, however, this catalyst was almost completely reduced in the first step. The first reduction peak was larger and had shifted to a higher temperature compared to the Co/Al<sub>2</sub>O<sub>3</sub> catalyst. The second peak centered at the same temperature as for Co/Al<sub>2</sub>O<sub>3</sub>, but was much smaller. Lacroix et al. [50] proposed that insufficient coverage of the Al<sub>2</sub>O<sub>3</sub>

wash-coat, leading to cobalt oxide particles in direct contact with SiC, could explain the lowered reduction temperature.

Co/SiC-catalysts studied by de la Osa et al. [28], showed the same TPR profile for reduction of Co as Lacroix et al. [50]. The complete reduction of  $\text{Co}_3\text{O}_4$  to  $\text{Co}^0$  was achieved at just above 600 K, for a 12.5 wt.% Co/SiC-catalyst. TPR profiles of two catalysts promoted with Ca, 1 and 2 wt.% respectively, were also reported. The catalyst promoted with 1 wt.% Ca showed an even lower temperature of the reduction peak, while the one promoted with 2 wt.% peaked at the same temperature as the un-promoted catalyst. All three catalysts showed a sharp peak around 950 K in addition, which the authors explain by the reduction of cobalt oxide species interacting with the  $\text{SiO}_2$  support [28].

According to Iglesia [44], cobalt oxide on  $\text{Al}_2\text{O}_3$  will only reduce completely at temperatures above 800 K, this leads to sintering of the cobalt metal particles. On  $\text{SiO}_2$  support cobalt oxides are reduced between 573–673 K without significant agglomeration.

## 2.7 Fischer-Tropsch synthesis

Important aspects regarding FT synthesis are included in the following sections. Previous FTS experiments and different aspects that can influence reaction activity and product selectivity, are presented.

### 2.7.1 Experimental FT synthesis work

As mentioned in section 2.1, SiC is a new and not widely applied support material for Fischer-Tropsch synthesis (FTS) catalysts. Yet, it was found some publications where FT synthesis was performed with Co/SiC catalysts.

Nguyen and Pham [59] prepared two 30 wt.% Co-catalysts on  $\text{Al}_2\text{O}_3$ - and SiC-foam, respectively. The catalyst activities were then examined in a fixed-bed reactor operated at 40 bar total pressure and a temperature of 493 K. FTS activity was expressed in terms of CO conversion and  $\text{C}_{5+}$  selectivity for the catalysts. After 25 hours on stream, the CO conversions of the catalysts were almost equal, while there was a large difference in the  $\text{C}_{5+}$  selectivities.

The Co/SiC foam showed a CO conversion of 71% and a  $\text{C}_{5+}$  selectivity of 85%, while the Co/ $\text{Al}_2\text{O}_3$  foam showed a CO conversion of 77% and a  $\text{C}_{5+}$  selectivity of 54%. It was also reported a lower selectivity to  $\text{CO}_2$  on the SiC-supported catalyst than on the  $\text{Al}_2\text{O}_3$ -supported one. Nguyen and Pham [59] suggested that the large pores of SiC allows for a faster evacuation of steam formed in the reaction, than the smaller pores of alumina does. Retained or condensed steam may react with CO according to the water-gas-shift reaction to produce  $\text{CO}_2$  (see table 1.1, section 1.2).

The unusually low CO conversion reported on the Co/ $\text{Al}_2\text{O}_3$  catalyst is possibly explained by a drift in the reaction temperature. Nguyen and Pham [59] had difficulties in measuring the temperature of the catalyst bed, and expected that the measured temperature was

lower than the real temperature, thus the experiment might have been performed at a wrong temperature.

In a publication by Lacroix et al. [50], where Nguyen and Pham participated, FTS experiments on SiC-, experiments on Al<sub>2</sub>O<sub>3</sub>- and Al<sub>2</sub>O<sub>3</sub>-SiC-foam supported catalysts were performed the same way as described by Nguyen and Pham [59]. This study reported the exact same CO conversions and C<sub>5+</sub> selectivities as was reported in the study of Nguyen and Pham [59], in addition to 75% CO conversion and 79% C<sub>5+</sub> selectivity for the Alumina-SiC supported catalyst.

de la Osa et al. have several publications regarding Co/SiC FTS catalysts [27, 28, 26]. A Co/SiC catalyst in extrudate form was examined along with Al<sub>2</sub>O<sub>3</sub>-, bentonite- and TiO<sub>2</sub>-supported Co catalysts in de la Osa et al. [26]. FTS activity was studied in a fixed bed reactor operated at 20 bar and temperatures varying from 493 to 573 K. The experimental data from FT synthesis show extremely high values for C<sub>5+</sub> selectivity on the bentonite and SiC supported catalysts, >99% and >90% respectively.

At a reaction temperature of 493 K the CO conversion was 7.4% and the corresponding product selectivity to C<sub>5+</sub> hydrocarbons was 93.33% for a 15 wt.% loaded Co/SiC catalyst. C<sub>5+</sub> selectivities on the Al<sub>2</sub>O<sub>3</sub> and TiO<sub>2</sub> supported catalysts were similar to findings of previous studies [15, 78], >80% for reaction temperatures in the interval 493–508 K.

de la Osa et al. [27] further investigated SiC supported Co catalysts for FT synthesis, and included Ca as a promoter to the catalyst. The same fixed bed reactor experimental setup was used and operated at 20 bar and temperatures of 493, 508 or 523 K. As in the previous publication by de la Osa et al. [26], the experimental data showed extremely high selectivity to C<sub>5+</sub> hydrocarbons. One Co/SiC catalyst with 20 wt% Co-loading and one CoCa/SiC catalyst with 20 wt.% Co- and 2 wt.% Ca-loading was run at a reaction temperature of 493 K. The Co/SiC catalyst reached a CO conversion of 34.1% and a C<sub>5+</sub> selectivity of 95.97%, while the CoCa/SiC catalyst reached a Co conversion of 31.1% and a C<sub>5+</sub> selectivity of 98.82%.

de la Osa et al. [27] pointed to the addition of alkali or alkaline earth metals for attributing to the high C<sub>5+</sub> selectivity obtained on the catalysts. It is also suggested that larger Co particle sizes, corresponding to the Co loading, favor the production of long-chained hydrocarbons.

Inspired by de la Osa et al. [28], table 2.1 was put together to give an overview of some previously reported FTS results. The table shows results from experiments on Al<sub>2</sub>O<sub>3</sub>-, SiO<sub>2</sub>, TiO<sub>2</sub> and SiC-supported catalysts. This might suggest what results can be expected for the catalysts of this work.

Table 2.1: Summary of FTS experimental results in the literature on Al<sub>2</sub>O<sub>3</sub>- and SiC-supported Co-catalysts.

Reference	Catalyst	Reaction conditions		X <sub>CO</sub> (%)	S <sub>CH<sub>4</sub></sub> (%)	S <sub>C<sub>5+</sub></sub> (%)	TOF (s <sup>-1</sup> )
S. Storsæter et al. [78]	(a) Co/γ-Al <sub>2</sub> O <sub>3</sub>	Fixed-bed reactor	(a)	42.6	9.7	80.2	0.052
	(b) Co/SiO <sub>2</sub>	483 K, H <sub>2</sub> /CO = 2	(b)	40.4	9.1	81.7	0.054
	(c) Co/TiO <sub>2</sub>	20 bar, 1-2 g catalyst Grain size 53-90 μm GHSV <sup>1</sup> = (a) 2982 (b) 3060 (c) 1885	(c)	39.8	10.2	81.6	0.054
Ø. Borg et al. [15]	CoRe/γ-Al <sub>2</sub> O <sub>3</sub>	Fixed-bed reactor	(a)	50.0	9.8	79.5	0.062
		483 K; H <sub>2</sub> /CO = 2.1	(b)	50.0	10.0	81.0	0.073
		20 bar, 1 g catalyst Grain size 53-90 μm GHSV <sup>1</sup> = (a) 8400 (b) 9100 (c) 6500	(c)	50.0	8.5	84.1	0.063
S. Rane et al. [69]	(a) Co/γ-Al <sub>2</sub> O <sub>3</sub>	Fixed-bed reactor	(a)	45.0	8.3	82.8	0.043
	(b) Co/δ-Al <sub>2</sub> O <sub>3</sub>	483 K; H <sub>2</sub> /CO = 2.1	(b)	47.0	7.2	86.0	0.028
	(c) Co/θ-Al <sub>2</sub> O <sub>3</sub>	20 bar, 1.7 g catalyst	(c)	46.0	8.1	83.1	0.043
	(d) Co/α-Al <sub>2</sub> O <sub>3</sub>	Grain size 53-90 μm GHSV <sup>1</sup> = (a) 2590 (b) 1840 (c) 1770	(d)	46.0	6.1	88.5	0.027
M. Lacroix et al. [50]	(a) Co/SiC	Fixed-bed reactor	(a)	71.0	-	85.0	0.020 <sup>4</sup>
	(b) Co/γ-Al <sub>2</sub> O <sub>3</sub> <sup>3</sup>	493 K; H <sub>2</sub> /CO = 2	(b)	77.0	-	54.0	0.016 <sup>4</sup>
	(c) Co/γ-Al <sub>2</sub> O <sub>3</sub> - SiC	40 bar, 10 g catalyst SiC- and Al <sub>2</sub> O <sub>3</sub> foam GHSV <sup>2</sup> = 330	(c)	75.0	-	79.0	0.023 <sup>4</sup>
de la Osa et al. [28, 26]	(a) Co/γ-Al <sub>2</sub> O <sub>3</sub>	Fixed-bed reactor	(a)	13.9	15.1 <sup>5</sup>	84.2	0.040 <sup>4</sup>
	(b) Co/SiC	493 K; H <sub>2</sub> /CO = 2	(b)	7.4	2.9 <sup>5</sup>	93.3	0.035 <sup>4</sup>
	(c) Co/SiC	20 bar, 5 g catalyst	(c)	34.1	3.4 <sup>5</sup>	96.0	-
	(d) Co-Ca/SiC	Grain size 2 mm GHSV <sup>1</sup> = 6000	(d)	31.1	1.0 <sup>5</sup>	98.8	-

<sup>1</sup> GHSV in units (ml/g<sub>cat</sub> - h).

<sup>2</sup> GHSV calculated as: Reactant volume flow (N cm<sup>3</sup>/h)/Catalyst apparent volume (cm<sup>3</sup>).

<sup>3</sup> Results were obtained under diluted reactant mixture: H<sub>2</sub>:CO/Ar of 50/50 vol.%.

<sup>4</sup> Reported values converted to [molCO/surface molCo - s].

<sup>5</sup> Selectivity to C<sub>1</sub>-C<sub>4</sub> hydrocarbons.

## 2.7.2 Selectivity

The FTS reaction network is regarded to be very complex [77]. Figure 2.1 gives a simplified rendering of the network and shows that the selectivities depend on the reaction rates of the different reactions. It shows that a hydrocarbon species on the cobalt surface can react in three different ways, i.e. by propagation to a higher hydrocarbon, by hydrogenation to a n-paraffin, or by hydrogen abstraction to an α-olefin. In addition, the α-olefin can undergo a second reaction, which is either hydrogenation to an n-paraffin. Or, it can



re-adsorb on the surface and undergo a subsequent chain propagation [78].

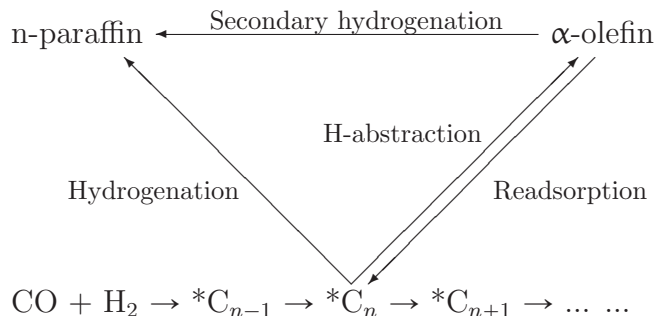


Figure 2.1: Simplified rendering of the FT synthesis reaction network.  $*C_{n-1}$ ,  $*C_n$  and  $*C_{n+1}$  represent the growing chain on the catalyst surface [78].

From the Anderson-Schulz-Flory (ASF) equation [3] the carbon chain growth distribution can be described. The chain growth distribution was calculated by equation 2.1 and presented in figure 2.2.

$$W_n = n \cdot (1 - \alpha)^2 \cdot \alpha^{n-1} \quad (2.1)$$

where  $W_n$  is the weight fraction of hydrocarbons with  $n$  carbon atoms in the chain and  $\alpha$  is the chain growth probability factor from equation 2.2.

$$\alpha = \frac{r_p}{r_p + r_t} \quad (2.2)$$

where  $\alpha$  is the chain growth probability,  $r_p$  is the rate of propagation and  $r_t$  is the rate of termination.

The selectivities of FT synthesis are in practice very different from thermodynamically calculated expectations. When methane, carbon dioxide and coke were expected to be the dominant product species from calculations, to the contrary, experiments showed that higher molecular weight hydrocarbons were the main products. According to Iglesia et al. [43], the deviation from ASF distribution yielded by the paraffinic heavy hydrocarbons in FT synthesis on cobalt catalysts, could be explained by diffusion-enhanced readsorption of  $\alpha$ -olefins and further chain growth.

Different parameters are important to and influence the selectivity, including: temperature, pressure, type of support and catalyst, promoters, feed gas composition and conversion (space velocity). Temperature has been found to influence the selectivity consistently for all FT catalysts. An increase in the temperature results in a selectivity shift toward lighter molecular mass products [2].

Increased pressure shifts the selectivity toward higher molecular mass hydrocarbons and oxygenated products. This effect is believed to be caused by either reactant or product partial pressures rather than the value of the total pressure itself [2]. Studies [15, 39, 43]



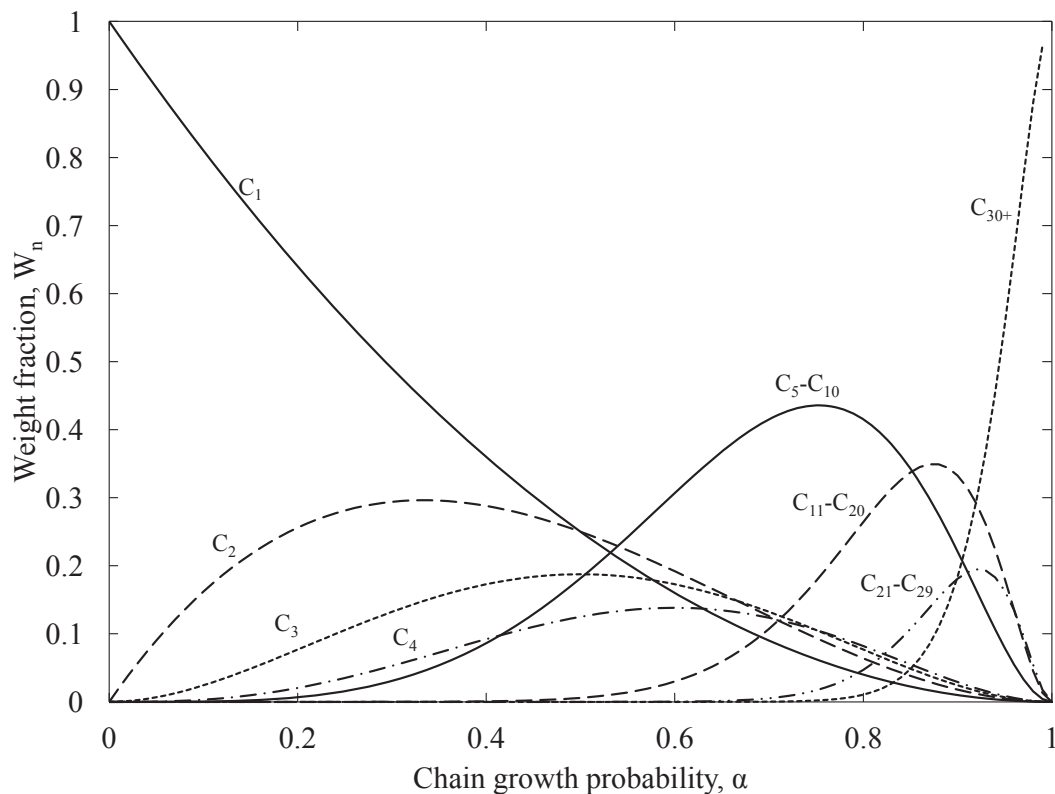


Figure 2.2: Distribution of FTS products in weight fraction as a function of the chain growth probability.

have showed that the  $C_{5+}$  selectivity increases with increasing CO conversion, either from increasing the cobalt dispersion/loading or decreasing the space velocity.

### 2.7.3 Turnover frequency

Turnover frequency (TOF) and site-time yield (STY) are two terms which are often used to describe the activity of a catalyst. Both terms describe the number of reactants converted into products per catalytic site per time unit. The author's preference seems to decide which term is used in a publication. Thus, to a reader that is unfamiliar with these terms, it might be confusing to see them used interchangeably in this and the following sections.

According to Borg [13], TOF is generally accepted to be independent of dispersion and support identity for supported cobalt catalysts.

Iglesia [44] found that at chain growth favoring conditions, i.e.  $C_{5+}$  selectivity  $> 80\%$ , the TOF was not influenced by dispersion of active metal or by support material effects. Alumina, silica, titania, silica-modified titania and magnesium chromate support materials were investigated with cobalt-loadings in the range of 1–12 wt.%, and no significant variation in TOF was found as shown in figure 2.3.

Bezemer et al. [8] investigated the relation between cobalt particle size and TOF on carbon nanofiber catalysts at FTS reaction conditions of 493 K, 1 bar and  $H_2/CO = 2$ . It was

found that the TOF increased sharply for particle sizes up to 6 nm, and that it leveled off at a practically constant value for particle sizes between 6 and 27 nm. The trend is shown in figure 2.4.

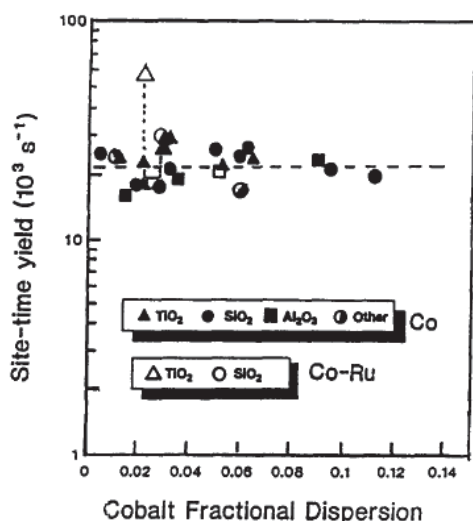


Figure 2.3: Effect of dispersion on turnover frequency in various cobalt supported catalysts [44].

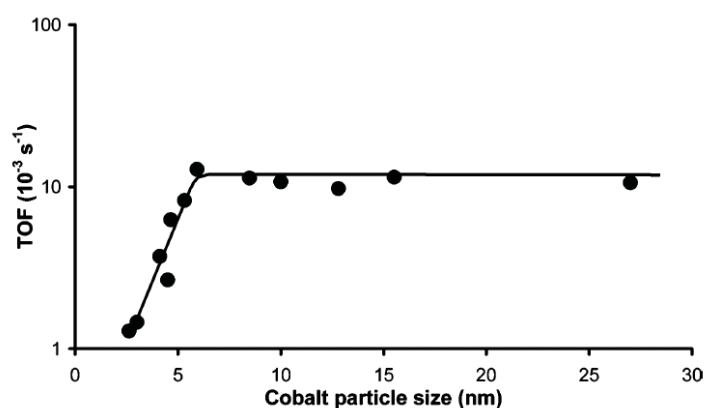


Figure 2.4: Influence of cobalt particle size on TOF [8].

### 2.7.4 Effect of water

The effect of water on FT synthesis has previously been studied widely and the results are published in several papers [39, 40, 71, 78]. Studies [40, 71] of Co-Re/ $\text{Al}_2\text{O}_3$  catalysts on the deactivation by water found that reoxidation of small cobalt particles was possibly the responsible mechanism. Hilmen et al. [40] also found a correlation between the presence of water and increased cobalt-alumina interactions. Figure 2.5 shows the effect of water addition on the hydrocarbon formation rate of a Co-Re/ $\text{Al}_2\text{O}_3$  catalyst run in a fixed-bed reactor at 483 K, 20 bar and  $\text{H}_2/\text{CO} = 2.1$  [39].

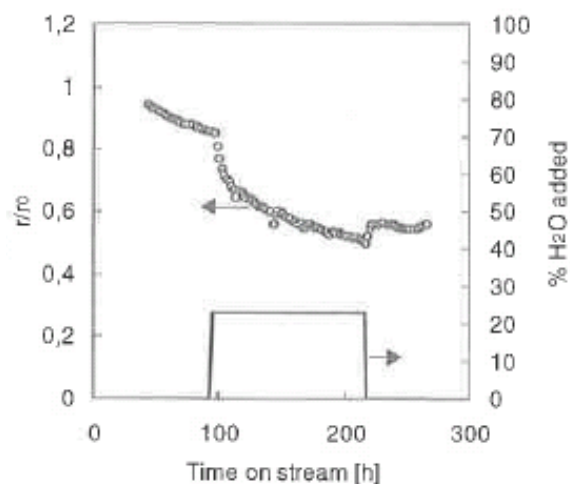


Figure 2.5: Effect of deactivation by water. Normalized rate of hydrocarbon formation as a function of time on stream for 20%Co-1%Re/ $\text{Al}_2\text{O}_3$  catalyst, amount of water in the feed flow on the right [39].

Storsæter et al. [78] studied the effect of water on  $\text{Al}_2\text{O}_3$ -,  $\text{SiO}_2$ - and  $\text{TiO}_2$ -supported Co and Co-Re catalysts. Results on the  $\text{Al}_2\text{O}_3$ -supported catalysts were in accordance with the previous results above. The  $\text{SiO}_2$ - and  $\text{TiO}_2$ -supported catalysts, however, reacted differently to the addition of water as shown in figure 2.6.

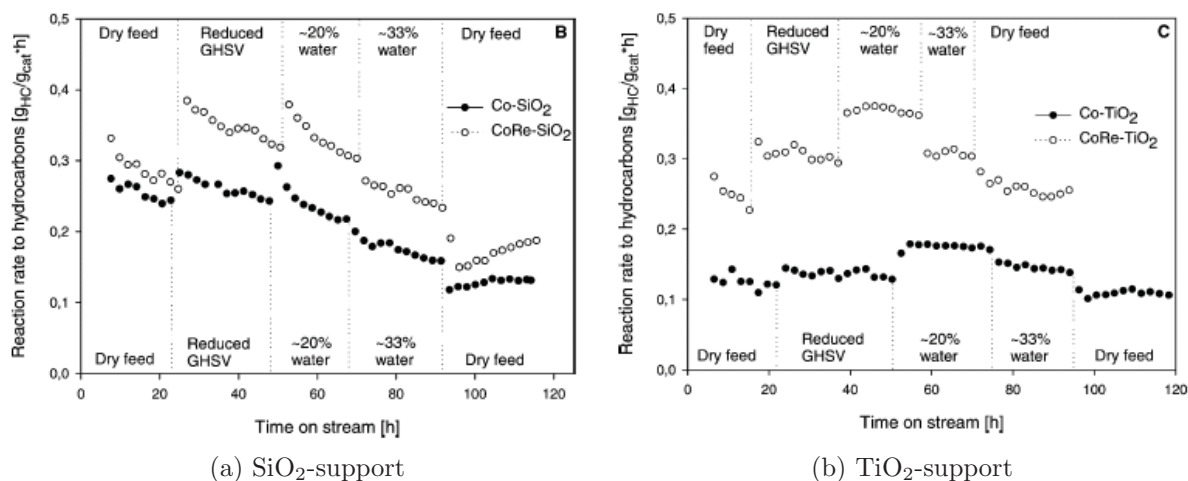


Figure 2.6: Observed hydrocarbon formation rate as function of time on stream at reaction conditions: 483 K, 20 bar and  $\text{H}_2/\text{CO} = 2.1$  [78].

Hilmen et al. [39] proposed that increased partial pressure of water, as a result of increased CO conversion, could contribute to increased  $\text{C}_{5+}$  selectivity by inhibiting hydrogenation reactions (i.e. termination of the chain growth to n-paraffins, figure 2.1). The effect of water on the remaining hydrocarbon selectivities (methane and  $\text{C}_2\text{-C}_4$ ) was decreased values. It was found that after the addition of water to the feed was stopped, selectivities to  $\text{C}_2\text{-C}_4$  and  $\text{C}_{5+}$  hydrocarbons did not return to the values observed before water addition. Water effects on the  $\text{CH}_4$  selectivity was found to be completely reversible, and this

was also found for  $C_2$  olefin selectivity.  $C_3$  and  $C_4$  olefin selectivities remained at almost the same values as during water addition. Hilmen et al. [39] notes that another study on a Co/SiO<sub>2</sub> catalyst reported that the effects of water was completely reversible.

### 2.7.5 Impurities

As some elements have promoting effects on cobalt catalysts, others have poisoning effects. Regarding FT catalysts it has been found that alkali elements have a poisoning effect on the cobalt catalysts.

Borg et al. [15] studied various effects of different support variables, one being the effect of sodium concentration in the support materials. Experiments were done with  $\gamma$ -alumina support materials from different suppliers and carried out in a fixed bed FT reactor at  $T = 483$  K,  $P = 20$  bar and  $H_2/CO = 2.1$ . The experiments showed that sodium concentrations above 50 ppm had a negative effect on the site-time yield of the catalysts. As shown in figure 2.7 the site-time yield decreases with increasing concentration of sodium in the catalysts. Borg et al. [15] also notes that no correlation between site-time yield and the physical parameters of the catalysts was found.

Borg et al. [17] studied a variety of impurities and their effect on cobalt FT synthesis. The effect of Na and Ca was found to be decreased TOF values with increasing amount of impurity loading. Na was found to have a positive effect on the  $C_{5+}$  selectivity, while Ca had a negative effect.

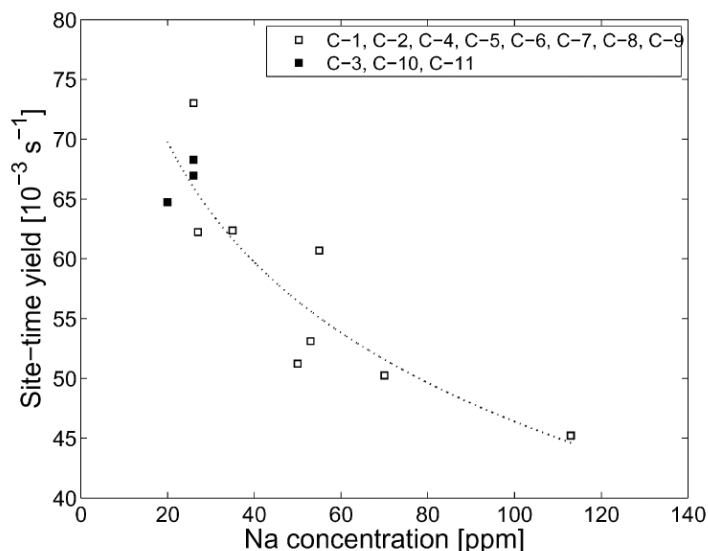


Figure 2.7: Effect of Na concentration in catalysts on the site-time yield measured after 8 h on stream [15].

Balonek et al. [5] studied the effect of alkali metal impurities on Co-Re catalysts supported on  $\gamma$ -alumina. Catalysts were loaded with four different alkali metals, Na (25–1000 ppm), Li, Ca and K (200–1000 ppm), and the experiments were carried out the same way as Borg et al. [15]; fixed bed reactor,  $T = 483$  K,  $P = 20$  bar and  $H_2/CO = 2.1$ . The

effects of alkali metal concentrations on the site-time yield and  $C_{5+}$ -selectivity are shown in figures 2.8.

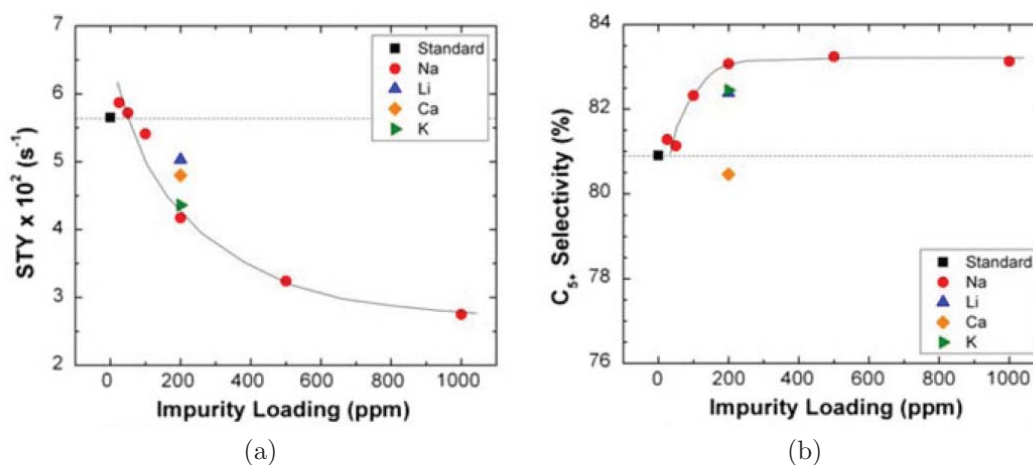


Figure 2.8: Effect of alkali metals on site-time yield and  $C_{5+}$  selectivity after 24 hours at 50 % CO conversion [5].

Balonek et al. [5] found the same correlation between catalyst sodium concentration and site-time yield as Borg et al. [15]. The results (figure 2.8a) showed that small concentrations of sodium, 25–100 ppm, gave equal values to the standard catalyst without sodium addition. Higher concentrations showed a sharp decrease in site-time yield from 100–500 ppm, and then a slower decrease from 500–1000 ppm.

Balonek et al. [5] also found that sodium had a positive effect on the  $C_{5+}$  selectivity, as shown in figure 2.8b, in a similar manner to the site-time yield effects. Sodium concentrations of 25–50 ppm showed small variations from the standard catalyst, then a sharp increase in  $C_{5+}$  selectivity from 50–200 ppm before it leveled off at a constant value between 200–1000 ppm. It was also found that the alkali metals increased the temperature needed to reduce cobalt oxide to metallic cobalt.

Sulfur is another element which is poisonous to FT cobalt catalyst, and causes permanent deactivation of the catalyst sites [30]. The threat of sulfur poisoning is greatest from the feed gas, thus great care is taken to remove as much sulfur as possible from it. Shell recommended for fixed bed reactors using cobalt catalysts, that the feed gas should be practically free of sulfur [46].

### 2.7.6 Effect of alkali metals

$H_2$  adsorb dissociatively on Pt(111), like it does on Co, and need two adjacent sites to do so.

Zhou and White [89] studied hydrogen adsorption on K-covered Pt(111) surfaces. It was proposed that, since hydrogen does not adsorb on metallic K, potassium would not only cover otherwise free sites, but also minimize the chance of two sites existing next to each other. Zhou and White [89] also proposed that adsorbed potassium increased the

electron density of the Pt surface. This resulted in a larger charge difference between the Pt surface and adsorbed hydrogen, which in turn increased the hydrogen desorption energy, thus stabilizing the bond between platinum and adsorbed hydrogen. Solymosi and Kovacs [75] investigated dissociative adsorption of  $H_2$  on K-covered Pd(100) surfaces and found the same effects of potassium coverage as Zhou and White [89] did on Pt(111).

The study of Gebhard and Koel [35] also supports the effects of K-coverage on Pt(111) surfaces that Zhou and White [89] found. It was found that the sticking coefficient for hydrogen, the number of adsorbed atoms/molecules by the number of atoms/molecules that hit a surface at a given time interval, drastically decreased on the K-covered surface compared to the K-free. Gebhard and Koel [35] observed an increased activation energy for dissociative  $H_2$  adsorption in line with Zhou and White [89].

It was proposed that mobile, weakly bound adsorbed molecular  $H_2$  was an important precursor to the dissociative adsorption of hydrogen. When potassium was introduced to the Pt(111) surface, it was suggested that the behavior of this  $H_2$  precursor changed. It was proposed two possible causes of this. Increased probability of desorption of the  $H_2$  precursor prior to finding a suitable site for dissociative adsorption. And, changes in the electronic structure of the platinum surface decreasing the probability of adsorption of  $H_2$  into the precursor state.

Berkó and Solymosi [7] studied adsorption of CO on K-covered Pd(100) surfaces, and found that potassium had a stabilizing effect on the adsorbed CO molecules too. It was proposed that potassium donated an electron to the adsorbed CO molecule creating a  $K^+ - CO^-$  complex. Potassium stabilized CO by increasing the binding energy, and adsorbed CO on K stabilized the weak bond between K and the Pd surface. It was pointed out that K was mainly ionic at low coverages, and electronic interaction between K and CO can not be expected then. Metallization of K occurred with increasing coverage of K, and complete metallization was first achieved at or above monolayer coverage.

Uner et al. [83] disagreed to the proposed electron density changes having caused the observed effects of alkali coverage of the metal surfaces as discussed above. [83] studied hydrogen interaction on ruthenium catalysts promoted with potassium. It was proposed that K was present on the catalyst surface in oxide or hydroxide form, and thus would not donate electron density to the metal surface. Instead, the decreased hydrogen adsorption rates and reduced mobility of hydrogen was attributed to alkali blocking of the sites available for hydrogen adsorption alone.

In a relating study Uner [82] theoretically investigated the effect of limited hydrogen adsorption/desorption mobility by changing the equilibrium constant in a model describing FT synthesis. Uner [82] claimed that alkali metal oxides and  $TiO_x$  exhibit similar properties on FTS catalyst metals. Studies by Komaya et al. [49, 48], on  $TiO_2$  promoted Ru/ $SiO_2$  catalysts, was used to support the assumptions made. It was concluded from the theoretical model that the methane formation and CO consumption rates would decrease with decreasing hydrogen adsorption equilibrium constant. The olefin/paraffin ratio was found to increase with decreasing hydrogen adsorption rate constant.

Borg et al. [17] looked at different possible reasons for the lowered activity caused by Na and Ca. Physical blocking of the active cobalt sites was found to be unlikely due to too small impurity concentrations on the catalysts. Cobalt particle size effects induced by

the impurities were also ruled out as no significant different in particle size was observed. Electronic effects via the oxygen ion of alkali and alkaline earth metal oxides was suggested as a more likely reason for the observed effects. However, Borg et al. [17] would not make any further detailed speculations regarding the electronic effects.





# Chapter 3

## Experimental

Experimental work done over the course of this thesis is described in this chapter. This includes preparation and characterization of the catalyst, and experimental Fischer-Tropsch synthesis (FTS) work. The preparation method used was incipient wetness impregnation and calcination in flowing air. Characterization methods used were volumetric adsorption, temperature programmed reduction (TPR), volumetric chemisorption, X-ray diffraction (XRD), steady-state isotopic transient kinetics (SSITKA) and electron microscopy. There was also done an elemental analysis on one support and one catalyst sample. The FTS experiments were performed in two parallel fixed-bed reactors.

### 3.1 Preparation of catalyst

This section includes specifications and properties of the support materials and the prepared catalysts, along with a detailed description of the impregnation and calcination steps in the catalyst preparation.

Table 3.1: Support properties provided by SICAT. Surface area measured by N<sub>2</sub> adsorption and pore volume measured by mercury porosimetry.

SICAT code	Sample notation	Phase	Surface area (m <sup>2</sup> /g)	Pore volume (cm <sup>3</sup> /g)
<b>First batch</b>				
SB0689A	S1	β-SiC	25-35	0.55
SB0700G	S2	β-SiC	25-35	0.60
SB0700C	S3	β-SiC	25-35	0.85
DA0558B	S4	TiO <sub>2</sub> -SiC	100	0.30
<b>Second batch</b>				
DI0234	S5	β-SiC	27	0.55
SD0035B <sub>2D</sub>	S6	β-SiC	24	N.A.
SD0037F <sub>G</sub>	S7	β-SiC	N.A.	N.A.

### 3.1.1 Support materials

Support materials for the catalysts were obtained from the commercial catalyst support producer SICAT [72] in Germany. Initially, three  $\beta$ -SiC samples and one TiO<sub>2</sub>-SiC sample were selected to be investigated in this thesis. Catalytic testing of the four support samples rose suspicions of impurities being present in the materials. Thus, three more support samples, which would contain fewer impurities, were investigated. Information is given in table 3.1 and appendix D.

### 3.1.2 Catalysts

Table 3.2 shows the notations that will be used for the catalysts throughout the report, along with the cobalt loading of the catalysts. Also included are cobalt and rhenium loadings of two reference catalysts. These will be used for comparison with results from the SiC-supported catalysts, and with previous experimental results. Catalyst C1 was prepared from support sample S1, etc.

Table 3.2: Properties of SiC- and reference Al<sub>2</sub>O<sub>3</sub>-catalysts.

Sample notation	Catalyst	Cobalt loading (wt.%)	Rhenium loading (wt.%)
<b>First batch</b>			
C1	Co/SiC	12.5	-
C2	Co/SiC	12.5	-
C3	Co/SiC	12.5	-
C4	Co/TiO <sub>2</sub> -SiC	12.5	-
<b>Second batch</b>			
C5	Co/SiC	12.5	-
C6	Co/SiC	12.5	-
C7	Co/SiC	12.5	-
<b>Reference</b>			
R1	Co/Al <sub>2</sub> O <sub>3</sub>	12.0	-
R2	CoRe/Al <sub>2</sub> O <sub>3</sub>	20.0	0.5

### 3.1.3 Impregnation and calcination

The support samples came in pellet form and were not suited for characterization or FTS experiments, thus each support sample was crushed in a mortar and sifted in a sieve into three fractions of differing particle size: >90  $\mu\text{m}$ , 53–90  $\mu\text{m}$  and <53  $\mu\text{m}$ .

Cobalt was added to the four support samples by the incipient wetness impregnation (IWI) method. The incipient wetness point (IWP) was determined for each support sample by wetting until full capillary condensation was achieved. The IWP was determined by eye when the support was starting to look wet. At IWP the support will release the absorbed fluid by gently knocking the container holding the support sample, against a solid surface.

Table 3.3: Molecular weights of Co and  $\text{Co}(\text{NO}_3)_2 \cdot 6\text{H}_2\text{O}$ .

Component	$M_W$ (g/mol)
Cobalt	58.93
Cobalt(II)nirate hexahydrate	291.07

The cobalt precursor used was 99.0% pure cobalt(II)nirate hexahydrate,  $\text{Co}(\text{NO}_3)_2 \cdot 6\text{H}_2\text{O}$ , from *Fluke*. All seven catalysts were prepared with a cobalt loading ( $x_{Co}$ ) of 12.5wt.%.

First, the IWP for a given sample was determined from equation 3.1, using deionized water and SiC particles with diameter  $<53 \mu\text{m}$ . This was due to low yield of support particles with the correct diameter after crushing. It was investigated that the amount of water absorbed by the supports were independent of the particle sizes. It was investigated that the amount of water absorbed by the supports were independent of the particle sizes.

$$IWP = \frac{m_{Water}}{m_{Support}} \quad (3.1)$$

where  $IWP$  is the ratio of water to support where full capillary condensation is achieved [ $g_{Water}/g_{Support}$ ], and  $m_{Water}$  and  $m_{Support}$  are the weights of water and SiC support, respectively, in [g].

Next, the desired mass of catalyst,  $m_{Cat}$ , (support +  $\text{Co}^0$ ) after calcination and reduction, was chosen to be 10 g. The mass of SiC support and mass of cobalt(II)nirate hexahydrate needed to achieve this, was calculated from equation 3.2 and equations 3.3 and 3.4, respectively.

$$m_{Support} = m_{Cat} \cdot (1 - x_{Co}) \quad (3.2)$$

$$m_{Co^0} = m_{Cat} \cdot x_{Co} \quad (3.3)$$

$$m_{Co(NO_3)_2 \cdot 6H_2O} = \frac{M_W(Co(NO_3)_2 \cdot 6H_2O)}{M_W(Co)} \cdot m_{Co^0} \quad (3.4)$$

where  $m_{Support}$ ,  $m_{Cat}$ ,  $m_{Co^0}$  and  $m_{Co(NO_3)_2 \cdot 6H_2O}$  are the mass of SiC support, calcined and reduced catalyst, cobalt metal and cobalt(II)nirate hexahydrate, respectively, in [g],  $x_{Co} = 0.125$  is the specified cobalt loading, and  $M_W(Co)$  and  $M_W(Co(NO_3)_2 \cdot 6H_2O)$  are the molecular weights of cobalt and cobalt(II)nirate hexahydrate, respectively, in [g/mol].

Equation 3.1 was then rearranged into equation 3.5. This, to calculate the mass of water that the amount of SiC support, calculated from equation 3.2, could absorb. The calculated amount of water was then weighed into a graduated cylinder, and the volume it corresponded to, was marked on the cylinder. The cylinder was then emptied and dried. Next, cobalt nirate was weighed into the cylinder and deionized water was added up to

the marking, thus giving the correct volume of liquid for impregnation. It should be noted that deionized water was used in all steps of the catalyst preparation.

$$m_{Water} = IWP \cdot m_{Support} \quad (3.5)$$

where all variables correspond to equation 3.1.

The cobalt(II)nitrate hexahydrate solution was poured onto the support sample while stirring. This was done to ensure a good distribution of cobalt(II)nitrate hexahydrate, avoiding a filtering effect from the support material. The impregnated support was then dried in a heating cabinet at 383 K for two hours, while stirring every 15 minutes the first hour, and every 30 minutes the second hour.

Finally, the impregnated support was calcined in flowing air at 573 K for 16 hours in a quartz glass reactor. The temperature was ramped from ambient to 573 K at a rate of 2 K/min. After calcination, the prepared catalyst was sifted one more time into the fractions: >90  $\mu\text{m}$ , 53–90  $\mu\text{m}$  and <53  $\mu\text{m}$ .

## 3.2 Characterizations

The experimental procedures of the different characterizations are thoroughly explained in this section along with calculations associated with them. As mentioned, these were volumetric adsorption, temperature programmed reduction (TPR), volumetric chemisorption, X-ray diffraction (XRD), steady-state isotopic transient kinetics (SSITKA) and electron microscopy.

### 3.2.1 Volumetric adsorption

Volumetric adsorption was used to find the surface area, pore volume and average pore diameter of both the un-impregnated support samples and the prepared catalysts.

A *TriStar II 3020* instrument was used to perform the experimental analysis. Support and catalyst samples of 0.2 g for S4 and C4, and 0.4 g for the remaining samples were placed in sample holders and mounted to the instruments vacuum pump. Degassing of the samples were then performed at ambient temperature for one hour, then at 473 K overnight, to remove water from the samples. The next day each sample holder was weighed again to determine the weight of sample without water, and then mounted back on the instrument. Finally, the liquid nitrogen container was filled to the correct level.

A computer software, called *TriStar II 3020 V1.03*, was performing the analysis automatically. For each sample an individual file was created on the computer where the measured weight after degassing was inputted together with analysis parameters.

Surface area was calculated from the experimental data, using the isotherm of Brunauer, Emmett and Teller, known as the BET isotherm [21]. Starting by plotting  $\frac{P}{P_0}$  against  $\frac{P}{P_0 - P}$ , to extract the slope and intersection of the slope with the Y-axis from the

resulting equation 3.6 [21]. The data points were collected from the report produced by the computer program *TriStar II 3020 V1.03*.

$$\frac{P}{V_a(P_0 - P)} = \frac{P}{P_0} \cdot \alpha + \eta \quad (3.6)$$

where  $P$  is the adsorption pressure [ $mmHg$ ],  $P_0$  is the equilibrium (saturation) pressure of the condensed gas [ $mmHg$ ],  $V_a$  is the volume of adsorbed gas [ $cm^3/g$  STP],  $\alpha$  is the slope [ $g/cm^3$  STP] and  $\eta$  is the intersection of the slope with the Y-axis [ $g/cm^3$  STP] [9].

With the slope and intersection values, the volume of gas adsorbed in the first monolayer was calculated by equation 3.7 [21].

$$V_0 = \frac{1}{\alpha + \eta} \quad (3.7)$$

where  $V_0$  is the volume of adsorbed gas in the first monolayer [ $cm^3/g$  STP],  $\alpha$  is the slope [ $g/cm^3$  STP] and  $\eta$  is the intersection of the slope with the Y-axis [ $g/cm^3$  STP].

The volume of adsorbed gas in the first monolayer was converted to the number of molecules adsorbed in the first monolayer by equation 3.8 [21].

$$N_0 = \frac{P_{STP} \cdot V_0 \cdot 10^{-6}}{T_{STP} \cdot k_B} \quad (3.8)$$

where  $N_0$  is the number of molecules adsorbed in the first monolayer [ $g^{-1}$ ],  $P_{STP} = 101300[Pa]$  is the pressure at STP conditions,  $V_0$  is the volume of adsorbed gas in the first monolayer [ $cm^3/g$  STP],  $10^{-6}[m^3/cm^3]$  is a correction for the volume unit,  $T_{STP} = 273.15[K]$  is the temperature at STP conditions and  $k_B = 1.38065 \cdot 10^{-23}[J/K]$  [4] is the Boltzmann constant.

Finally, the BET surface area was calculated by equation 3.9 [21].

$$A_{BET} = N_0 \cdot A_0 \quad (3.9)$$

where  $A_{BET}$  is the BET surface area [ $m^2/g$ ],  $N_0$  is the number of molecules adsorbed in the first monolayer [ $g^{-1}$ ] and  $A_0 = 16.2 \cdot 10^{-20}[m^2]$  is the surface area a nitrogen gas molecule occupies at the analysis conditions (77.15 K).

Pore volumes and pore diameters were measured by the *TriStar II 3020* instrument using the Barrett, Joyner and Halenda [6] (BJH) isotherm. These results were collected from the report produced by the computer program *TriStar II 3020 V1.03*.

### 3.2.2 Temperature programmed reduction

Temperature programmed reduction (TPR) was used to find the reducibility of cobalt on the different supports.

A TPR apparatus was used to perform the reductions, a schematic drawing of the apparatus can be found in [11]. Catalyst samples of approximately 0.2 g were placed in a quartz glass reactor and mounted to the apparatus. The reducing gas, 7 % H<sub>2</sub>/Ar, was passed through a gas purifier, an oxy-trap and a molecular sieve, all manufactured by *Alltech*.

With the help of a valve and a manometer, the gas pressure was set to  $0.8 \pm 0.1$  bar. Then the gas was split in two, one line for the reducing gas and one line for reference gas to the gas chromatograph. The reducing gas was passed through the reactor and a cold trap, before entering the gas chromatograph. Water produced during the reduction of cobalt was condensed and removed from the gas in the cold trap, with dry ice (CO<sub>2</sub>(s)) in 2-isopropanol as cooling agent.

Reactor temperature was increased with a furnace by ramping the temperature at 10 K/min from ambient to 1200 K. The gas chromatograph used was a *Shimadzu GC-8A* with a thermal conductivity detector (TCD) running at a current of 60 mA and a column temperature of 373 K. The data from the gas chromatograph was logged on a computer using a software called EasyView.

### 3.2.3 Volumetric chemisorption

To find the metal dispersion and metallic surface area of the catalysts, volumetric chemisorption of hydrogen was performed.

An *ASAP 2020C* instrument was used to conduct the chemisorption experiments. Catalyst samples of approximately 0.3 g was placed in a U-tube quartz glass reactor and mounted to the instrument. The catalyst samples were situated between two layers of quartz wool inside the reactor. A manual leak test was done by evacuating the reactor and letting the pressure stabilize (approx. 20 min.) before closing the valves to the vacuum pumps to see if the pressure would increase rapidly or not. A preprogrammed file, *fts-10h.anc*, containing analysis condition settings was loaded and information about the sample weight and cobalt loading was entered in the computer program *ASAP 2020C v1.09*. The preprogrammed file was used to enable comparison with earlier metal dispersion results obtained on the same instrument using this file. Then the instrument was started.

The preprogrammed file guided the instrument through seven "tasks", deciding temperatures, temperature ramping rates and durations of the tasks:

1. The reactor was heated to 313 K at a rate of 10 K/min while the reactor was evacuated for 60 minutes.
2. A leak test was performed.
3. The reactor was heated to 623 K at a rate of 1 K/min and reduced with hydrogen for a total of 16 hours.
4. Cooling of the sample to 603 K at 10 K/min while evacuated for one hour.
5. Further cooling to 373 K at 10 K/min while evacuated for 30 minutes.

6. Another leak test was performed.
7. The sample was cooled to 313 K at 10 K/min before the analysis was performed with hydrogen, to obtain the chemisorption isotherms.

Dispersion of metal on the support surface and average particle diameter was then calculated. The straight part of the collected isotherms was extrapolated to zero pressure, and the corresponding volume of adsorbed H<sub>2</sub> was noted. Two isotherms were collected, one chemisorption + physisorption isotherm and one physisorption isotherm. Neither of the isotherms yield the true dispersion, however, the chemisorption + physisorption isotherm was used in this work. Since the "real" isotherm was not possible to find, this isotherm was used as it was the most common practice [53].

The dispersion,  $D_{H_2,ads}$  (fraction of cobalt surface atoms by total number of cobalt atoms), was calculated using equation 3.10 [41]:

$$D_{H_2,ads} = \frac{v_{ads} \cdot M_W(Co) \cdot F}{x_m} \quad (3.10)$$

where  $D_{H_2,ads}$  is the dispersion of cobalt on the support,  $v_{ads}$  is the adsorbed amount of H<sub>2</sub> by selective chemisorption [mol/g STP],  $M_W(Co) = 58.933[g/mol]$  is the molecular mass of cobalt,  $F$  is the adsorption stoichiometry, i.e. the number of surface atoms covered by one adsorbed molecule (2Co:1H<sub>2</sub>) and  $x_m$  is the mass fraction of cobalt in the sample.

The average metal particle size was then calculated from equation 3.14 [41].

$$d_{H_2,ads} = f \cdot \frac{V_{sp}}{S_m} \quad (3.11)$$

where  $d_{H_2,ads}[nm]$  is the metal particle size,  $f$  is a factor describing the particle shape (chosen to 6 assuming spherical particles [41]), and  $V_{sp}[cm^3/g]$  is the specific volume of the cobalt particles and  $S_m[m^2/g]$  is the specific surface area of cobalt calculated by equations 3.12 and 3.13, respectively.

$$V_{sp} = \frac{1}{\rho} \quad (3.12)$$

and

$$S_m = \sigma \cdot \frac{N_A}{M_W} \cdot D_{H_2,ads} \quad (3.13)$$

where  $V_{sp}[cm^3/g]$  is the specific volume of the cobalt particles [ $cm^3/g$ ],  $\rho = 8,9[g/cm^3]$  is the density of cobalt,  $S_m[m^2/g]$  is the specific surface area of cobalt,  $\sigma = 6.62 \cdot 10^{-16}[cm^2]$  [54] is the average surface area occupied by a cobalt surface atom,  $N_A = 6.022 \cdot 10^{23}[mol^{-1}]$  is Avogadro's number,  $M_W = 58.933[g/mol]$  is the molecular mass of cobalt and  $D_{H_2,ads}$  is the dispersion calculated by equation 3.10. This gives the following equation:



$$d_{H_2,ads} = \frac{f \cdot M_W}{\sigma \cdot \rho \cdot N_A \cdot D_{H_2,ads}} \cdot 10^7 [nm/cm] \quad (3.14)$$

where all variables and constants correspond to equations 3.11, 3.12 and 3.13.

### 3.2.4 X-ray diffraction

X-ray diffraction (XRD) was used to identify the crystalline phases of the support samples and the catalysts. And to find the particle sizes of cobalt oxide on the catalysts.

XRD spectra were obtained using a *Siemens D8 focus* instrument. Initially, a catalyst sample was run quickly from  $2\theta$  angles  $5^\circ$  to  $90^\circ$  to establish the  $2\theta$  range where the peaks were located. Samples were prepared on special sample holders for the instrument. The aim was to achieve a monolayer of particles by placing sample on the holders and spread the particles by applying ethanol. After the ethanol had evaporated the sample holders were placed in the instrument.

A computer software controlled the instrument and could automatically run through up to eight samples without human interference. Parameters on  $2\theta$  range, step length and step time were selected prior to running the instrument. Scanning range was set to  $2\theta = [20^\circ-80^\circ]$ , step length to  $0.021^\circ$ , step time to 96 s and the slit size was 1 mm.

After the XRD spectra were collected, the software *EVA* was used to determine the phases of cobalt oxide, silicon carbide and titanium oxide. Spectra from a library in the program were compared and matched to the collected spectra. Another software, *TOPAS*, was used to calculate the particle sizes directly from the "full width at half maximum" (FWHM) method. Data on SiC, TiO<sub>2</sub> and Co<sub>3</sub>O<sub>4</sub> was inputted, and the software calculated ideally fitted peaks to calculate the particle size from an average of all Co<sub>3</sub>O<sub>4</sub> peaks. Since XRD was done on oxidized samples, equation 3.15 [77] was used to estimate the particle sizes of cobalt metal from the cobalt oxide particle sizes.

$$d_{XRD}(Co^0) = 0.75 \cdot d_{XRD}(Co_3O_4) \quad (3.15)$$

where  $d_{XRD}(Co^0)[nm]$  is the particle size of cobalt metal and  $d_{XRD}(Co_3O_4)[nm]$  is the particle size of cobalt oxide.

Cobalt metal dispersion from XRD,  $D_{XRD}$ , was then found from equation 3.16 [77].

$$D_{XRD} = \frac{f \cdot M_W}{\rho \cdot \sigma \cdot N_A} \cdot \frac{S}{V} \quad (3.16)$$

where  $D_{XRD}[nm]$  is the cobalt dispersion,  $f$  is the fraction of the surface of the active atom which is effectively exposed to the reactants, equal to 1.  $M_W = 58.993[g/mol]$  is the molecular mass of cobalt,  $\rho = 8.9 \cdot 10^6[g/m^3]$  is the density of cobalt,  $\sigma = 0.0662 \cdot 10^{-18}[m^2]$  is the average surface area occupied by a surface atom,  $N_A = 6.022 \cdot 10^{23}[mol^{-1}]$  is Avogadro's number, and  $S/V$  is equal to  $6/d$  for spherical particles. Numbers inserted gives:



$$D_{XRD} = \frac{1 \cdot 58.933[g/mol] \cdot 10^9[nm/m]}{8.9 \cdot 10^6[g/m^3] \cdot 0.0662 \cdot 10^{-18}[m^2] \cdot 6.022 \cdot 10^{23}[mol^{-1}]} \cdot \frac{6}{d_{XRD}} \cdot 100\%$$

$$D_{XRD} = \frac{99.66}{d_{XRD}[nm]} \quad (3.17)$$

where  $D_{XRD}[nm]$  is the cobalt dispersion and  $d_{XRD}(Co^0)[nm]$  is the particle size of cobalt metal.

### 3.2.5 SSITKA

Steady state isotopic transient kinetic analysis (SSITKA) characterization was done on catalysts C1 and C3. The experiments were carried out by *postdoc. Jia Yang* [87] with the *Department of Chemical Engineering* at *NTNU*. Experimental procedures are thoroughly explained in [33].

### 3.2.6 Electron microscopy

Transmission electron microscopy (TEM) and scanning transmission electron microscopy (STEM) characterizations was performed by *Senior Scientist John Walmsley* [86] with *SINTEF Materials and Chemistry* on catalyst C1. The experimental work was done similarly to what is described in [79].

### 3.2.7 Elemental analysis

Two samples, support S1 and catalyst C1, was sent to *Molab AS* for an elemental analysis of their composition. Of interest were elements that could have an impact on the FTS activity and selectivity, thus it was requested that the samples were analyzed for iron, sodium, calcium, phosphorus and sulfur content. Analysis techniques used were Inductively Coupled Plasma (ICP) on Fe, Na, Ca and P, and combustion analysis on S.

## 3.3 Fischer-Tropsch synthesis

FTS experiments were carried out in two parallel fixed-bed reactors, two catalysts each run. The reactors were made in stainless steel and had an inner diameter of 10 mm. A schematic drawing of the apparatus is given in figure 3.1.

At first the FTS rig was flushed with helium to remove any remaining synthesis gas from the previous experiment, and then the reactors were disassembled from the electrical furnaces. The old catalyst beds were removed and the reactors were cleaned. Catalyst samples (53–90  $\mu\text{m}$ ) were weighed in, 2 g of the SiC supported catalysts and 0.2 g of the reference  $\gamma$ -alumina catalyst, diluted with 15 g of inert SiC (*Saint-Gobain Sika*, 75–150

$\mu\text{m}$ ). The diluted catalysts were then placed in the reactors between two layers of quartz wool and the reactors were reassembled in the electrical furnaces. An overnight leak test was performed by pressurizing the rig to 20 bar with helium as a safety measure.

If the leak test was passed, the pressure was decreased to 1.5 bar and reduction of the catalysts in flowing  $\text{H}_2$  (supplied by *Yara Praxair*) was started. The catalysts were heated from ambient temperature to 623 K at a ramping rate of 1 K/min, reduced for 16 hours, and then cooled to 443 K. Simultaneously, as the reduction was performed, a small flow of synthesis gas (supplied by *Yara Praxair*) was sent to the gas chromatograph (GC) in order to calibrate the  $\text{N}_2/\text{CO}$  ratio of the synthesis gas bottle. This was done prior to every experiment due to drifting in the  $\text{N}_2/\text{CO}$  ratio within the same gas bottle over time.

As the temperature reached 443 K, the hydrogen flow was replaced by helium, and the pressure increased to 20 bar. When the rig was pressurized, helium was replaced with synthesis gas and the temperature was ramped up to reach the reaction temperature of 483 K. Ramping was done in three steps, from 443–463 K at 2 K/min, from 463–473 K at 0.5 K/min and finally from 473–483 K at  $\sim 0.2$  K/min. The first two ramping steps were done by a temperature controller while the last was done manually. After the temperature had reached 483 K and was stabilized, a temperature profile of the catalyst bed was logged using an adjustable thermocouple.

- Catalysts C1, C2, C3 and R2 were run for 48 hours with a synthesis gas flow of 150 NmL/min.
- Catalysts C4 and C5 were run for 26 hours with a synthesis gas flow of 150 NmL/min. Then the synthesis gas flow was reduced to 34 and 18 NmL/min respectively, in order to reach a CO conversion of 50%.
- Catalysts C6 and C7 were run for 26 hours with a synthesis gas flow of 150 NmL/min. Then the synthesis gas flow was reduced to 100 and 81 NmL/min to reach CO conversions of 9 and 15%, respectively.

Liquid products were collected from the hot- and cold pots, while the lighter gaseous products were analyzed in a gas chromatograph. A thermal conductivity detector (TCD) analyzed for  $\text{H}_2$ ,  $\text{N}_2$ ,  $\text{CO}$ ,  $\text{CO}_2$  and  $\text{CH}_4$ , which were first separated in a 3.048 m by 3.175 mm inner diameter Carbosieve SII packed column. And a flame ionization detector (FID) analyzed for the hydrocarbons, previously separated in a 30 m by 0.53 mm inner diameter GS-Q capillary column. Methane was used to link the results from TCD and FID analyses.

Equation 3.18 was used to calculate the  $\text{CO}/\text{N}_2$  ratio of the feed synthesis gas. The ten last GC analyses was calculated, and the average value was used.

$$R_{\text{CO}/\text{N}_2, \text{in}} = \frac{1}{10} \cdot \sum_{i=1}^{10} \frac{A_{\text{CO},i}}{A_{\text{N}_2,i}} \quad (3.18)$$

where  $R_{\text{CO}/\text{N}_2, \text{in}}$  is the  $\text{CO}/\text{N}_2$  feed ratio,  $A_{\text{CO}}$  and  $A_{\text{N}_2}$  are the peak area of the respective compound from the GC TCD signal, and  $i$  denotes one of the ten last GC analyses.

Since the composition of the synthesis gas varied between different synthesis gas bottles, and the supplier (*Yara Praxair*) only certified the quantitative amount of nitrogen in the gas bottles, the amounts of carbon monoxide and hydrogen were calculated by equations 3.19 and 3.20.

$$\chi_{CO} = \chi_{N_2} \cdot R_{CO/N_2,in} \cdot \frac{f_{N_2}}{f_{CO}} \quad (3.19)$$

$$\chi_{H_2} = 1 - \chi_{CO} - \chi_{N_2} \quad (3.20)$$

where  $\chi_{CO}$ ,  $\chi_{N_2}$  and  $\chi_{H_2}$  are component mole fractions in the feed flow,  $f_{N_2}$  and  $f_{CO}$  are the response factors of the two components in the GC. The different response factors that were used are listed in table 3.4.

GC TCD response factors were used to correct for the amount of an analyte compared to the analyte signal detected. The ratio between peak areas belonging to the different components detected, could not be directly compared to each other with respect to the amount of the components.

Table 3.4: Calibrated response factors to the thermal conductivity detector of the gas chromatograph.

Component, $i$	N <sub>2</sub>	CO	CO <sub>2</sub>	CH <sub>4</sub>
Response factor, $f_i$	616.70	619.38	698.68	469.50

Feed flow rates of the three components in the synthesis gas, in units [ $mol/g \cdot h$ ], were calculated by equations 3.21 and 3.22.

$$\dot{V}_{i,in} = \dot{V}_{tot,in} \cdot \chi_i \quad (3.21)$$

$$\dot{F}_{i,in} = \frac{\dot{V}_{i,in}}{m_{cat} \cdot V_m^{i,g.}} \quad (3.22)$$

where  $\dot{V}_{i,in}$  is the feed flow rate in [ $ml/h$ ],  $\dot{V}_{tot,in}$  is the total feed flow rate in [ $ml/h$ ],  $\chi_i$  is the component mole fraction,  $\dot{F}_{i,in}$  is the feed flow rate in [ $mol/g_{cat} \cdot h$ ],  $m_{cat}$  is the amount of catalyst used in [ $g$ ],  $V_m^{i,g.} = 22414$  [ $ml/mol$ ] is the molar volume of ideal gas at 273.15 K and 1 atm, and  $i$  denotes one of the components in the feed gas.

Using the calculated feed flow rate of nitrogen, which is equal to the exit flow rate due to its inertness, flow rates of the remaining components detected in the TCD, i.e. H<sub>2</sub>, CH<sub>4</sub>, CO and CO<sub>2</sub>, was calculated by equation 3.23.

$$\dot{F}_{i,out} = \dot{F}_{N_2,in} \cdot \frac{f_{N_2} \cdot A_i}{f_i \cdot A_{N_2}} \quad (3.23)$$

where  $\dot{F}_{i,out}$  is the exit flow rate of component  $i$  in  $[mol/g_{cat} \cdot h]$ ,  $\dot{F}_{N_2,in}$  is the  $N_2$  feed flow rate calculated by equation 3.22 in  $[mol/g_{cat} \cdot h]$ ,  $f$  is the GC TCD response factors and  $A$  is the GC TCD peak area. The indices  $N_2$  and  $i$  denote nitrogen and components detected in the TCD, respectively.

Flow rates of the hydrocarbons with 2–4 carbon atoms detected in the FID was calculated by equation 3.24. In this equation the calculated flow rate of methane detected in the TCD was used as a reference to calculate the flow rates of components detected in the FID.

$$\dot{F}_{j,out} = \dot{F}_{CH_4,out} \cdot \frac{A_j}{A_{CH_4} \cdot n_C} \quad (3.24)$$

where  $\dot{F}_{j,out}$  is the exit flow rate of component  $j$  in  $[mol/g_{cat} \cdot h]$ ,  $\dot{F}_{CH_4,out}$  is the methane product flow  $[mol/g_{cat} \cdot h]$  calculated by equation 3.23,  $A$  is the GC FID peak area,  $n_C$  is the number of carbon atoms in the given component. The indices  $CH_4$  and  $j$  denote methane and components detected in the FID, respectively.

Amount of carbon monoxide in the synthesis feed gas converted into products,  $X_{CO}$ , was calculated by equation 3.25.

$$X_{CO} = \frac{\dot{F}_{CO,in} - \dot{F}_{CO,out}}{\dot{F}_{CO,in}} \quad (3.25)$$

where  $X_{CO}$  is the conversion of carbon monoxide,  $\dot{F}_{CO,in}$  is the CO feed flow rate  $[mol/g_{cat} \cdot h]$  calculated by equation 3.22 and  $\dot{F}_{CO,out}$  is the CO exit flow rate  $[mol/g_{cat} \cdot h]$  by equation 3.23.

The selectivity to carbon dioxide and methane was calculated by equation 3.26.

$$S_i = \frac{\dot{F}_{i,out} \cdot m_{cat} \cdot V_m^{i,g}}{\dot{V}_{CO,in} \cdot X_{CO}} \cdot 100 \quad (3.26)$$

where  $S_i$  is the selectivity in [%],  $\dot{F}_{i,out}$  is the exit flow rate of component  $i$  in  $[mol/g_{cat} \cdot h]$  calculated by equation 3.23,  $m_{cat}$  is the amount of catalyst used in  $[g]$ ,  $V_m^{i,g} = 22414 [ml/mol]$  is the molar volume of ideal gas at 273.15 K and 1 atm,  $\dot{V}_{CO,in}$  is the feed flow of CO in  $[ml/h]$ ,  $X_{CO}$  is the conversion of CO and  $i$  denotes either  $CO_2$  or  $CH_4$ .

Selectivity to hydrocarbons containing 2–4 carbon atoms were calculated by equation 3.27.

$$S_j = \frac{\dot{F}_{j,out} \cdot m_{cat} \cdot V_m^{j,g} \cdot n_C}{\dot{V}_{CO,in} \cdot X_{CO}} \cdot 100 \quad (3.27)$$

where  $S_j$  is the selectivity in [%],  $\dot{F}_{j,out}$  is the exit flow rate of component  $j$  in  $[mol/g_{cat} \cdot h]$  calculated by equation 3.24,  $m_{cat}$  is the amount of catalyst used in  $[g]$ ,  $V_m^{j,g} = 22414 [ml/mol]$  is the molar volume of ideal gas at 273.15 K and 1 atm,  $n_C$  is the number

of carbon atoms in the given component,  $\dot{V}_{CO,in}$  is the feed flow of CO in  $[ml/h]$ ,  $X_{CO}$  is the conversion of CO and  $j$  denotes hydrocarbon components with 2–4 carbon atoms.

Selectivities to hydrocarbons containing more than four carbon atoms were combined and presented as the selectivity to  $C_{5+}$  hydrocarbons, this was calculated by equation 3.28.

$$\begin{aligned}
 S_{C_{5+}} = & 100 - S_{CO_2} - S_{CH_4} \\
 & - S_{ethane} - S_{ethene} \\
 & - S_{propane} - S_{propene} \\
 & - S_{n-butane} - S_{i-butane} - S_{1-butene} - S_{i-butene} \\
 & - S_{trans-2-butene} - S_{cis-2-butene}
 \end{aligned} \tag{3.28}$$

where  $S_{C_{5+}}$  is the selectivity to higher hydrocarbons,  $S_{CO_2}$  and  $S_{CH_4}$  are selectivities calculated by equation 3.26 and the rest are selectivities calculated by equation 3.27, all in [%].

The reaction rate of CO was calculated by equation 3.29.

$$-r_{CO} = \frac{\dot{V}_{CO,in} \cdot X_{CO}}{m_{cat} \cdot V_m^{i.g.}} \tag{3.29}$$

where  $-r_{CO}$  is the reaction rate of CO being consumed in  $[molCO/g_{cat} \cdot h]$ ,  $\dot{V}_{CO,in}$  is the feed flow of CO in  $[ml/h]$ ,  $X_{CO}$  is the conversion of CO,  $m_{cat}$  is the amount of catalyst used in  $[g]$  and  $V_m^{i.g.} = 22414[ml/mol]$  is the molar volume of ideal gas at 273.15 K and 1 atm.

Turnover frequency (TOF) was calculated by equation 3.30 [41].

$$TOF = \frac{-r_{CO} \cdot M_W(Co)}{D_{H_2,ads} \cdot X_{CO} \cdot 3600} \tag{3.30}$$

where  $TOF$  is the turnover frequency in  $[s^{-1}]$ ,  $-r_{CO}$  is the reaction rate of CO in  $[molCO/g_{cat} \cdot h]$ ,  $M_W(Co) = 58,933[g/mol]$  is the molecular weight of cobalt,  $D_{H_2,ads}$  is the dispersion calculated by equation 3.10 in section 3.2.3,  $X_{CO}$  is the conversion of CO and 3600 converts hours to seconds.

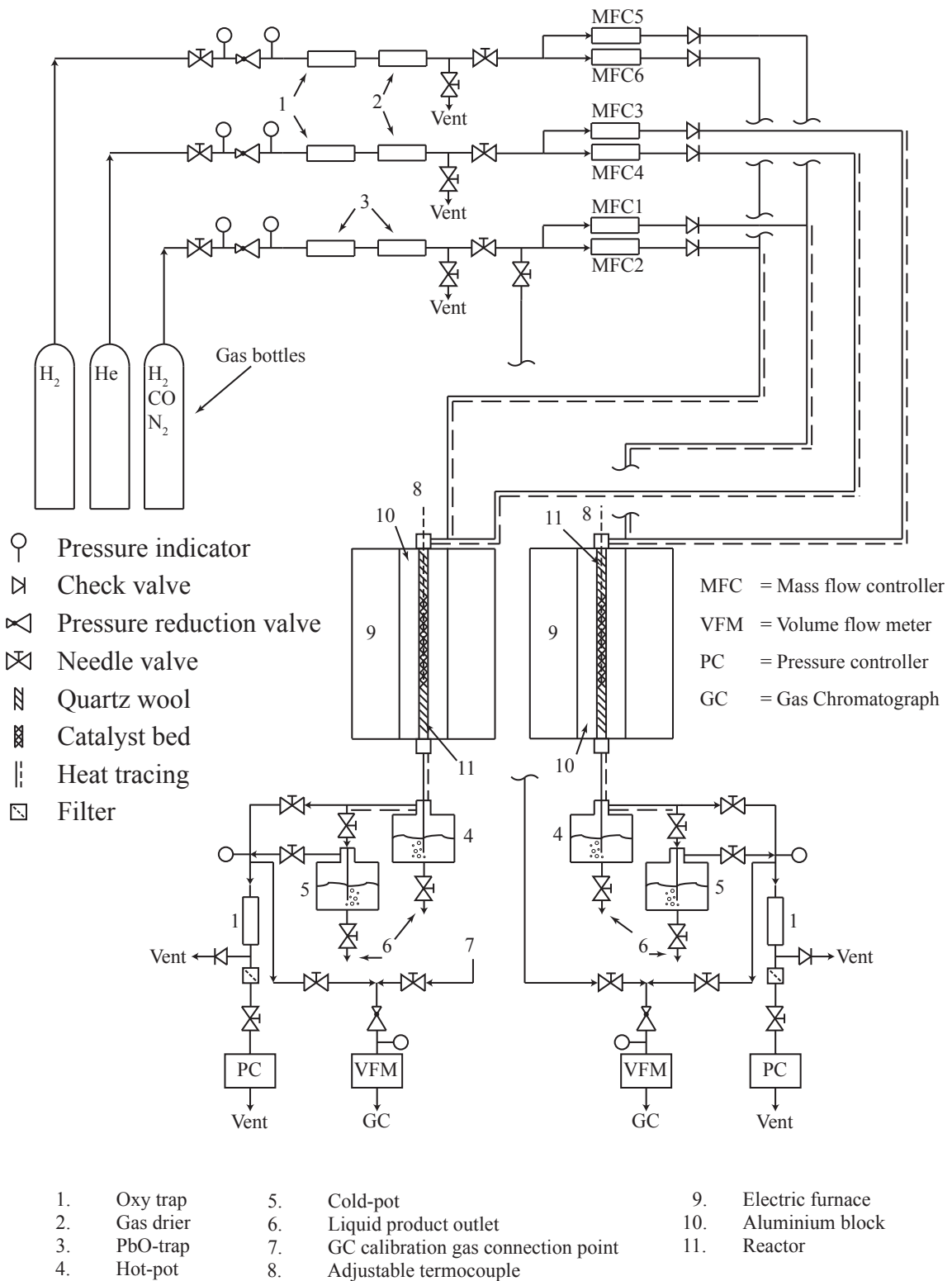


Figure 3.1: Schematic drawing of the experimental rig used in the FTS experiments.

# Chapter 4

## Results and discussion

This chapter shows the results from the experimental work done in this thesis. The observed results are also discussed here. The chapter will first show and discuss results from the characterizations, and then the same is done with the results from the Fischer-Tropsch synthesis experiments. Results that were found unfit to be presented in this chapter, can be found in appendix A.

### 4.1 Characterizations

Results from the different characterization methods are displayed and discussed in the following sections. Since it was convenient, XRD and chemisorption results are presented together. This was done to arrange for the best structure of the discussion of these results.

#### 4.1.1 Electron microscopy

TEM and STEM images collected by *John Walmsley* [86] of catalyst C1 are shown in figures 4.1 and 4.2.

Figure 4.1 shows TEM images of catalyst C1 where the areas of brighter contrast are SiC support, and the areas of darker contrast are  $\text{Co}_3\text{O}_4$ . In figure 4.1a the upper arrow points to a  $\text{Co}_3\text{O}_4$  particle, and the two lower arrows point to areas of SiC support.

STEM images are shown in figure 4.2 of catalyst C1. These images show  $\text{Co}_3\text{O}_4$  in brighter contrast and SiC in darker contrast, opposite of the TEM images. The lower arrow in figure 4.2c points to an area of SiC support, and the upper one to a  $\text{Co}_3\text{O}_4$  particle. Figure 4.2d suggests that the  $\text{Co}_3\text{O}_4$  particles have agglomerated into clusters of  $\text{Co}_3\text{O}_4$  and have a porous structure. Images of figure 4.2 showed that the  $\text{Co}_3\text{O}_4$  clusters had irregular shapes which were different from what Storsæter et al. [79] found on alumina-, silica- and titania-supported catalysts. These showed more spherical clusters of  $\text{Co}_3\text{O}_4$  on the different supports than what was seen on the SiC-supported catalysts.

Unfortunately, an instrument was unavailable when the catalyst was tested, thus an elemental composition of the sample could not be obtained. Using Energy-Dispersive X-ray



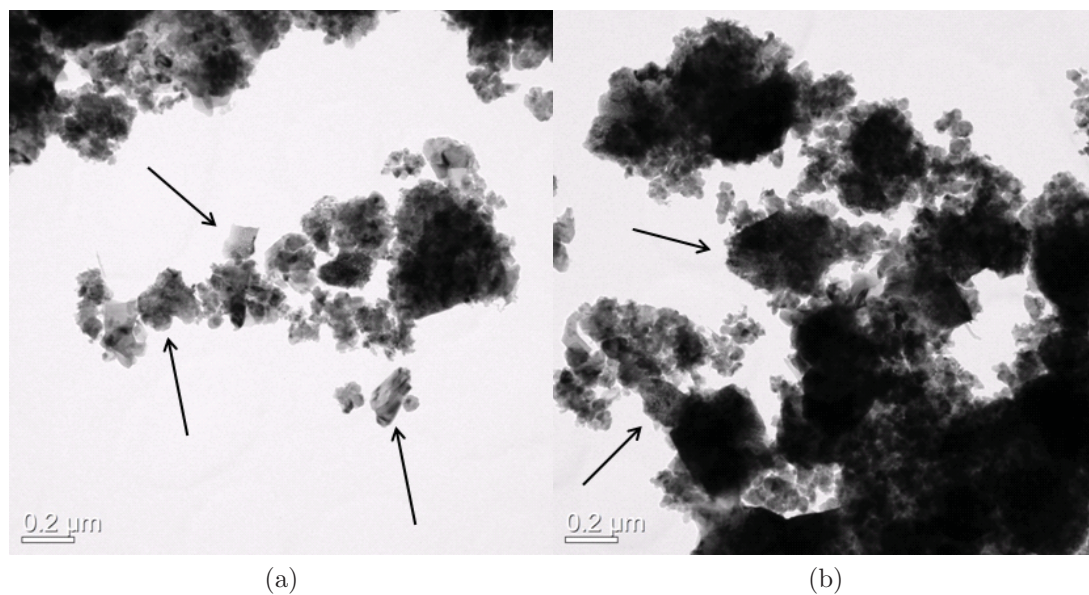


Figure 4.1: Experimental results: TEM images of catalyst C1.

Spectroscopy (EDS), a map of the elements in the sample could have been made, as was done in Storsæter et al. [79]. This would have made measuring of the cobalt particle sizes easier and more reliable.



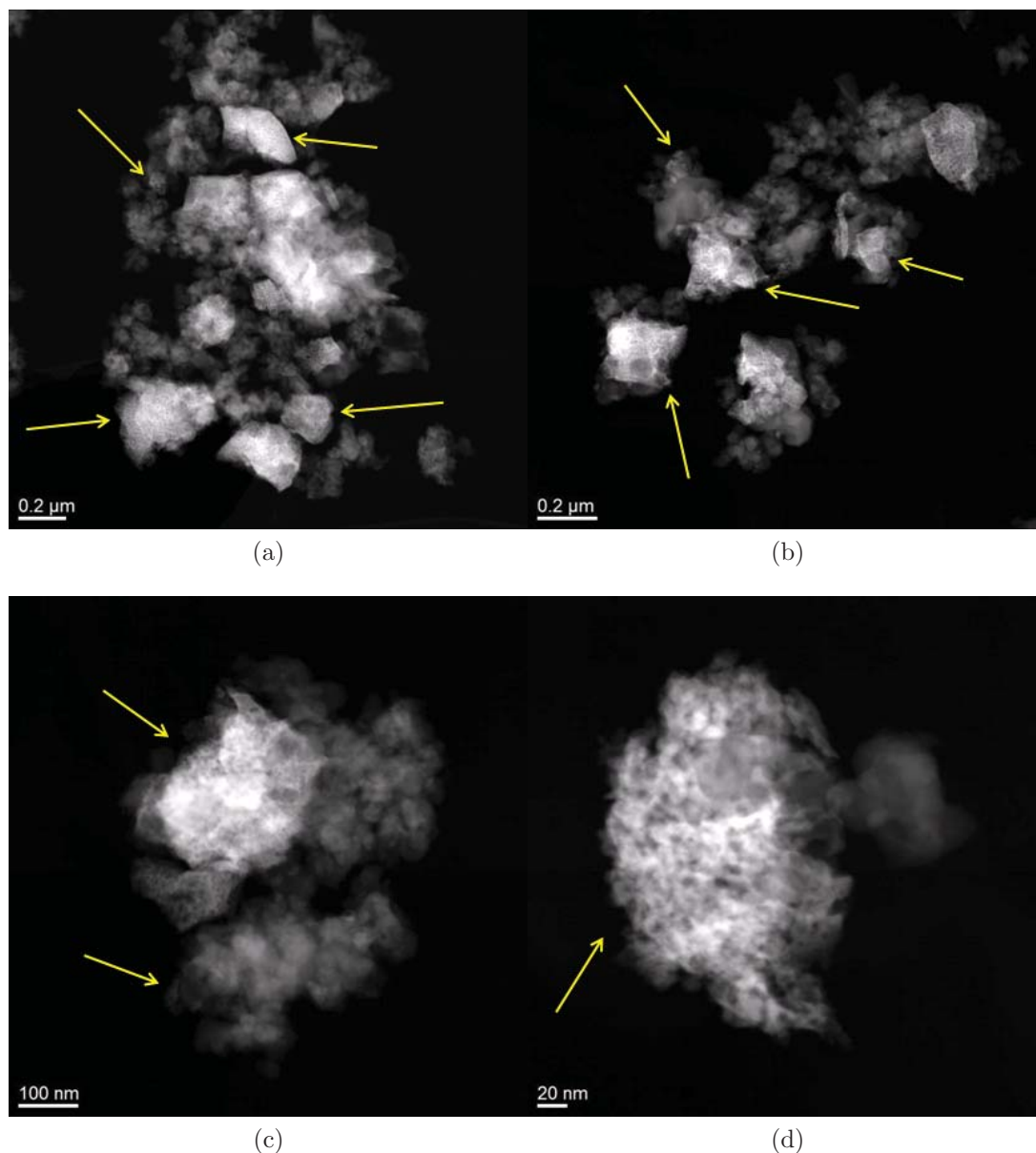


Figure 4.2: Experimental results: STEM images of catalyst C1.

#### 4.1.2 Volumetric adsorption

Volumetric adsorption was done on all support and catalyst samples, both to confirm data provided by SICAT (appendix D), and to obtain exact values for each support/catalyst. Results are given in table 4.1 and in appendix A.

Compared to that declared by SICAT (table 3.1 section 3.1.1), the results from BET measurements of the support samples S1–S7 yielded approximately the same values. The experimental uncertainty in the measurements was rather large though, with respect to the surface areas. This might explain why there was a significant difference between the surface area of support samples and corresponding catalyst samples, but there was no consistent trend in the difference. Some support-catalyst pairs showed an increase in

Table 4.1: Experimental results: Volumetric adsorption.

Sample	Surface area <sup>a,d</sup> (m <sup>2</sup> /g)	Pore volume <sup>b</sup> (cm <sup>3</sup> /g)	Pore diameter <sup>c</sup> (nm)
S1	26	0.13	19.0
C1	27	0.11	14.2
S2	34	0.15	16.1
C2	31	0.11	12.8
S3	24	0.12	18.9
C3	24	0.09	13.4
S4	112	0.09	5.1
C4	34	0.12	14.9
S5	29	0.14	17.9
C5	29	0.11	13.5
S6	28	0.14	18.6
C6	32	0.11	12.2
S7	29	0.15	18.2
C7	32	0.11	12.7
R2 <sup>e</sup>	174	0.71	12.0

<sup>a</sup> BET isotherm.

<sup>b</sup> BJH desorption cumulative volume of pores between 1.7 and 300 nm diameter.

<sup>c</sup> BJH desorption average pore diameter.

<sup>d</sup> Uncertainty ( $\pm 2\sigma$ ) calculated from three catalyst C2 samples:  $\pm 2$  m<sup>2</sup>/g.

<sup>e</sup> Data collected from Balonek et al. [5].

surface area after impregnation of Co, some showed a decrease and some showed almost no difference.

The S4/C4 pair was an exception with a large decrease of two thirds of the surface area after impregnation of cobalt. The experimental error was possibly introduced with the procedure for weighing of samples. Since the samples had to be weighed before and after degassing to determine the amount of water removed, and thus the true sample weight. As the sample containers were made of glass, they were very easily statically charged. This had an influence on the scale, making it unstable. It constantly drifted and would not settle at a fixed number. Even though the scale drifted within 0.5-1.0 mg, such a deviation could have a significant impact on the results of the experiments when subtracting the amount of water removed during degassing.

### Pore volume measurements

Results from pore volume measurements (table 4.1) yielded different values from what was declared by SICAT (section 3.1.1, table 3.1). The results showed lower pore volumes than what was declared by SICAT, and also the trend of increasing pore volumes of S1–S3 was not seen in the results. Pore volumes and pore diameters were of fairly equal values for all

supports and catalysts with the exception of the S4/C4 pair. The trend was a decrease of pore volume and pore diameter after cobalt was loaded onto the supports. Which was expected, since more matter was introduced to the pores of the support samples, taking up free space and making the pores narrower.

A possible explanation of the differing pore volume values was thought to be the shape of the support samples when analyzed. The values reported in table 4.1 was obtained from analyzing support- and catalyst samples of 53–90  $\mu\text{m}$  grains sizes. As mentioned in the experimental chapter (section 3.1.3), SICAT shipped the support samples in pellet shapes. The pellet shaped samples of S1, S2 and S3 were analyzed to investigate this possibility. However, only a small increase in pore volume was found, see appendix A.3.

Another possible explanation could be the fact that two different experimental techniques were used for the measurements; results in table 4.1 were obtained by volumetric adsorption of  $\text{N}_2$ , while results from SICAT were obtained by mercury intrusion porosimetry. Nitrogen adsorption have been known to give differing results compared to mercury intrusion on low surface area materials. Borg et al. [15] used mercury intrusion to detect macropores in some of the catalysts in the study. However, the difference between the results of mercury intrusion and  $\text{N}_2$  adsorption in [15] was much smaller than the discussed difference in this work.

According to literature [58, 67], in the mesoporous range of the pores in the analyzed samples, both techniques should give equally good results. Nevertheless, the results from the volumetric adsorption could be used for comparison between the prepared SiC-supported catalysts.

### Loss of surface area in the S4/C4 system

As mentioned above, there was a great loss of surface area when support S4 was impregnated and calcined to become C4 (table 4.1). The surface area was decreased from 112  $\text{m}^2/\text{g}$  in S4, to 34  $\text{m}^2/\text{g}$  in C4. There was also an increase in both pore volume and pore diameter. This suggested that the structure of the pore system was changed in C4, compared to S4.

Figure 4.3 shows that the BET isotherms were different for the support and the catalyst samples. The support sample (figure 4.3a) showed a typical type II adsorption isotherm, and the catalyst sample (figure 4.3b) showed a typical type III adsorption isotherm. Typical for materials showing these isotherms are multilayer adsorption on the surface, and the ratio of macropores in the materials are low [9].

The first inclining part of the isotherm in figure 4.3a represents the formation of a submonolayer, the part where the isotherm slowed its incline represents formation of monolayer and multilayer, and last inclining part represents formation of multilayer. Since there is no completely horizontal part of this isotherm there was most likely not formed a uniform monolayer before the formation of multilayer started. Instead, it suggested that the multilayer formation started before the first monolayer was completed. The isotherm in figure 4.3b showed little or no formation of submonolayer, and formation of multilayer right from the start. Suggesting that the micropores of S4 were lost during the preparation of C4.

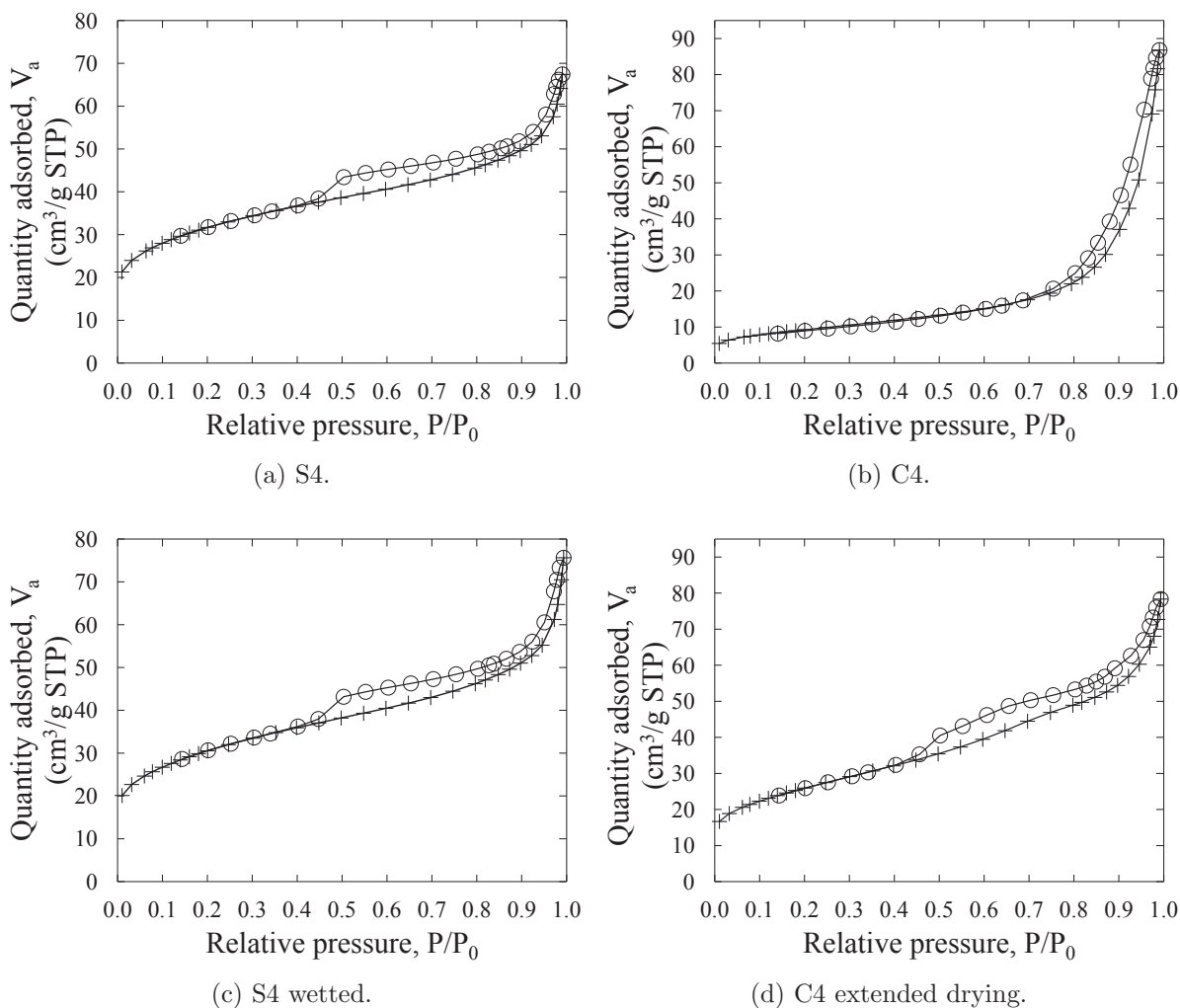


Figure 4.3: BET adsorption and desorption isotherms of S4 and C4.

Table 4.2: Experimental results: BET surface area of differently pretreated support S4.

Sample	Surface area <sup>a</sup> (m <sup>2</sup> /g)	Comment
S4	112	Untreated.
S4	113	Only calcined.
S4	108	Wetted with water (IWP), dried for two hours at 383 K, and calcined.
C4	93	Impregnated with cobalt (IWI), dried for 24 hours at 383 K, then 24 hours at room temperature, and calcined.

<sup>a</sup> BET isotherm.

Table 4.2 shows surface areas of three S4 samples and one C4 sample after different treatments prior to the analysis. This was done to investigate the cause of the lowered surface area and increased pore volumes observed for catalyst C4. BET isotherms of wetted S4 and long dried C4 are shown in figure 4.3c,d, respectively. The results showed

that running the normal synthesizing steps, but without cobalt loading, did not yield a significant loss in surface area (or pore volume and pore diameter, not shown).

When the prolonged drying period was used, the catalyst maintained the surface area to a much greater extent than when the two hour drying was used. Thus, it would be beneficial to extend the drying period for high surface area (HSA)  $\text{TiO}_2\text{-SiC}$  catalysts in the future. However, it should be mentioned that the preparation method used in this work, was used in previous works on HSA catalysts [15, 78]. Borg et al. [15] used the same method as this work, except for a drying period of three hours, and had an average loss of only 22 % surface area.

### 4.1.3 Temperature programmed reduction

Temperature programmed reduction (TPR) was done on all SiC-supported catalysts, C1–C7. One  $\text{Co}/\text{Al}_2\text{O}_3$ -supported catalyst, R1, provided by prof. Anders Holmen [42]. And, one  $\text{CoRe}/\text{Al}_2\text{O}_3$ -supported catalyst, R2, provided by Andreas Lillebø [53] (see table 3.2 section 3.1.2).

A 7 %  $\text{H}_2/\text{Ar}$  flow was used, and the temperature was ramped from ambient to around 1150 K at 10 K/min. Results from the TPR experiments are given in table 4.3 and figures 4.4 and 4.5.

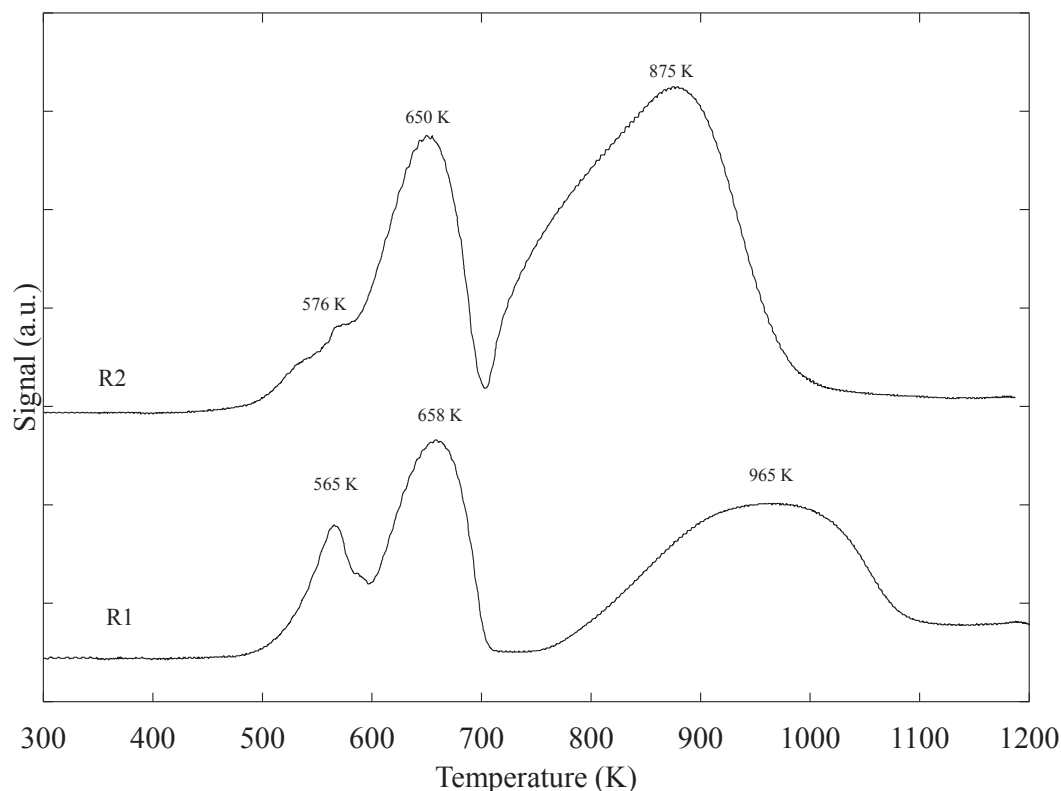


Figure 4.4: TPR curves of catalysts R1 and R2.

To ensure that TPR results from this project could be compared with earlier experimental work done at the same apparatus, the  $\text{Co}/\text{Al}_2\text{O}_3$  catalyst (R1) was run. Figure 4.4 shows

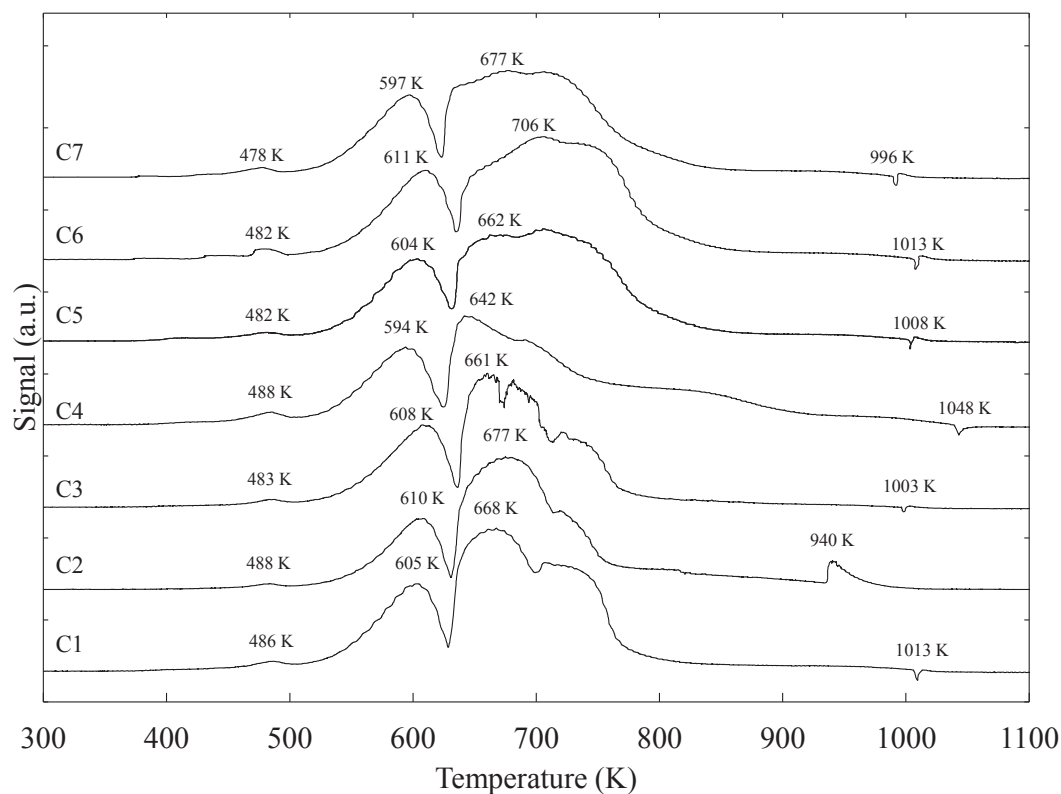


Figure 4.5: TPR curves of catalysts C1-C7.

three distinctive peaks at about 565 K, 659 K and 968 K, respectively. The first peak can be attributed to residual nitrates from the catalyst preparation, while the other two can be attributed to the reduction of cobalt. The results showed that cobalt oxide on alumina support was completely reduced at a high temperature, i.e. 968 K. These results are well in accordance with earlier experiments [15, 78] using the same apparatus. Thus, it was reasonable to compare results from this work with previous findings.

TPR was done on the CoRe/Al<sub>2</sub>O<sub>3</sub>-catalyst to see the promoting effects of rhenium. Results in figure 4.4 show three peaks for R2 at 576 K, 650 K and 875 K, respectively. The first two peaks are in accordance with the corresponding peaks in TPR of R1. Peak number three, however, is shifted to the left in figure 4.4 indicating complete reduction of cobalt oxide at a lower temperature with the promotion of rhenium.

Results from TPR of the SiC-supported catalyst (figure 4.5), were very similar to each other. The Co peaks of catalyst C4 showed a little lower temperatures than the rest of the SiC-supported catalysts. Catalysts C5–C7 showed a higher temperature for the second Co peak compared to catalysts C1–C3. All seven catalysts showed a nitrate peak between 478–488 K.

In contrast to the reduction of cobalt on the Al<sub>2</sub>O<sub>3</sub> support which was completed at a high temperature, the reduction of cobalt on SiC support was completed at a significantly lower temperature. Results of C1-C7 were in accordance with the findings of Lacroix et. al. [50], and C4 showed accordance with the findings of Storsæter et. al. [78] on Co/TiO<sub>2</sub>-catalysts. The lowered reduction temperatures were presumably due to a lower degree of

Table 4.3: Experimental results: Temperature programmed reduction.

Catalyst	NO <sub>3</sub> peak [K]	Co peak 1 [K]	Co peak 2 [K]	$\Delta T$ Co-peaks
C1	488	605	668	63
C2	483	610	677	67
C3	488	608	661	53
C4	486	594	642	48
C5	482	604	705	101
C6	482	611	706	95
C7	478	597	677	80
R1	565	658	965	280
R2	576	650	875	225

interaction between Co<sub>3</sub>O<sub>4</sub> and SiC-support compared to Al<sub>2</sub>O<sub>3</sub>-support, also reported by Moene et. al. [57]. The tailing peak in C4 was likely due to reduction of surface species for which there exists a range of degrees of interaction between cobalt oxide and the TiO<sub>2</sub> part of the support [45, 78].

The increased temperature of the second peak of catalysts C5–C7, might suggest that these catalysts had stronger MSI between the Co<sub>3</sub>O<sub>4</sub> and the SiC support. There were similarities to the difference between un-promoted and promoted Al<sub>2</sub>O<sub>3</sub>-supported catalysts. Indicating that catalysts C1–C4 might have contained a promoting material, which possibly was not present in C5–C7. The fact that catalysts C5–C7 were prepared on supposedly purer support samples supports this.

Dispersion of Co was increased on catalysts C5–C7, however there were not found any literature that suggested such a correlation. Another explanation might be experimental error. The characterizations of C1–C4 were done six months apart from C5–C7. However, since the nitrate and first cobalt peaks showed little change, experimental error seemed less likely.

The last peak, or possibly disturbance, for each catalyst was hard to explain why appeared. Lacroix et al. [50] suggests formation of CH<sub>4</sub>, via the reaction  $\text{Co} + 2\text{SiC} + \text{H}_2 \rightarrow \text{CoSi}_2 + 2\text{CH}_4$ , to cause a peak in their study which is similar to the one at 940 K for C2. The suggestion fits very well for the peak in C2, however, since there were no such peak at the same temperature for any of the other catalysts, it will only stand as a possible explanation. It was not found any literature proposing explanations for the peaks in the other three catalysts.

Yet, the temperature of about 1000 K where this occurred, was relatively high. A possibility would be something other than Co<sub>3</sub>O<sub>4</sub> being reduced at this point. It could be contaminants in the catalysts, or contaminants introduced during the preparation of samples for the experiments.



### 4.1.4 Chemisorption and XRD

H<sub>2</sub>-chemisorption at 313 K was done for catalysts C1–C7 to obtain the metal dispersion, and the average metal particle sizes were calculated by equation 3.14. XRD was done to find the cobalt oxide particle sizes in catalysts C1–C4, the cobalt metal particle sizes and dispersions were calculated by equations 3.15 and 3.17. Results are given in table 4.4, together with the XRD patterns in figures 4.6 and 4.7. Chemisorption isotherms can be found in appendix A.4.

Table 4.4: Characterization results: H<sub>2</sub>-chemisorption and XRD.

Catalyst	Dispersion <sup>#</sup> , $D_{H_2,ads}(Co^0)$ (%)	Particle size <sup>*</sup> , $d_{H_2,ads}(Co^0)$ (nm)	Particle size <sup>#</sup> , $d_{XRD}(Co_3O_4)$ (nm)	Particle size <sup>*</sup> , $d_{XRD}(Co^0)$ (nm)	Dispersion <sup>*</sup> , $D_{XRD}(Co^0)$ (%)
C1	2.3	43.8	23.7	17.7	5.54
C2	2.2	44.7	25.7	19.3	5.25
C3	2.3	43.5	23.8	17.8	5.54
C4	2.8	35.4	14.5	10.9	9.06
C5	3.3	30.1	-	-	-
C6	2.8	35.8	-	-	-
C7	3.3	30.2	-	-	-

<sup>#</sup> Experimental values

<sup>\*</sup> Calculated values

Chemisorption results yielded low dispersion of cobalt metal on all seven catalysts. Catalysts C1-C3 showed similar dispersions, while catalysts C4-C7 showed slightly improved dispersions compared to the first three. Related to the dispersion, the average cobalt particle sizes were relatively large.

The greater dispersions of the catalysts prepared in the second batch compared to C1–C3 of the first batch, might be explained by the air flow used during the calcinations. Due to a misunderstanding, the air flow during the calcinations of the first batch was much lower than what it should have been. This was discovered between the preparation of the first and second batches of catalysts. When the second batch catalysts were calcined, an increased flow of air was used. Since an uncalibrated rotameter was used to adjust the flow, exact flow rates used were not available.

The author of this work changed the air flow without reflecting on any consequences that could follow. Later, it was found that Borg et al. [14] reported a correlation between air flow used during calcination and Co dispersion on Al<sub>2</sub>O<sub>3</sub>-supported catalysts. The increased air flow was the only difference made in the preparation method between the first and second batch.

XRD patterns, figure 4.6 and 4.7, showed that Co<sub>3</sub>O<sub>4</sub> was the only cobalt oxide phase present in the calcined catalysts. They also showed that SiC and TiO<sub>2</sub> were the only phases present in the support materials.

Chemisorption and XRD results were not in agreement with each other and showed very different dispersions and particle sizes for the catalysts. XRD showed particle sizes less



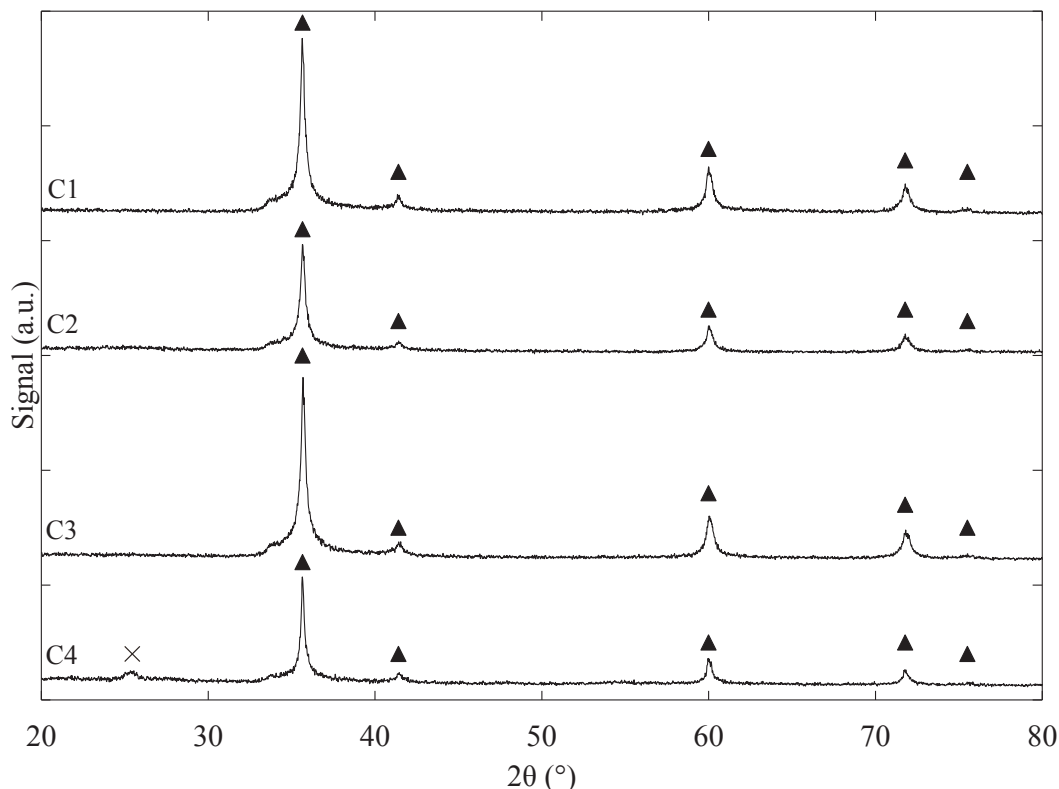


Figure 4.6: Collected XRD patterns of support materials S1-S4. ▲: SiC, and ×: TiO<sub>2</sub>.

than half of what the chemisorption showed, and the opposite regarding dispersion (table 4.4). However, the results followed the same trend for both characterization methods.

Catalysts C1–C3 showed equal dispersions and particle sizes, while C4 showed a lower average particle size and a higher dispersion in comparison. Results from XRD were in accordance with dispersions and particle sizes usually achieved by incipient wetness impregnation on other support materials [69, 78], however, these studies reported greater similarities between XRD and chemisorption results.

Studies [26, 50] on SiC-supported catalysts reported Co<sub>3</sub>O<sub>4</sub> particle sizes in the same range as was found from chemisorption in this work. Thus, XRD results from this work was not in accordance with the literature on the given support material.

The observed trend of smaller cobalt particle sizes on catalyst C4 could have been explained by the difference in pore diameter. Studies on different cobalt supported catalysts [78, 15, 47] showed that cobalt oxide particle size increased with increasing support pore size. Yet, as it was evident from the volumetric adsorption results (table 4.1), this catalyst seemed to have lost its microporous structure during the preparation. Which limited the validity of this explanation.

The addition of TiO<sub>2</sub> in the support of C4 might be an explanation to the increased Co dispersion. Depending on which phases the Co<sub>3</sub>O<sub>4</sub> was in contact with, the TiO<sub>2</sub> could have introduced stronger MSI to the catalyst. This could have resulted in a greater dispersion.

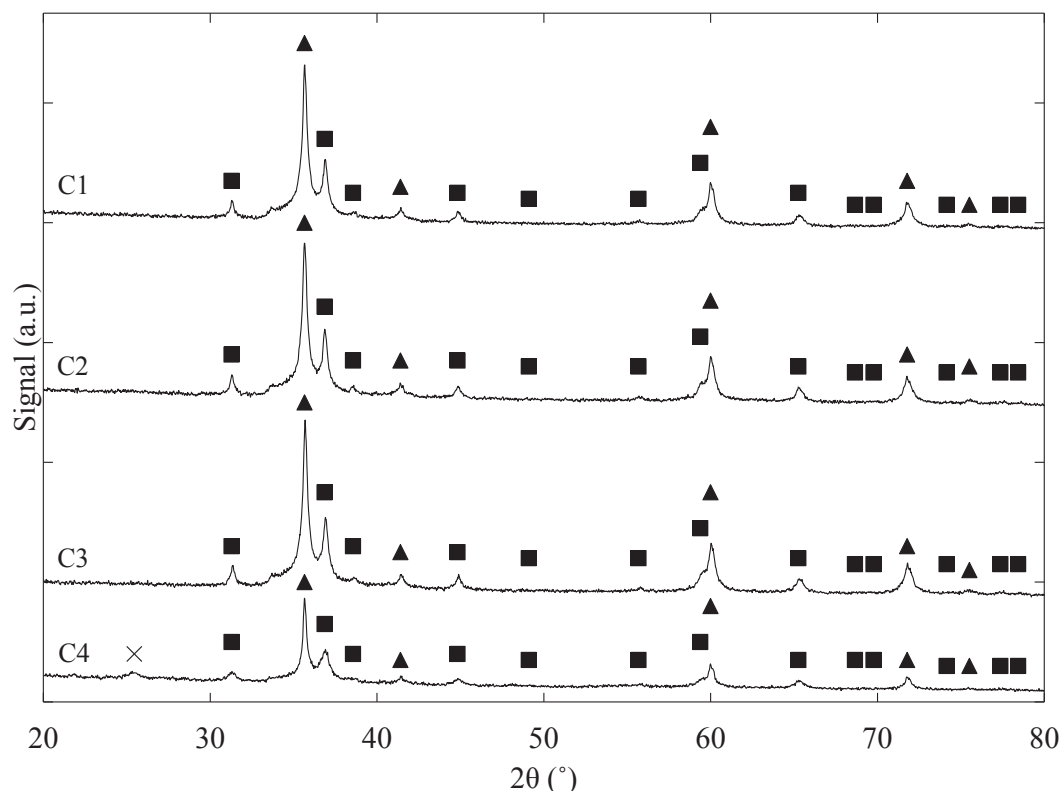


Figure 4.7: Collected XRD patterns of catalysts C1-C4. ▲: SiC, ■:  $\text{Co}_3\text{O}_4$  and ×:  $\text{TiO}_2$ .

XRD was done on the calcined catalysts in their oxidized states, while  $\text{H}_2$ -chemisorption was done in their reduced states. Since XRD and chemisorption usually yield dispersion and particle size measurements in better agreement with each other [13, 77], than what was found in this work. A change in cobalt dispersion during the reduction step of the chemisorption might explain the observed results.

TPR results in tables 4.5 and 4.4 indicated weaker MSI in the Co/SiC catalysts than in the Co/ $\text{Al}_2\text{O}_3$  catalyst. On weakly interacting supports, poorly dispersed cobalt oxide intermediates and correspondingly large cobalt metal crystallites are formed according to Soled et al. [74]. If agglomeration of the cobalt oxide intermediates happened during the reduction step of the  $\text{H}_2$ -chemisorption, it could possibly explain the difference between the observed XRD and chemisorption results.

An earlier study by Storsæter et al. [78], showed results on Co/ $\text{SiO}_2$  catalysts that were contradicting to this hypothesis. The catalysts were prepared very similarly, and calcined at the same temperature as the Co/SiC catalysts in this work. TPR results of the Co/ $\text{SiO}_2$  catalysts showed two reduction peaks for cobalt oxide at 615 K and 685 K, respectively, indicating an even lower MSI than what was found for the Co/SiC catalysts. In the study of Storsæter et al. [78], the XRD and chemisorption results were in good accordance with each other. Thus indicating no change in the cobalt oxide dispersion during the reduction prior to  $\text{H}_2$ -chemisorption, which is also supported by Iglesia [44].

Poor experimental data from the chemisorption runs could have explained the low dispersion. However, the collected isotherms (presented in appendix A) were relatively linear in

the points that were used for calculation, and were all very similar to each other. Further investigation is needed to make a conclusion on this.

Bjørn Christian Enger [31] suggested to do a reduction/oxidation cycle and then collect XRD patterns on the samples, to compare with the results in table 4.4. If the proposed hypothesis were to be pointing in a correct direction, literature [57] suggest calcination at higher temperatures to induce stronger MSI, which may hinder agglomeration of cobalt oxide intermediates.

Since H<sub>2</sub>-chemisorption results were in accordance with the literature and these were the results used in the calculation of FTS results, catalysts C5–C7 were not analyzed in XRD. It was not believed that XRD results on these catalysts would reveal any new, useful information. Especially, since the issue of the differing results between XRD and chemisorption was not resolved.

## 4.2 Fischer-Tropsch synthesis

Fischer-Tropsch synthesis was performed with catalysts C1–C7 and R2 at 483 K, 20 bar and H<sub>2</sub>/CO = 2.1 to obtain activity and selectivity results of the SiC-supported catalysts and the reference catalyst. Results after 24 hours on stream are presented in table 4.5.

Table 4.5: Fischer-Tropsch synthesis results for catalysts C1–C7 and R2 after 24 hours on stream. D<sub>H<sub>2</sub>,ads</sub>, X<sub>CO</sub>, S<sub>C<sub>5+</sub></sub>, S<sub>C<sub>2</sub>–C<sub>4</sub></sub>, S<sub>CH<sub>4</sub></sub>, S<sub>CO<sub>2</sub></sub> and TOF denotes cobalt dispersion from H<sub>2</sub>-chemisorption, CO conversion, C<sub>5+</sub> selectivity, C<sub>2</sub>–C<sub>4</sub> selectivity, methane selectivity, CO<sub>2</sub> selectivity and turnover frequency, respectively.

Catalyst	D <sub>H<sub>2</sub>,ads</sub> (%)	X <sub>CO</sub> (%)	S <sub>C<sub>5+</sub></sub> (%)	S <sub>C<sub>2</sub>–C<sub>4</sub></sub> (%)	S <sub>CH<sub>4</sub></sub> (%)	S <sub>CO<sub>2</sub></sub> (%)	TOF <sup>a</sup> (s <sup>-1</sup> )
C1	2.3	7.43	74.6	11.5	12.3	1.2	0.026
C2	2.2	9.09	74.2	11.4	13.5	1.0	0.032
C3	2.3	7.00	74.5	11.2	13.4	0.9	0.024
C4	2.8	11.09	76.9	9.4	13.1	0.6	0.031
C5	3.3	15.14	78.8	9.4	11.7	0.8	0.036
C6	2.8	5.30	68.8	11.8	16.8	1.1	0.015
C7	3.3	9.33	81.2	8.3	10.4	0.4	0.022
R2	7.8	7.14	72.0	12.8	14.0	1.3	0.045

<sup>a</sup> Based on H<sub>2</sub>-chemisorption data.

Figure 4.8 shows the initial conversion levels of all catalysts run in the FTS rig. For each experiment on the SiC-supported catalysts, a loading of 2 g and a feed flow of 150 NmL/min was used with the intent to reach an initial Co conversion of 25%. This was empirically calculated from previous results on the reference catalyst R2, expecting that the SiC-supported catalysts would have a similar activity and compensating for the difference in cobalt dispersion and loading.

However, as shown in table 4.5 and figure 4.8, none of the SiC-supported catalysts reached

the intended 25% initial CO conversion. There was also a greater difference in the activity between the SiC-supported catalysts than expected. Because of this, catalyst R2 was run with a low amount of catalyst and reduced feed flow (0.2 g and 150 NmL/min) to obtain low conversion results that could be compared with the results from the SiC-supported catalysts.

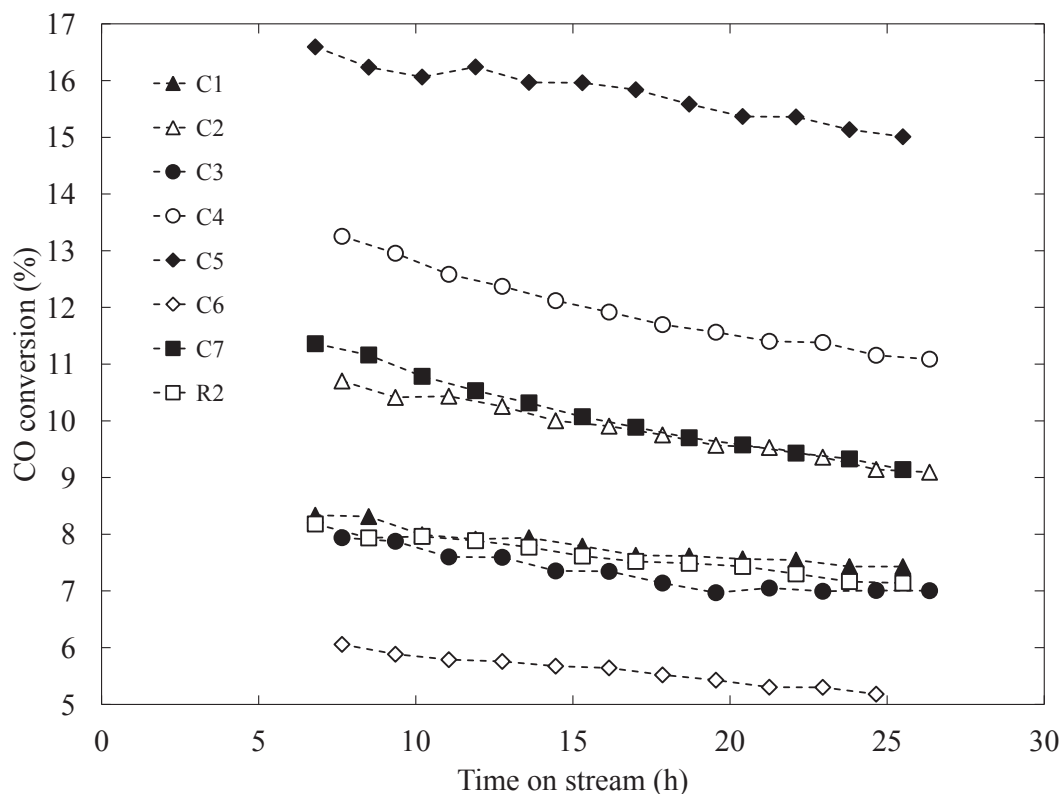


Figure 4.8: CO conversion as a function of time on stream for catalysts C1–C7 and R2 at 483 K, 20 bar and  $H_2/CO = 2.1$ .

### 4.2.1 First batch

Catalysts C1–C4 were prepared from the first batch of support samples obtained from SICAT. Results showed low TOF values for these catalysts compared to the reference catalyst R2. This was not in line with what was found in the literature (section 2.7.3), which said that TOF should be independent of support material and dispersion of Co. The CO conversion, on the other hand, was found to affect both the TOF and the  $C_{5+}$  selectivity. This should be kept in mind when viewing the results.

C1, C3 and R2 all had an initial CO conversion of approximately 7%. As mentioned, low TOF values were observed for C1 and C3, in fact 40% lower than that observed for R2. Yet, C1 and C3 showed a significantly higher  $C_{5+}$  selectivity than R2 (table 4.5). Correspondingly, the other reported selectivities were lower for the SiC-supported catalysts compared to R2.

C2 and C4 showed a little higher TOF values than C1 and C3, yet 30% lower than R2.

Table 4.5 shows that, in line with the increased TOF, C2 and C4 had higher initial CO conversions. The higher CO conversion of C4 compared to C2 was likely caused by the difference in Co dispersion on the catalysts.  $C_{5+}$  selectivity was also higher for C4 than C2, which might be explained by the difference in CO conversion, as previous studies suggested [15, 39, 43]. However, the results of C2 compared with C1 and C3 was not in line with this explanation. All three catalysts showed the same  $C_{5+}$  selectivity, even though C2 showed a significant higher CO conversion than the other two.

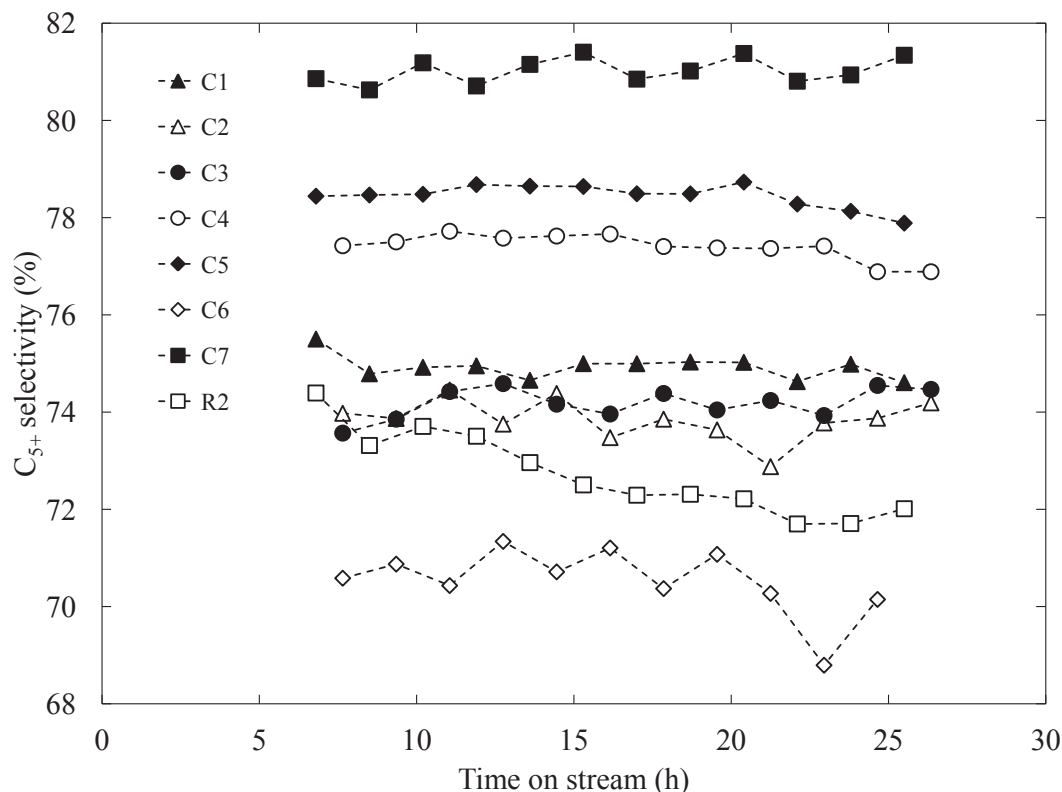


Figure 4.9:  $C_{5+}$  selectivity as a function of time on stream for catalysts C1–C7 and R2 at 483 K, 20 bar and  $H_2/CO = 2.1$ .

Figure 4.9 presents the  $C_{5+}$  selectivity as a function of time on stream. It shows that the  $C_{5+}$  selectivity for the SiC-supported catalysts was very stable throughout the experiments. The reference catalyst on the other hand showed a significant decay in  $C_{5+}$  selectivity, from  $\sim 74\%$  after 7 hours, to  $\sim 72\%$  after 24 hours on stream. Figure 4.8 shows that there was a similar decay for both the SiC-supported catalysts and the reference catalyst, with respect to CO conversion. According to literature [15, 39, 43], as mentioned above, the case of R2 was what would be expected.

Borg et al. [15] observed the same trend of stable  $C_{5+}$  selectivity with decreasing activity, as was observed for the SiC-supported catalyst. It was proposed that both sintering and oxidation led to increased particle sizes of Co. This was observed by Borg et al. [15] to lead to an increase in  $C_{5+}$  selectivity. It was therefore believed, that the combined effects of decreasing CO conversion and increasing average Co particle size, caused the stability in  $C_{5+}$  selectivity for the SiC-supported catalysts in this work.

In the case of R2, the deactivation might have been caused by oxidation of small cobalt

oxide particles as suggested in the literature [40, 71], see section 2.7.4. Due to the stronger interactions between cobalt species and  $\text{Al}_2\text{O}_3$ -support, sintering of small cobalt particles into larger particles might not have occurred on R2. Instead, cobalt might have reacted with the alumina surface, making it inaccessible to the reactions. Thus, explaining the decay in  $\text{C}_{5+}$  selectivity of R2.

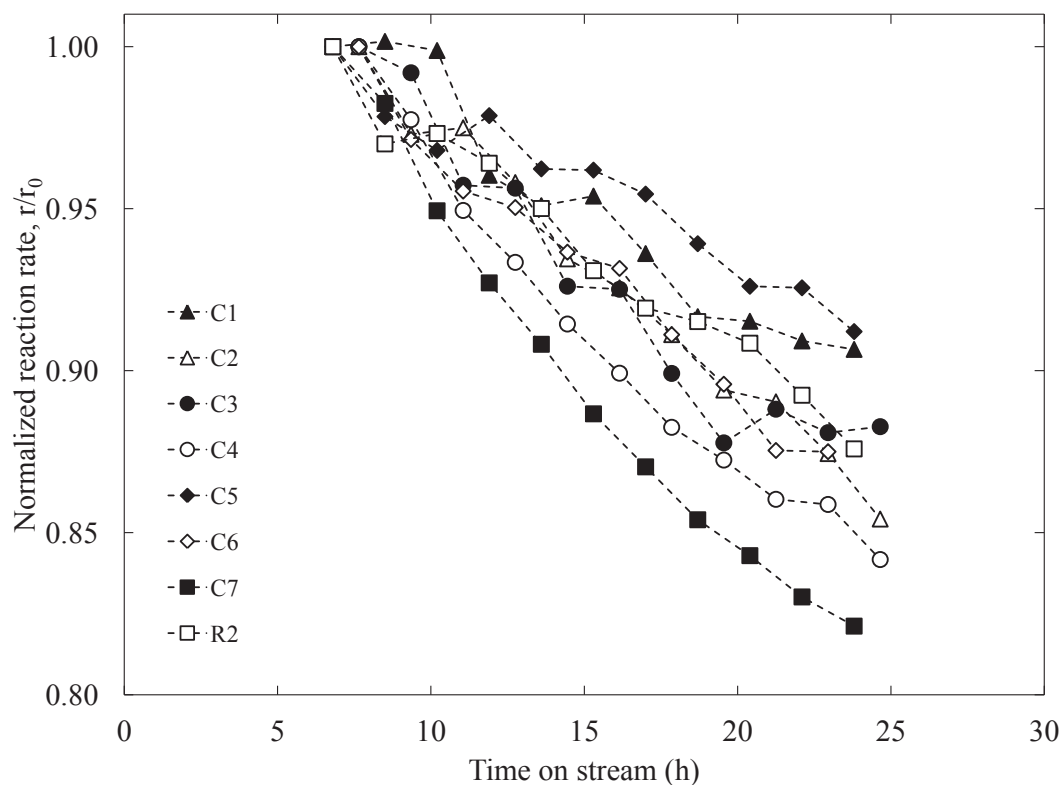


Figure 4.10: Normalized reaction rate plotted against time on stream for C1–C7 and R2 at 483 K, 20 bar and  $\text{H}_2/\text{CO} = 2.1$ .

Figure 4.10 shows the deactivation of the catalysts as normalized reaction rates plotted against time on stream. The figure showed no obvious trends in the deactivation with regards to support material. Neither was there a trend with regards to the stability of  $\text{C}_{5+}$  selectivity, which was discussed above. Nevertheless, the mechanism responsible for the lower TOF did not seem to have affected the rate of deactivation on the SiC-supported catalysts.

A possible explanation of the observed trends for the SiC-supported catalysts, might be found in the studies of Balonek et al. [5] and Borg et al. [17]. The studies found that alkali and alkaline earth metals decreased catalyst activity significantly. It was also found that sodium increased, and potassium decreased the  $\text{C}_{5+}$  selectivity. Comparing the results from the SiC-supported catalysts in this work with the results of [5, 17], the observed decrease in TOF roughly corresponded to either 1000 ppm Na, or 1000 ppm Ca loading in the catalysts.

With respect to catalyst activity and  $\text{C}_{5+}$  selectivity, contaminated SiC-supported catalysts could explain the observed results. Both, the differences between C1, C3 and R2,

and the similar  $C_{5+}$  selectivities of C1–C3. The latter case suggesting that C2 contains less alkali than C1 and C3. And, that the effect of increased CO conversion on  $C_{5+}$  selectivity for C2, was masked by the opposite effect of less alkali content.

This explanation was supported on the elemental analysis of catalyst C1, appendix A, and the impurity content declaration from SICAT, appendix D. Both stating, that alkali and alkaline earth metals were present in the support samples. Nevertheless, results from a SiC-supported catalyst, completely free of alkali and alkaline earth metals, would be needed to fully connect the results of this thesis with the literature. Until such results were to be obtained, effects from the support material itself, SiC, would remain a possibility.

It should also be mentioned that, in addition to alkali and alkaline earth metals, sulfur and phosphorus were possibly present in the support samples. These were found to reduce catalytic activity of Co by permanently adsorbing onto, and thus blocking active sites [17, 30]. Some of the activity loss might have been caused by S- and P effects, however, their poisoning effects would not explain the increased  $C_{5+}$  selectivity.

$N_2$  adsorption results showed that all SiC-supported catalysts, had roughly the same surface areas, average pore volumes, and average pore diameters, table 4.1. The reference  $Al_2O_3$ -supported catalyst had a greater surface area and a little lower pore volume, but similar pore diameter. Thus, the increased  $C_{5+}$  selectivities of C1 and C3 compared to R2 would most likely not be attributed to differing pore diameters, which Borg et al. [15] found to be a possibility.

The presented results were most likely affected by experimental errors, which might have been misleading when interpreting the results. None of the catalysts were run more than once in the FTS rig, thus, not allowing for any experimental error to be confirmed. Borg et al. [15] found that the TOF varied between  $62\text{--}73 \cdot 10^{-3} \text{ s}^{-1}$  for four catalysts with approximately equal Na loading. All SiC-supported catalysts except for C5 and C6, would fit inside such a span. Thus, making the observed differences between these catalysts merely experimental error.

## 4.2.2 Second batch

The second batch of catalysts (C5–C7), although treated to, or synthesized to contain fewer impurities, did not reach the intended 25% CO conversion when run in the FTS rig. Table 4.5 shows that there was a greater spread in TOFs between these catalysts, compared to the first batch. Nevertheless, all catalysts from the second batch showed lower TOF than R2, suggesting that the attempted purification measures were unsuccessful.

Catalyst C5 was made from the acid washed support material, and showed activity results closet to the reference catalyst. Indicating that this was the most successful of the attempted purification methods, yet, it had not been completely successful. A proposed explanation to this result, might be a slight difference in the preparation of this catalyst.

Contrary to the other support samples, which were shipped in pellet shapes from SICAT, the support material of C5 was shipped as grains ( $<500 \mu\text{m}$ ). The entire sample was sifted to extract the fraction of  $53\text{--}90 \mu\text{m}$  grains, which yielded about half the amount of



material needed. Then, the remaining half was obtained from the normal crushing and sifting method.

It was suspected that crushing of the support samples freed more impurities otherwise trapped in the material structure, and made them available on the surface. The new surface area that was due to the crushing had not been subjected to the washing with acid. Thus, it was likely to assume that in reality, only about 50% of the support material that C5 was prepared on, was acid washed. Suggesting that acid washing was an effective measure against the impurities, but the full effect of it was not seen in the results.

Rather surprisingly, the least active catalyst, C6, was prepared on the supposedly purest support material. This support material was synthesized from pure starting materials and without additives that SICAT suspected would introduce impurities. The results either showed that SiC-supported catalysts have lower TOF than catalysts on other supports, or that this attempt of purification had failed. The former was not a likely explanation, since this would mean that the other SiC-supported catalysts were promoted to have increased TOFs.

Although it might seem odd, that the catalyst prepared from the purest support material showed the lowest activity, this was what the results showed. Theoretically calculated amounts of impurities are shown in appendix D. However, an elemental analysis of the support, or preferably the catalyst, would be needed to conclude on this catalyst. The results showed, in accordance with the low activity, a low CO conversion and low a C<sub>5+</sub> selectivity.

SICAT did not state which measures for improvement of the impurity was done for catalyst C7. However, it was described as an "intermediate grade" material. C7 showed a similar TOF as C3, but due to the higher Co dispersion on C7, it showed a higher CO conversion. This catalyst also showed the highest C<sub>5+</sub> selectivity of the SiC-supported catalysts. The C<sub>5+</sub> selectivity on C7 was greatly increased compared to that on C2, both at approximately 9% conversion.

The observed difference in C<sub>5+</sub> selectivity between C2 and C7, was much greater than the maximum increase Balonek et al. [5] found in their study, see figure 2.8 section 2.7.5. The figure shows that the selectivity increased from approximately 81% to 83% with 200 ppm Na loading, however it was not increased more with further increased Na loading. Nevertheless, such comparisons were not trivial to make. Too many unknown variables could possibly have contributed to the differing results of the two SiC-supported catalysts.

As mentioned previously, experimental errors might have been misleading when the results were interpreted. The explanations were still based on the assumption, that alkali and alkali earth metals were present to an extent that led to the observed results. Thus, no conclusions should be drawn as long as the presence of these metals remain unknown. Preferably, it should be both qualitatively and quantitatively confirmed.

### 4.2.3 CO conversion of 50%

Figure 4.11 shows the CO conversion and C<sub>5+</sub> selectivity plotted against time on stream. All catalysts were aimed to stabilize at 50% CO conversion, yet the results varied within



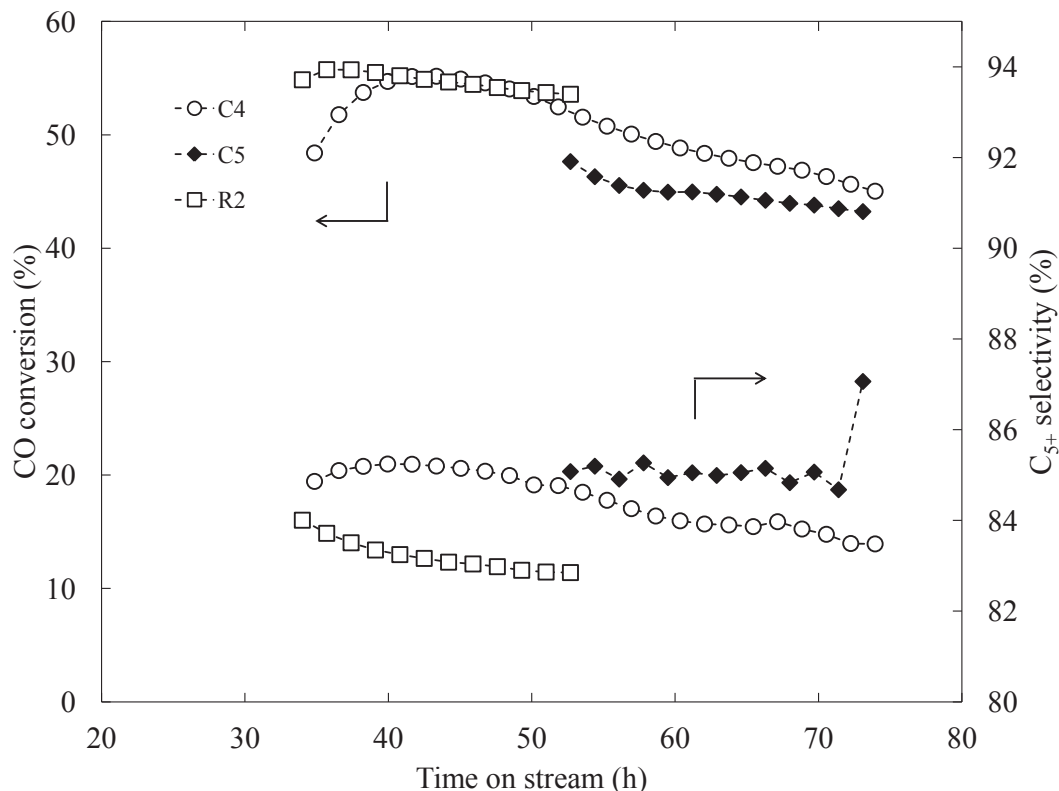


Figure 4.11: CO conversion and C<sub>5+</sub> selectivity as a function of time on stream for catalysts C4, C5 and R2 at 483 K, 20 bar and H<sub>2</sub>/CO = 2.1.

±5% of this. Adjusting of the CO conversion was not a straight forward task with the SiC-supported catalysts. Due to the lower activity, it was hard to predict how much adjustment would be needed. The 50% CO conversion results for R2 were obtained from the work of co-supervisor Andreas H. Lillebø [53].

As is visible in the figure, not all SiC-supported catalysts were tested at 50% CO conversion. This was due to the very low space velocities needed, if 50% CO conversion were to be achieved on the little active SiC catalysts. Running the FTS experiments with too low space velocity would have added experimental uncertainty to the results. It was believed that such a low feed flow would take to long time to displace the entire gas volume in the rig. This could lead to wrongful or useless results.

In accordance with the low conversion results, the SiC-supported catalysts showed higher C<sub>5+</sub> selectivity than the reference catalyst at 50% CO conversion. A good comparison was possible between 40–50 hours for C4 and R2, clearly showing higher C<sub>5+</sub> selectivity at the same conversion level. Catalyst C5, though at a significantly lower conversion, still showed higher C<sub>5+</sub> selectivity compared to R2.

C5 and R2 showed the same trends of deactivation in terms of CO conversion and C<sub>5+</sub> selectivity, as figure 4.11 shows. The same mechanisms that were discussed for the low conversion results in section 4.2.1, would also explain the high conversion results. Figures 4.8 and 4.11 does not show it clearly, due to the axis proportions, yet there was a greater deactivation of catalyst activity at high conversion. Which was in accordance

with the literature [40, 71].

Catalyst C4, on the other hand, did not show the same stability in terms of  $C_{5+}$  selectivity at high conversion compared to low conversion. Figure 4.11 shows that C4 was deactivating at a faster rate than C5 and R2, and that the  $C_{5+}$  selectivity decayed along with the conversion. This was in accordance with the low conversion results, as shown in figure 4.10. However, the mechanism causing the deactivation seemed to have been changed in a way that it no longer sustained the  $C_{5+}$  selectivity at a fixed level.

Proposing what this change involved was not easy, since little was known about the interaction between cobalt and the  $TiO_2$ -SiC structure of C4. The increased partial pressure of  $H_2O$  from the increased CO conversion, might have contributed to a more aggressive deactivation disfavoring  $C_{5+}$  selectivity. However, since the results were from only one run of the catalyst, it was dangerous to say that these results represented the whole truth.

#### 4.2.4 Olefin/paraffin ratio

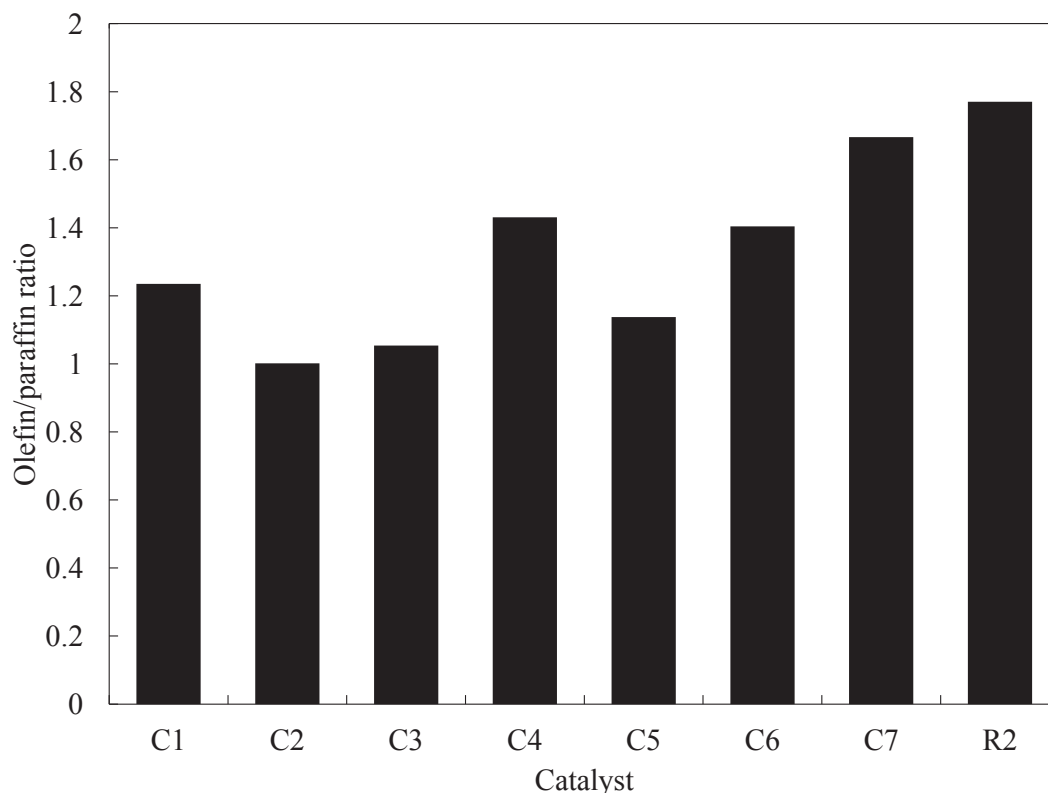


Figure 4.12: Olefin/paraffin ratio for catalysts C1–C7 and R2 at 483 K, 20 bar and  $H_2/CO = 2.1$ .

Figure 4.12 shows the olefin/paraffin (O/P) ratio for the catalysts tested in this work. All SiC-supported catalysts showed lower O/P ratios compared to the reference catalyst. There was not observed any correlation between the O/P ratio and the TOF value for the catalysts.

This, together with the increased  $C_{5+}$  selectivity, was not in line with the findings of Borg et al. [17] and Trépanier et al. [81]. These studies observed increased O/P ratios with increased  $C_{5+}$  selectivity as an effect of alkali metal loading.

#### 4.2.5 CO conversion vs. $C_{5+}$ selectivity

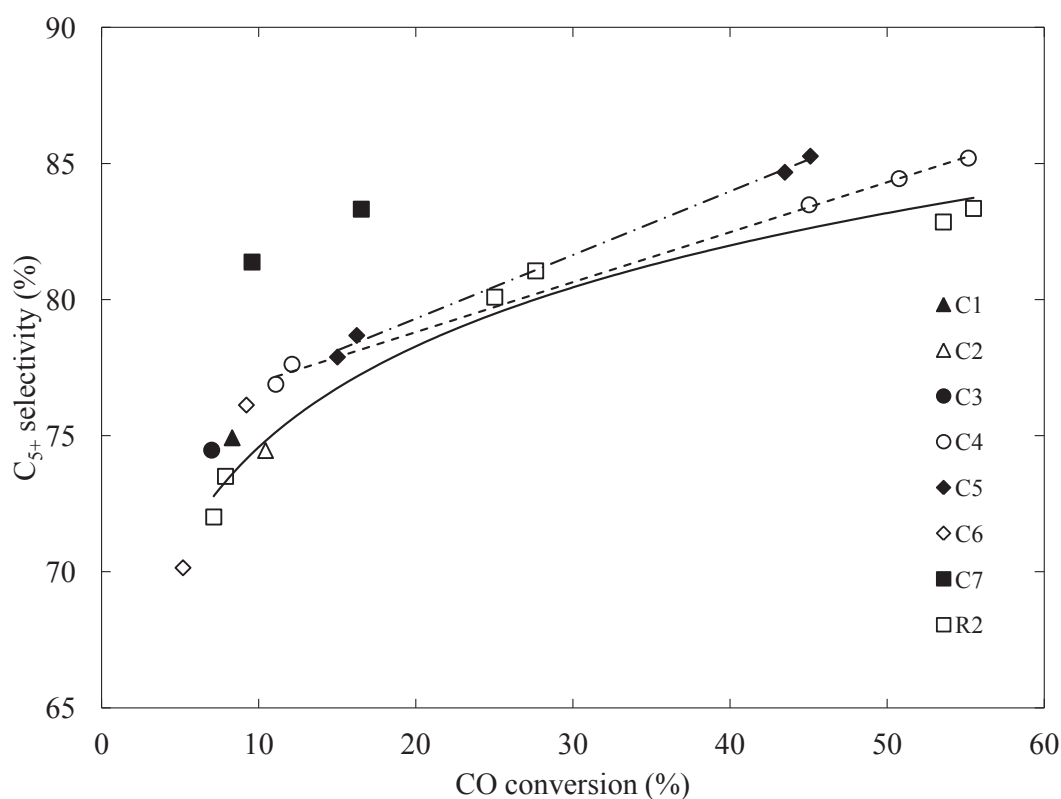


Figure 4.13:  $C_{5+}$  selectivity as a function of CO conversion for catalysts C1-C7 and R2 at 483 K, 20 bar and  $H_2/CO = 2.1$ .

Figure 4.13 shows the  $C_{5+}$  selectivity plotted against the CO conversion for all catalysts tested in this work, and the 50% CO conversion results obtained from Andreas H. Lillebø [53]. Assuming that the relation between CO conversion and  $C_{5+}$  selectivity was not influenced by any unknown effects, the results showed a tendency of steeper decrease in  $C_{5+}$  selectivity in the low conversion region for R2. The same could not be proposed for the SiC-supported catalysts due to the suspected influence of alkali on the  $C_{5+}$  selectivity.

Tendencies for C4 and C5 were also suggested in the figure. The line of C4 (- - -) suggested a linear relation between 12–45% CO conversion. However, this was not by far enough data points to make any conclusions based on the observed tendencies. Neither for R2 or the two SiC-supported catalysts.

## 4.2.6 FTS results in the literature

Section 2.7.1 presents the previous publications regarding FTS with Co/SiC catalysts that were found. A summary is given in table 2.1.

Lacroix et al. [50] also reported low TOF on the SiC-supported catalyst that was tested. The experiments were run at very different reaction conditions than what was used in this work. Results were also reported at a very high CO conversion ( $>70\%$ ). Thus, it was difficult to make much comparisons between the two sets of results. Lacroix et al. [50] reported very low TOFs on all three catalysts that were tested, including a  $\gamma$ - $\text{Al}_2\text{O}_3$ -supported catalyst. The TOF was actually reported to be lower on the  $\text{Al}_2\text{O}_3$ -supported than on the SiC-catalyst. This was different from what was observed in this study. However, it might be explained by other factors caused by the difference in reaction conditions.

de la Osa et al. [50] reported a lower TOF on SiC-supported catalyst than on  $\text{Al}_2\text{O}_3$ -supported catalyst. It was used a higher temperature and a different catalyst grain size in the study, than was used in this work. Nevertheless, at a reaction temperature of 493 K and  $\text{TOF} = 0,035 \text{ s}^{-1}$ , the CO conversion and  $\text{C}_{5+}$  selectivity were 7.4% and 93.3%, respectively. Compared to C5 of this work, there was a significant difference in the CO conversion. However, the fact that the catalyst run at higher reaction temperature showed lower conversion was strange. The higher  $\text{C}_{5+}$  selectivity of 93.3%, was likely caused by the higher reaction temperature.

de la Osa et al. [28] also proposed effects from alkali and alkaline earth metals, rather than surface characteristics, to be the cause of the higher selectivity observed on SiC-supported catalysts. It was reported that Ca had an promoting effect on the  $\text{C}_{5+}$  selectivity by de la Osa et al. [28], which was in contradiction to what Borg et al. [17] found. Since the actual amounts of alkali and alkaline earth metals were not confirmed on the catalysts of this work, the results could not support any of the two proposed effects of Ca.

It should be mentioned that de la Osa et al. [28] loaded a significantly larger amount of Ca on their catalysts than Borg et al. [17], 2 wt.% and 0.1 wt.% respectively. This might have attributed to the different effects reported. If the support samples (obtained from SICAT) that de la Osa et al. [28] used, were contaminated in a similar way to those tested in this work, this could also have attributed to the differences.

## 4.2.7 Mechanism of alkali and alkali earth metals effects

Which role alkali and alkaline earth metals holds that effects cobalt FT synthesis, has not yet been discovered. Nevertheless, some theories on the subject are presented in section 2.7.6. This section reflects on these theories.

Studies of alkali and alkaline earth metals on FTS catalysts proposed that these species adsorbed on the surface of the active metal [5, 81, 83]. The same was proposed for the poisoning of sulfur [18, 65] and phosphorus [17]. Since all these elements deactivated the catalysts, but only the alkali and alkaline earth metals affected the selectivity of the catalysts, there might be a slight difference in mechanisms of the deactivations.

Changes in the adsorption of H<sub>2</sub> and CO on alkali and alkaline earth metal promoted transition metal surfaces have been attributed to various effects. Electronic effects [89], decreased sticking coefficients [35] and site blocking effects [83]. However, the same effects were proposed for sulfur adsorption on these surfaces too [18, 37].

According to Goodman and Kiskinova [37], sulfur on Ni(100) poisoned CO adsorption and decreased the hydrogen sticking factor at low coverages. Potassium was found by Sun et al. [80] to decrease the sticking factor of hydrogen on Ni(100). However, Campbell and Goodman [20] found no limitations to CO adsorption when Ni(100) was promoted with potassium.

Thus, it seemed that sulfur affected the adsorption of both CO and H<sub>2</sub>, while potassium only affected the adsorption of H<sub>2</sub> on Ni(100) surfaces.

Oudar [63] stated it was well established, that sulfur adsorbs on the sites of maximum symmetry. Potassium on the other hand, was found by Norris et al. [60] to firstly cover the step edge sites, and then subsequently cover terrace sites of Ni(100) surfaces. Zhou and White [89] proposed that dissociative adsorption of H<sub>2</sub> on Pt(111) depended on defect sites initiating it. The hydrogen molecules then moved from the defect sites to more symmetrical sites where they adsorbed. Conrad et al. [22] stated that adsorbed CO molecules were mainly located at highly symmetrical sites.

It might be proposed that, due to site blocking effects, adsorption of H<sub>2</sub> was affected more by the presence of potassium, than the adsorption of CO were. While in the presence of sulfur, the adsorption of CO and H<sub>2</sub> were equally affected.

Trepanier et al. [81] proposed that the H<sub>2</sub> adsorption limiting effects of potassium led to lower conversion of CO. Also, that the decreased adsorption of H<sub>2</sub> caused a decrease in hydrogenation reactions, see figure 2.1 section 2.7.2. The increased amount of  $\alpha$ -olefin products led to an increase in olefin re-adsorption and further chain growth. Thus, an increased selectivity to higher hydrocarbons.

Viewing the results of Na loading by Balonek et al. [5] (figure 2.8, section 2.7.5), keeping the above proposed effects of potassium in mind. The observed effect of Na on the C<sub>5+</sub> selectivity reached a maximum, before the effect of Na on the CO conversion.

This might be explained by Na firstly adsorbing on the edge sites only affecting H<sub>2</sub> adsorption. Then, both CO conversion and C<sub>5+</sub> selectivity would be affected by the decrease in adsorbed H<sub>2</sub> as explained by Trépanier et al. [81]. Later, when the loading was increased, Na adsorbed on the terrace sites. Thus, blocking adsorption of both H<sub>2</sub> and CO. Now, the CO conversion would still be decreased by the site blocking, while the C<sub>5+</sub> selectivity would not be further increased.

It should be mentioned, that the author of this work was not personally familiar with studies on the mechanism of the poisoning elements. Since the proposed explanations above were supported on knowledge from the literature, some assumptions and connections may have been made, that should not have been made. Borg et al. [17] proposed that site blocking was an unlikely explanation due to too low impurity loading (up to 1000 ppmw). Impurity loadings for Na and Ca in catalyst C1 was found to be <1000 and <500 ppmw, respectively (see appendix A.2).

Studies of alkali and alkaline earth metal effects [5, 17] did not observe any significant difference in Co dispersion with regards to the impurity loadings. If the impurities had site blocking effects, it might be expected to see a decrease in hydrogen chemisorption. Prof. Edd A. Blekkan [10] mentioned the possibility that the impurities could have been mobile, and transported onto the Co surface during FT synthesis, which might explain the unaffected dispersion values.

However, Borg et al [17] reported no variations in deactivation rates, suggesting that the effect of the impurity was present from the start. Figure 4.10 shows that there were no significant variations in the deactivation rates of the catalysts tested in this work either. Nevertheless, it should be noted that the reaction rates in the figure were normalized to the first stable data point, after approximately six hours on stream.

The correct reaction conditions were reached after four hours, which leaves two hour were impurities could have moved around on the catalyst. This could not be observed due to the unstable data points collected in this period. However, it suggested that mobility of the impurities during FT synthesis could not be ruled out, based on the results from this work.

# Chapter 5

## Conclusion

Cobalt as active phase on SiC-supported catalysts was studied by characterization methods: Volumetric adsorption, temperature programmed reduction, volumetric chemisorption, X-ray diffraction, SSITKA, electron microscopy and elemental analysis. The catalysts were also tested in an experimental Fischer-Tropsch synthesis rig.

All seven SiC-supported catalysts prepared, were reduced at lower temperatures than Al<sub>2</sub>O<sub>3</sub>-supported Co- and CoRe-catalysts. H<sub>2</sub>-chemisorption showed poor dispersion of cobalt metal (2-3%) on the SiC-supported catalysts.

In total, seven SiC-supported catalysts and one Al<sub>2</sub>O<sub>3</sub>-supported reference catalyst, were run in the experimental Fisher-Tropsch synthesis rig. The SiC-supported catalysts showed varying activity results, and were all less active than the Al<sub>2</sub>O<sub>3</sub>-supported reference catalyst. However, at the same CO conversion level, SiC-supported catalysts yielded an increased C<sub>5+</sub> hydrocarbon selectivity compared to the reference catalyst.

The decreased activity and increased C<sub>5+</sub> selectivity of SiC-supported catalysts were suspected to be caused by alkali and alkaline earth metal impurities in the support samples. After the first batch of catalysts were tested and found little active, a second set of purer support samples were tested. However, the results suggested that there were still enough impurities present to cause significant loss of activity compared to the reference catalyst.





# Chapter 6

## Future work

In the future, the main focus should be to either test SiC-supported catalysts completely free of alkali and alkaline earth metal impurities. Or, if this is not possible, the exact type, and preferably the exact amount of impurities should be known.

The results on catalyst C5 was interesting and should be further investigated, with respect to the acid washing. Since this catalyst showed activity results closest to the reference catalyst, it suggested that the purification treatment had worked to some extent, as was discussed in section 4.2.2. If more catalysts expected to contain impurities are to be run in the FTS rig, an acid wash treatment should be performed prior to the testing. It may be further discussed whether the treatment should be performed on the support samples, after they are crushed. Or, if the treatment can be performed on prepared catalyst samples.

It might be interesting to perform EDS experiments on one or more catalysts, as was discussed in section 4.1.1. As mentioned, this would make it easier to measure particle sizes from the collected images. And also, this might contribute to answering which of the measured dispersions are more correct.

Finally, since catalyst C1 was found to qualitatively contain both sodium and calcium, the author of this work would like to propose an experiment. It might not be very constructive, but still. It was found in the literature that sodium increases C<sub>5+</sub> selectivity, while calcium decreases it. However, the catalysts tested in this work showed increased selectivity (true for the catalysts that could be compared with the reference). Thus, it might be interesting to study the combined effect of sodium and calcium in a controlled manner.



# Bibliography

- [1] A.A. Adesina. Hydrocarbon synthesis via Fischer-Tropsch reaction: trivials and triumphs. *Applied Catalysis A: General*, 138:345–367, 1996.
- [2] J.R. Anderson and M. Boudart. *Catalysis - Science and Technology*. Springer-Verlag, 1981.
- [3] R.B. Anderson. Schulz-Flory equation. *Journal of Catalysis*, 55:114–115, 1978.
- [4] G. Aylward and T. Findlay. *SI Chemical Data*. John Wiley & Sons Australia, 5th edition, 2002.
- [5] C.M. Balonek, A.H. Lillebø, S. Rane, E. Rytter, L.D. Schmidt, and A. Holmen. Effect of Alkali Metal Impurities on Co-Re Catalysts for Fischer-Tropsch Synthesis from Biomass-Derived Syngas. *Catalysis Letters*, 138:8–13, 2010.
- [6] E.P. Barrett, L.G. Joyner, and P.P. Halenda. The Determination of Pore Volume and Area Distributions in Porous Substances. I. Computations from Nitrogen Isotherms. *Journal of the American Chemical Society*, 73:373–380, 1951.
- [7] A. Berkó and F. Solymosi. The properties of CO and K adsorbed on Pd(100). *The Journal of Chemical Physics*, 90:2492–2503, 1989.
- [8] G.L. Bezemer et al. Cobalt Particle Size Effects in the Fischer-Tropsch Reaction Studied with Carbon Nanofiber Supported Catalysts. *Journal of the American Chemical Society*, 128:3956–3964, 2006.
- [9] E.A. Blekkan. Catalyst characterization. Lecture slides TKP4515, 2011.
- [10] E.A. Blekkan. Personal communication, 2012. edd.blekkan@chemeng.ntnu.no.
- [11] E.A. Blekkan, A. Holmen, and S. Vada. Alkali Promotion of Alumina-Supported Cobalt Fischer-Tropsch Catalysts Studied by TPR, TPD and Pulse Chemisorption. *Acta Chemica Scandinavica*, 47:275–280, 1993.
- [12] E.A. Blekkan and H. Venvik. Fischer-Tropsch synthesis. Lecture slides TKP4150, 2011.
- [13] Ø. Borg. *Role of Alumina Support in Cobalt Fischer-Tropsch Synthesis*. PhD thesis, NTNU, 2007.
- [14] Ø. Borg et al. Effect of calcination atmosphere and temperature on  $\gamma$ -Al<sub>2</sub>O<sub>3</sub> supported cobalt Fischer-Tropsch catalysts. *Topics in Catalysis*, 45:39–43, 2007.

- [15] Ø. Borg et al. Fischer-Tropsch synthesis over  $\gamma$ -alumina-supported cobalt catalysts: Effect of support variables. *Journal of Catalysis*, 248:89–100, 2007.
- [16] Ø. Borg et al. Fischer-Tropsch synthesis over un-promoted and Re-promoted  $\gamma$ -Al<sub>2</sub>O<sub>3</sub> supported cobalt catalysts with different pore sizes. *Catalysis Today*, 142:70–77, 2009.
- [17] Ø. Borg et al. Effect of biomass-derived synthesis gas impurity elements on cobalt Fischer-Tropsch catalyst performance including *in situ* sulphur and nitrogen addition. *Journal of Catalysis*, 279:163–173, 2011.
- [18] J.L. Brand, A.A. Deckert, and S.M. George. Surface diffusion of hydrogen on sulfur-covered Ru(001) surfaces studied using laser-induced thermal desorption. *Surface Science*, 194:457–474, 1988.
- [19] British Petroleum. BP Statistical Review of World Energy June 2011. [www.bp.com/statisticalreview](http://www.bp.com/statisticalreview). Downloaded 29.10.2011.
- [20] C.T. Campbell and D.W. Goodman. A surface Science investigation of the role of potassium promoters in nickel catalysts for CO hydrogenation. *Surface Science*, 123:413–426, 1982.
- [21] I. Chorkendorff and J.W. Niemantsverdriet. *Concepts of Modern Catalysis and Kinetics*. WILEY-VCH Verlag, 2007.
- [22] H. Conrad, G. Ertl, K. Koch, and E.E. Latta. Adsorption of CO on Pd single crystal surfaces. *Surface Science*, 43:462–480, 1974.
- [23] E. Corporan et al. Emissions Characteristics of a Turbine Engine and Research Combustor Burning a Fischer-Tropsch Jet Fuel. *Energy & Fuels*, 21(5):2615–2626, 2007.
- [24] B.H. Davis. Fischer-Tropsch synthesis: current mechanism and futuristic needs. *Fuel Processing Technology*, 71:157–166, 2001.
- [25] B.H. Davis. Fischer-Tropsch Synthesis: Reaction mechanisms for iron catalysts. *Catalysis Today*, 141:25–33, 2009.
- [26] A.R. de la Osa, A. De Lucas, A. Romero, J.L. Valverde, and P. Sánchez. Influence of the catalytic support on the industrial Fischer–Tropsch synthetic diesel production. *Catalysis Today*, 176:298–302, 2011.
- [27] A.R. de la Osa, A. De Lucas, J. Díaz-Maroto, A. Romero, J.L. Valverde, and P. Sánchez. FTS fuels production over different Co/SiC catalysts. *Catalysis Today*, 187:173–182, 2012.
- [28] A.R. de la Osa, A. De Lucas, L. Sánchez-Silva, J. Díaz-Maroto, J.L. Valverde, and P. Sánchez. Performing the best composition of supported Co/SiC catalyst for selective FTS diesel production. *Fuel*, 95:587–598, 2012.
- [29] M.E. Dry. High quality diesel via the Fischer-Tropsch process - a review. *Journal of Chemical Technology and Biotechnology*, 77:43–50, 2001.
- [30] M.E. Dry. The Fischer–Tropsch process: 1950–2000. *Catalysis Today*, 71(3-4):227–241, 2002.

- [31] B.C. Enger. Personal communication, 2011. bjornce@chemeng.ntnu.no.
- [32] F. Fischer and H. Tropsch. Preparation of synthetic oil mixtures (synthol) from carbon monoxide and hydrogen. *Brennstoff-Chem.*, 4:276–285, 1923.
- [33] V. Frøseth, S. Storsæter, Ø. Borg, E.A. Blekkan, M. Rønning, and A. Holmen. Steady state isotopic transient kinetic analysis (SSITKA) of CO hydrogenation on different Co catalysts. *Applied Catalysis A: General*, 289:10–15, 2005.
- [34] Vidar Frøseth. *A steady-state isotopic transient kinetic study of Co catalysts on different supports*. PhD thesis, NTNU, 2006.
- [35] S.C. Gebhard and B.E. Koel. Influence of Potassium on the Adsorption of hydrogen on Pt(111). *The Journal of Physical Chemistry*, 96:7056–7063, 1992.
- [36] M.I. Gonzalez, B. Kraushaar-Czarnetzki, and G. Schaub. Process comparison of biomass-to-liquid (BtL) routes Fischer–Tropsch synthesis and methanol to gasoline. *Biomass Conversion and Biorefinery*, 1:1–15, 2011.
- [37] D.W. Goodman and M. Kiskinova. Chemisorption and reactivity studies of H<sub>2</sub> and CO on sulfided Ni(100). *Surface Science*, 105:L265–L270, 1981.
- [38] G.L. Haller and D.E. Resasco. Metal-support interaction: Group VIII metals and reducible oxides. *Advances in Catalysis*, 36:173–235, 1989.
- [39] A.M. Hilmen, O.A. Lindvåg, E. Bergene, D. Schanke, S. Eri, and A. Holmen. Selectivity and activity changes upon water addition during Fischer-Tropsch synthesis. *Studies in Surface Science and Catalysis*, 136:295–300, 2001.
- [40] A.M. Hilmen, D. Schanke, K.F. Hansen, and A. Holmen. Study of the effect of water on alumina supported cobalt Fischer-Tropsch catalysts. *Applied Catalysis A: General*, 186:169–188, 1999.
- [41] A. Holmen. *Heterogen katalyse*. IKP, NTNU, 2010.
- [42] A. Holmen. Personal communication, 2011–2012. anders.holmen@chemeng.ntnu.no.
- [43] E. Iglesia, S.C. Reyes, R.J. Madon, and S.L. Soled. Selectivity Control and Catalyst Design in the Fischer-Tropsch Synthesis: Sites, Pellets, and Reactors. *Advances in Catalysis*, 39:221–302, 1993.
- [44] E. Inglesia. Design, synthesis, and use of cobalt-based Fischer-Tropsch synthesis catalysts. *Applied Catalysis A: General*, 161:59–78, 1997.
- [45] G. Jacobs, T.K. Das, Y. Zhang, J. Li, G. Racoillet, and B.H. Davies. Fisher-Tropsch synthesis: support, loading and promoter effects on the reducibility of cobalt catalysts. *Applied Catalysis A: General*, 233:263–281, 2002.
- [46] B. Jager and R. Espinoza. Advances in low temperature Fischer-Tropsch synthesis.
- [47] A.Y. Khodakov, R. Bechara, and A. Griboval-Constant. Fischer-Tropsch synthesis over silica supported cobalt catalysts: mesoporous structure versus cobalt surface density. *Applied Catalysis A: General*, 254:273–288, 2003.

- [48] T. Komaya et al. Effects of Dispersion and Metal-Metal Oxide Interactions on Fischer-Tropsch Synthesis over Ru/TiO<sub>2</sub> and TiO<sub>2</sub>-Promoted Ru/SiO<sub>2</sub>. *Journal of Catalysis*, 150:400–406, 1994.
- [49] T. Komaya et al. The Influence of Metal-Support Interactions on the Accurate Determination of Ru Dispersion for Ru/TiO<sub>2</sub>. *Journal of catalysis*, 149:142–148, 1994.
- [50] M. Lacroix et al. Silicon carbide foam composite containing cobalt as a highly selective and re-usable Fischer–Tropsch synthesis catalyst. *Applied Catalysis A: General*, 397:62–72, 2011.
- [51] M.J. Ladoux, S. Hantzer, C. Pham-Huu, J. Guille, and M.P. Desaneaux. New synthesis and uses of high-specific-surface SiC as a catalytic support that is chemically inert and has high thermal resistance. *Journal of Catalysis*, 144:176–185, 1988.
- [52] M.J. Ledoux and C. Pham-Huu. High specific surface area carbides of silicon and transition metals for catalysis. *Catalysis Today*, 15:263–284, 1992.
- [53] A.H. Lillebø. Personal communication, 2011–2012. andreli@chemeng.ntnu.no.
- [54] M.C. Lok, G.J. Kelly, and G. Gray. Catalysts with high cobalt surface area. United States Patent No.: 6,927,190 B2, 2005.
- [55] R. Moene, L.F. Kramer, J. Schoonman, M. Makkee, and J.A. Moulijn. Synthesis of high surface area silicon carbide by fluidized bed chemical vapour deposition. *Applied Catalysis A: General*, 162:181–191, 1997.
- [56] R. Moene, M. Makkee, and J.A. Moulijn. Novel application of catalysis in the synthesis of catalysts. *Catalysis Letters*, 34:285–291, 1995.
- [57] R. Moene, E.P.A.M Tijssen, M. Makkee, and J.A. Moulijn. Synthesis and thermal stability of Ni, Cu, Co, and Mo catalysts based on high surface area silicon carbide. *Applied Catalysis A: General*, 184:127–141, 1999.
- [58] K.L. Murray, N.A. Seaton, and M.A. Day. Use of Mercury Intrusion Data, Combined with Nitrogen Adsorption Measurements, as a probe of Pore Network Connectivity. *Langmuir*, 15:8155–8160, 1999.
- [59] P. Nguyen and C. Pham. Innovative porous SiC-based materials: From nanoscopic understandings to turntable carriers serving catalytic needs. *Applied Catalysis A: General*, 391:443–454, 2011.
- [60] A.G. Norris et al. An STM study of the potassium-induced removal of the Ni(100)(2 x 2)p4g-N reconstruction. *Surface Science*, 424:74–81, 1999.
- [61] OECD. OECD Factbook 2010. [http://www.oecd-ilibrary.org/economics/oecd-factbook-2010\\_factbook-2010-en](http://www.oecd-ilibrary.org/economics/oecd-factbook-2010_factbook-2010-en). Downloaded 29.10.2011.
- [62] Society of petroleum engineers. Unit Conversion factors. [www.spe.org/industry/docs/UnitConversion.pdf](http://www.spe.org/industry/docs/UnitConversion.pdf). Downloaded 29.10.2011.
- [63] J. Oudar. Sulfur Adsorption and Poisoning of Metallic Catalysts. *Catalysis Reviews: Science and Engineering*, 22:171–195, 1980.

- [64] P. Panagiotopoulou, D.I. Kondarides, and X.E. Verykios. Selective methanation of CO over supported Ru catalysts. *Applied Catalysis B: Environmental*, 88:470–478, 2009.
- [65] S.S. Pansare and J.D. Allison. An investigation of the effect of ultra-low concentrations of sulfur on a Co/ $\gamma$ -Al<sub>2</sub>O<sub>3</sub> Fischer–Tropsch synthesis catalyst. *Applied Catalysis A: General*, 387:224–230, 2010.
- [66] J. Parmentier, J. Patarin, J. Dentzer, and C. Vix-Guterl. Formation of SiC via carbothermal reduction of a carbon-containing mesoporous MCM-48 silica phase: a new route to produce high surface area SiC. *Ceramics International*, 28:1–7, 2002.
- [67] C. Pierce. Computation of pore sizes from physical adsorption data. *The Journal of Physical Chemistry*, 57:149–152, 1953.
- [68] P.P. Prosini. *Iron Phosphate Materials as Cathodes for Lithium Batteries*. Springer-Verlag, 2011. Chapter 1.
- [69] S. Rane, Ø. Borg, J. Yang, E. Rytter, and A. Holmen. Effect of alumina phases on hydrocarbon selectivity in Fischer-Tropsch synthesis. *Applied Catalysis A: General*, 388:160–167, 2010.
- [70] D. Reinalda and J. Kars. Process for the preparation of a catalyst or catalyst precursor suitable for the preparation of hydrocarbons from carbon monoxide and hydrogen, and said catalyst. European Patent No. 0,421,502, 1994.
- [71] D. Schanke et al. Study of the deactivation mechanism of Al<sub>2</sub>O<sub>3</sub>-supported cobalt Fischer-Tropsch catalysts. *Catalysis Letters*, 34:269–284, 1995.
- [72] SICAT. <http://www.sicatcatalyst.com/>. 5.12.2011.
- [73] S.T. Sie and R. Krishna. Fundamentals and selection of advanced Fischer–Tropsch reactors. *Applied Catalysis A*, 186:55–70, 1999.
- [74] S.L. Soled, E. Inglesia, R.A. Fiato, J.E. Baumgartner, H. Vroman, and S. Mieso. Control of metal dispersion and structure by changes in the solid-state chemistry of supported cobalt Fischer–Tropsch catalysts. *Topics in Catalysis*, 26:101–109, 2003.
- [75] F. Solymosi and I. Kovacs. Effects of Potassium Adlayer on the Adsorption and Desorption of Hydrogen on a Pd(100) Surface. *The Journal of Physical Chemistry*, 93:7537–7539, 1989.
- [76] A.P. Steynberg and M.E. Dry. Fischer-Tropsch Technology. *Studies in Surface Science and Catalysis*, 152:1–63, 2004.
- [77] S. Storsæter. *Fischer-Tropsch synthesis over cobalt supported catalysts*. PhD thesis, NTNU, 2005.
- [78] S. Storsæter, Ø. Borg, E.A. Blekkan, and A. Holmen. Study of the effect of water on Fischer-Tropsch synthesis over supported cobalt catalysts. *Journal of Catalysis*, 231:405–419, 2005.



- [79] S. Storsæter, B. Tøtdal, J.C. Walmsley, B.S. Tanem, and A. Holmen. Characterization of alumina-, silica-, and titania-supported cobalt Fischer-Tropsch catalysts. *Journal of Catalysis*, 236:139–152, 2005.
- [80] Y.-M. Sun, H.S. Luftman, and J.M. White. Potassium and coadsorbed potassium and deuterium on Ni(100). *Surface Science*, 139:379–395, 1984.
- [81] M. Trépanier, A. Tavasoli, A.K. Dalia, and N. Abatzoglou. Co, Ru and K loadings effects on the activity and selectivity of carbon nanotubes supported cobalt catalyst in Fischer-Tropsch synthesis. *Applied Catalysis A: General*, 353:193–202, 2009.
- [82] D.O. Uner. A Sensible Mechanism of Alkali Promotion in Fischer-Tropsch Synthesis: Adsorbate Mobilities. *Industrial & Engineering Chemistry Research*, 37:2239–2245, 1998.
- [83] D.O. Uner, M. Pruski, B.C. Gerstein, and T.S. King. Hydrogen Chemisorption on Potassium Promoted Supported Ruthenium Catalysts. *Journal of Catalysis*, 146:530–536, 1994.
- [84] J. van de Loosdrecht et al. Calcination of Co-based Fischer-Tropsch synthesis catalysts. *Topics in Catalysis*, 26:121–127, 2003.
- [85] A.M. Vannice, Y-L Chao, and R.M. Friedman. The preparation and use of high surface area silicon carbide catalyst supports. *Applied Catalysis*, 20:91–107, 1986.
- [86] John Walmsley. Personal communication, 2012. john.walmsley@sintef.no.
- [87] Jia Yang. Personal communication, 2012. jia.yang@chemeng.ntnu.no.
- [88] Y. Zhang, Y. Liu, G. Yang, S. Sun, and N. Tsubaki. Effects of impregnation solvent on Co/SiO<sub>2</sub> catalyst for Fischer-Tropsch synthesis: A highly active and stable catalyst with bimodal sized cobalt particles. *Applied Catalysis A: General*, 321:79–85, 2007.
- [89] X.-L. Zhou and J.M. White. Stabilization by potassium of adsorbed hydrogen on pt(111). *Surface Science*, 185:450–456, 1987.
- [90] M. Zhuo, K.F. Tan, A. Borgna, and M. Sayes. Density Functional Theory Study of the CO Insertion Mechanism for Fischer-Tropsch Synthesis over Co Catalysts. *J. Phys. Chem. C*, 113:8357–8365, 2009.



# Appendix A

## Additional results

This appendix includes experimental results that were not practical to include in chapter 4: Results and discussion.

### A.1 SSITKA

SSITKA experiments were performed by *Jia Yang* [87] at NTNU. The results are presented in table A.1. These results did not reveal any information that could explain the low activity of the SiC-supported catalysts tested in this work.

Table A.1: SSITKA results at 483 K, 1.85 bar and  $\text{H}_2/\text{CO}/\text{inert} = 15/1.5/33.5$  NmL/min.  $\text{CH}_{(4)}$  indicates surface intermediates leading to  $\text{CH}_4$ ,  $\tau_i$ : concentration of surface intermediates.

Catalyst	$R_{\text{CO}}$ ( $\mu\text{mol}/\text{g}_{\text{cat}}\text{s}$ )	$\text{TOF}_{\text{CH}_4}^a$ ( $10^{-3}\text{s}^{-1}$ )	$S_{\text{CH}_4}$ (%)	$X_{\text{CO}}$ (%)
C1	1.14	18.09	76.5	10.2
C3	0.96	14.96	75.8	8.7
$\text{Co}/\alpha\text{-Al}_2\text{O}_3^b$	0.80	10.20	71.0	-
	$\tau_{\text{CH}_{(4)}}$ (s)	$\tau_{\text{CO}}$ (s)	$N_{\text{CH}_{(4)}}$ ( $\mu\text{mol}/\text{g}_{\text{cat}}\text{s}$ )	$N_{\text{CO}}$ ( $\mu\text{mol}/\text{g}_{\text{cat}}\text{s}$ )
C1	7.0	2.9	6.1	29.4
C3	8.1	2.8	5.9	28.6
$\text{Co}/\alpha\text{-Al}_2\text{O}_3^b$	11.0	2.0	6.0	22.0

<sup>a</sup> Based on  $\text{H}_2$ -chemisorption.

<sup>b</sup> Data collected from doctoral thesis of Vidar Frøseth [34].

## A.2 Elemental analysis

Elemental analysis of support S1 and catalyst C1 was performed by *Molab AS*. Confirmed that both samples contained alkali and alkaline earth metals Na and Ca. There was also found measurable amounts of P and Fe, and trace amounts of S, in the samples. Table A.2 shows the results, which can also be found in the document received from *Molab AS* included in appendix D.

Table A.2: Elemental analysis of S1 and C1.

Sample		S1	C1
Parameter	Unit		
Ca	%	<0.05	<0.05
Fe	%	0.24	0.19
Na	%	<0.010	<0.010
P	%	0.015	0.011
S	%	<0.02	<0.02

## A.3 Volumetric adsorption

This section shows the experimental results from volumetric adsorption for all supports and catalysts analyzed. Figures A.1 through A.12 shows adsorption/desorption isotherms,  $\alpha$  and  $\eta$  values for calculations, and pore size distributions.

Support S4 and catalysts C1–C3 were analyzed multiple times to ensure good results, and the values reported in table 4.1 are average values. The complete results for these catalysts are shown in table A.3.

Results for S1–S3 extrudates are presented in table A.4.

Table A.3: Complete results from parallel analyses of S4 and C1–C3

Sample	Surface area <sup>a,d</sup> (m <sup>2</sup> /g)	Pore volume <sup>b</sup> (cm <sup>3</sup> /g)	Pore diameter <sup>c</sup> (nm)
S4	33	15.2	0.14
S4	33	15.4	0.13
S4	33	15.0	0.13
S4	34	13.8	0.13
C1	26	14.5	0.10
C1	27	14.1	0.11
C1	27	14.4	0.11
C2	30	12.8	0.11
C2	32	13.0	0.12
C2	32	12.8	0.12
C3	24	13.3	0.09
C3	24	13.3	0.09
C3	25	13.6	0.10

<sup>a</sup> BET isotherm.

<sup>b</sup> BJH desorption cumulative volume of pores between 1.7 and 300 nm diameter.

<sup>c</sup> BJH desorption average pore diameter.

<sup>d</sup> Uncertainty ( $\pm 2\sigma$ ) calculated from three catalyst C2 samples:  $\pm 2$  m<sup>2</sup>/g.

Table A.4: Volumetric adsorption results for S1–S3 extrudates.

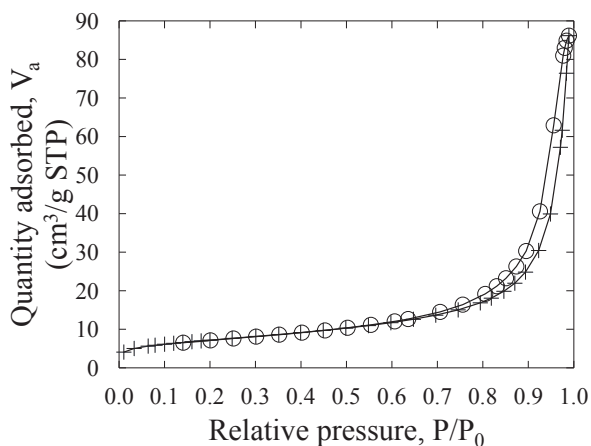
Sample	Surface area <sup>a,d</sup> (m <sup>2</sup> /g)	Pore volume <sup>b</sup> (cm <sup>3</sup> /g)	Pore diameter <sup>c</sup> (nm)
S1	24	21.6	0.13
S2	31	16.6	0.14
S3	23	19.1	0.11

<sup>a</sup> BET isotherm.

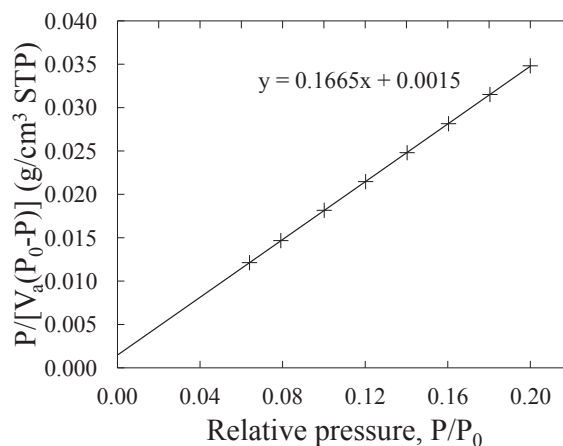
<sup>b</sup> BJH desorption cumulative volume of pores between 1.7 and 300 nm diameter.

<sup>c</sup> BJH desorption average pore diameter.

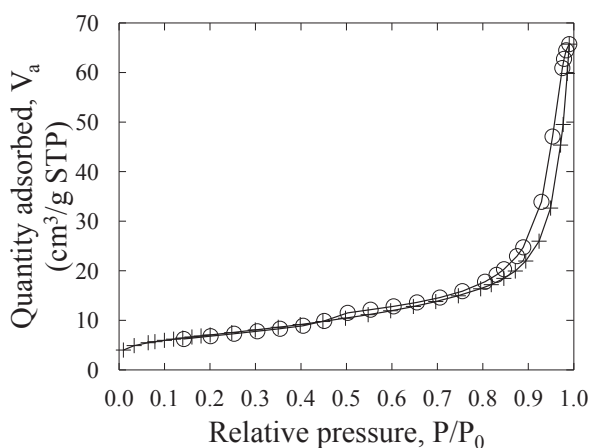
<sup>d</sup> Uncertainty ( $\pm 2\sigma$ ) calculated from three catalyst C2 samples:  $\pm 2$  m<sup>2</sup>/g.



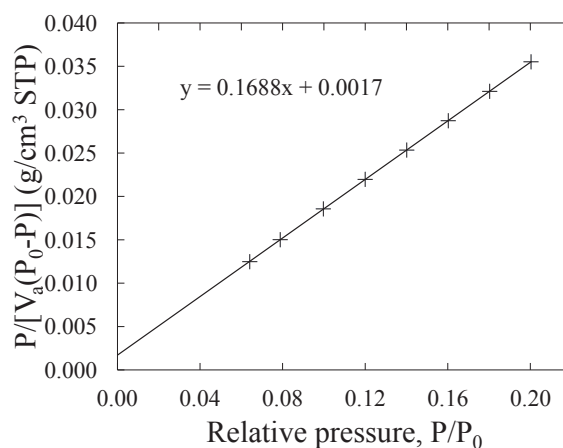
(a) Adsorption and desorption isotherm linear plot for S1.



(b) BET surface area plot for S1.



(c) Adsorption and desorption isotherm linear plot for C1.



(d) BET surface area plot for C1.

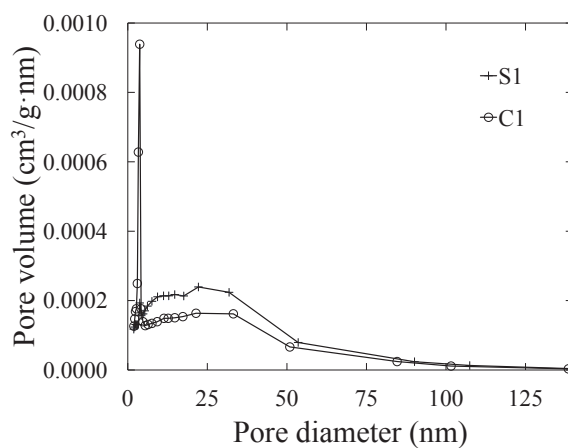
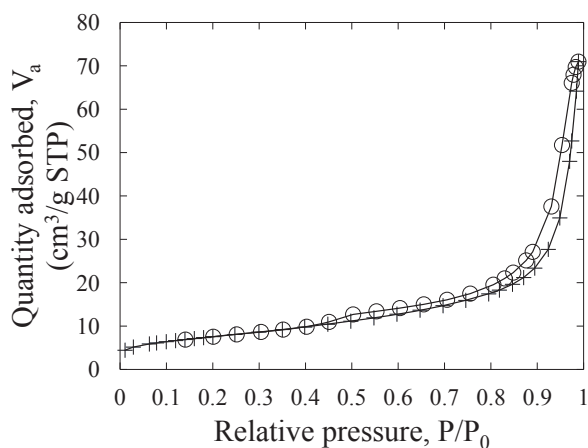
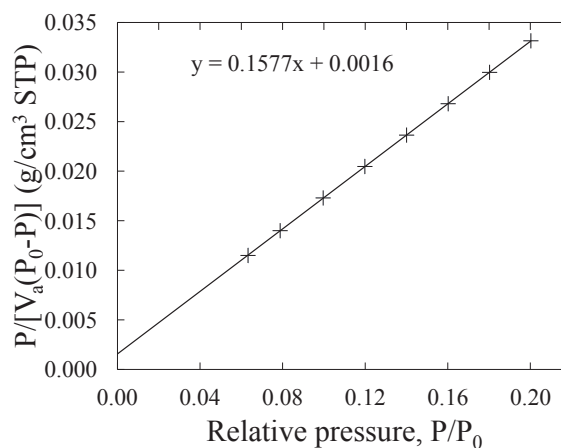
(e) BJH desorption  $dV/dD$  pore volume.

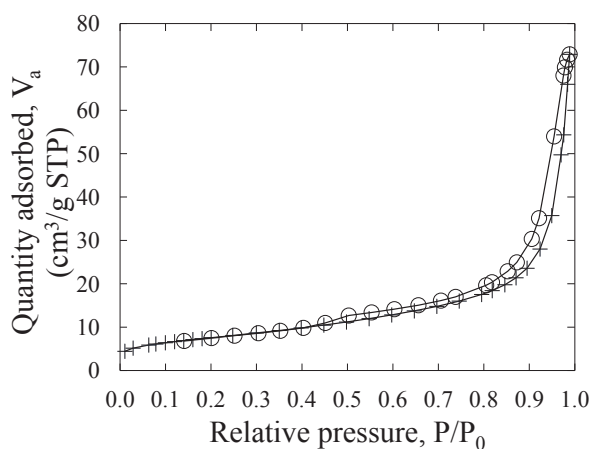
Figure A.1: Volumetric adsorption results for support S1 and catalyst C1.



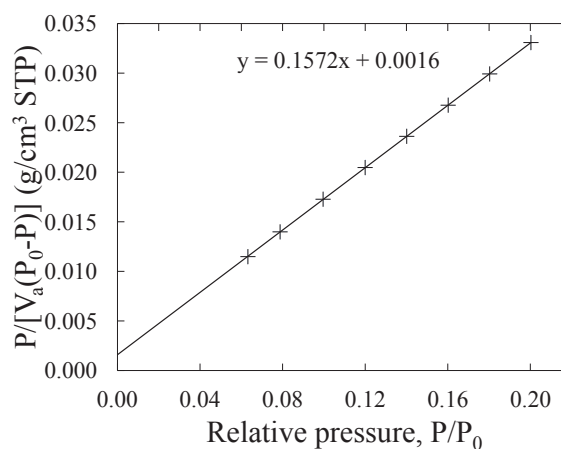
(a) Adsorption and desorption isotherm linear plot for C1.



(b) BET surface area plot for C1.

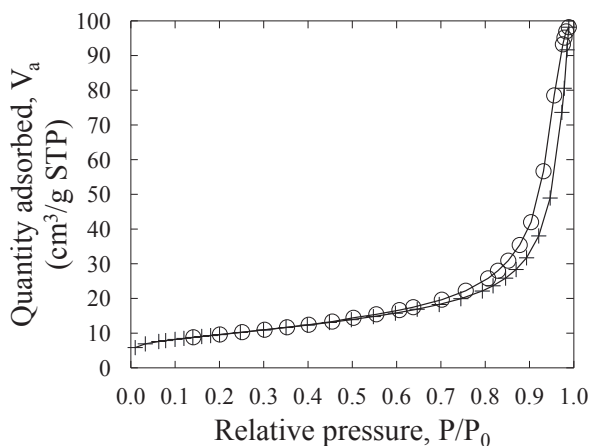


(c) Adsorption and desorption isotherm linear plot for C1.

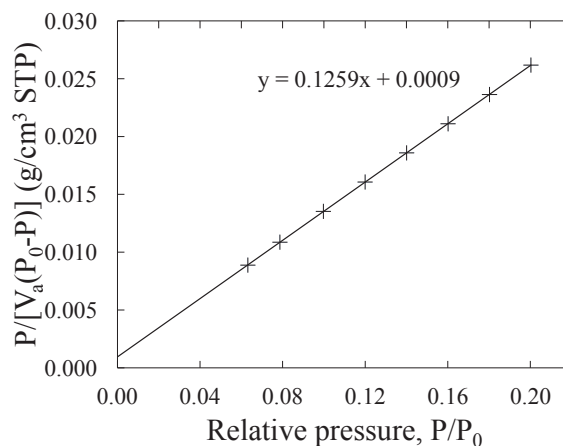


(d) BET surface area plot for C1.

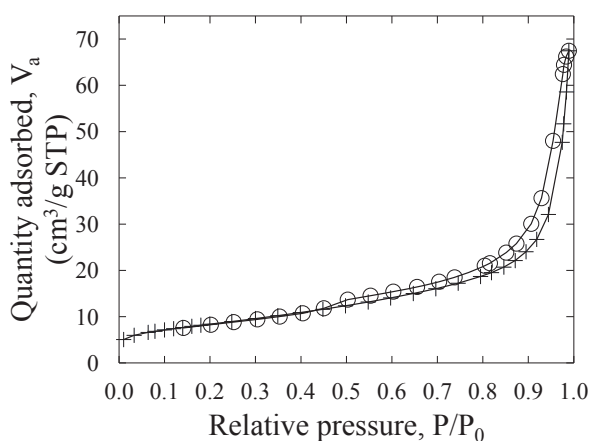
Figure A.2: Volumetric adsorption results for catalyst C1. Parallel runs.



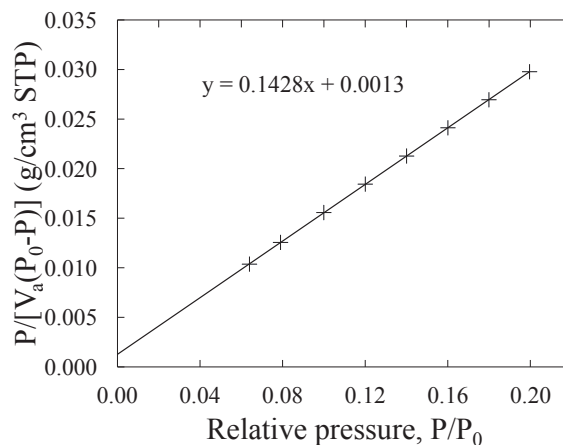
(a) Adsorption and desorption isotherm linear plot for S2.



(b) BET surface area plot for S2.



(c) Adsorption and desorption isotherm linear plot for C2.



(d) BET surface area plot for C2.

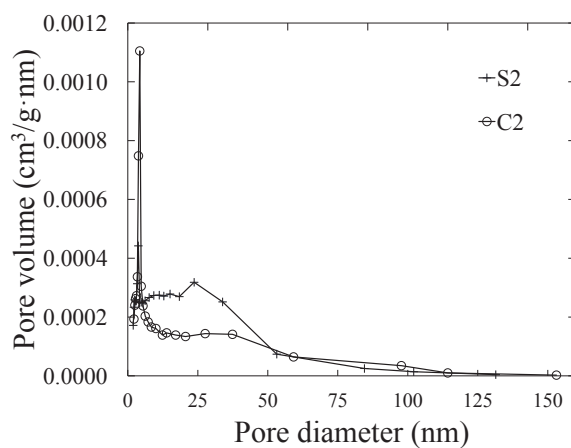
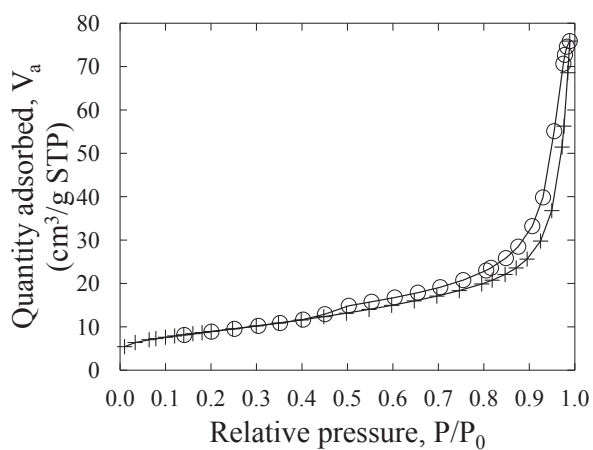
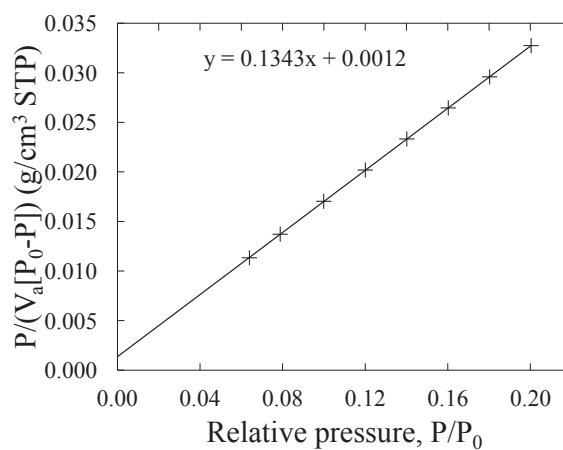
(e) BJH desorption  $dV/dD$  pore volume.

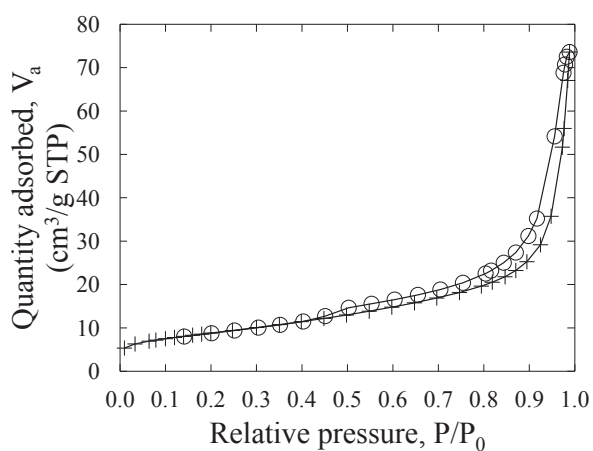
Figure A.3: Volumetric adsorption results for support S2 and catalyst C2.



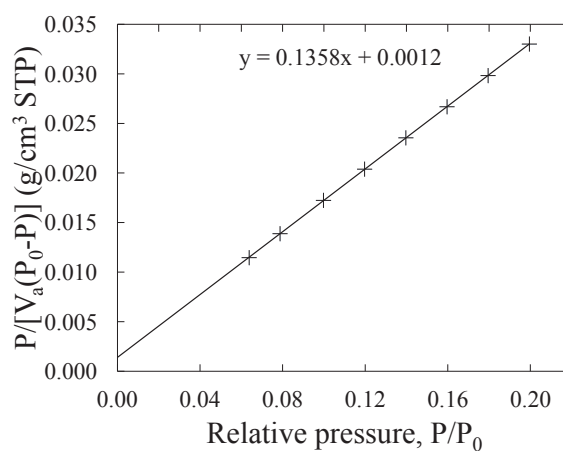
(a) Adsorption and desorption isotherm linear plot for C2.



(b) BET surface area plot for C2.

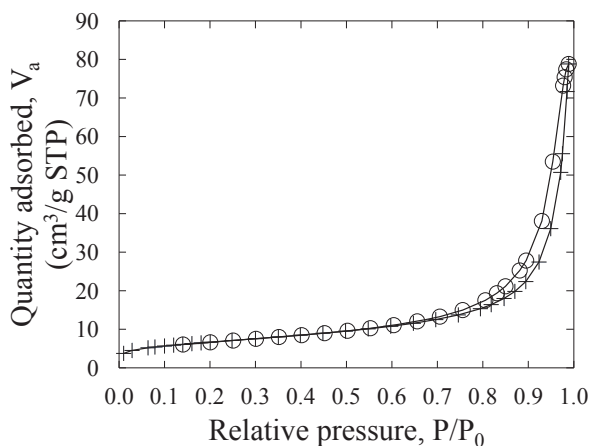


(c) Adsorption and desorption isotherm linear plot for C2.

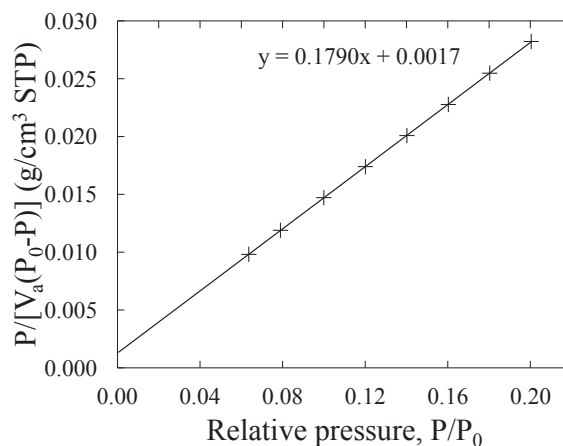


(d) BET surface area plot for C2.

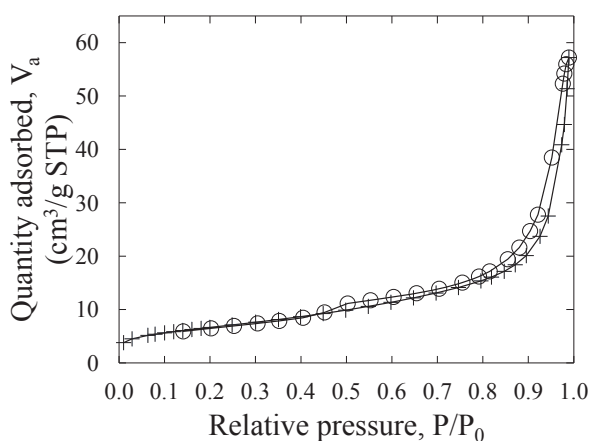
Figure A.4: Volumetric adsorption results for catalyst C2. Parallel runs for calculation of experimental uncertainty.



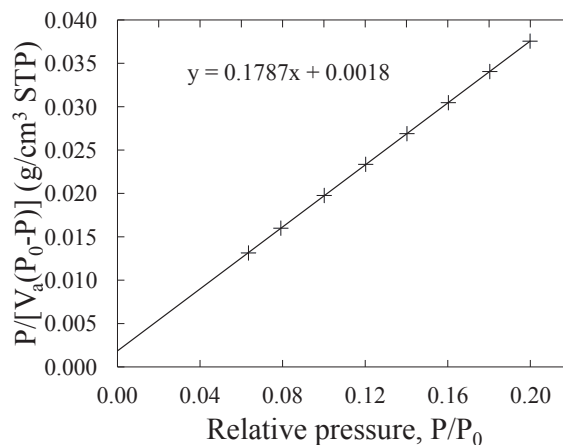
(a) Adsorption and desorption isotherm linear plot for S3.



(b) BET surface area plot for S3.



(c) Adsorption and desorption isotherm linear plot for C3.



(d) BET surface area plot for C3.

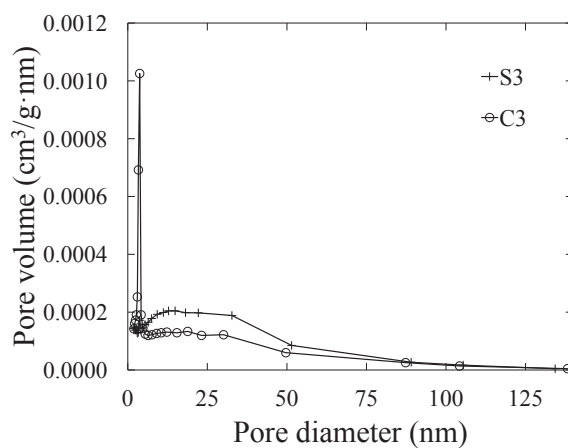
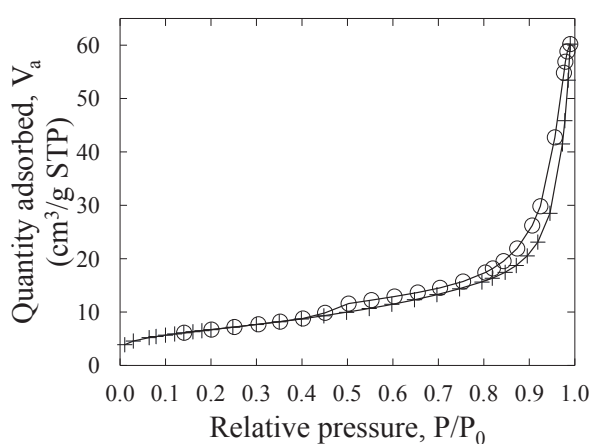
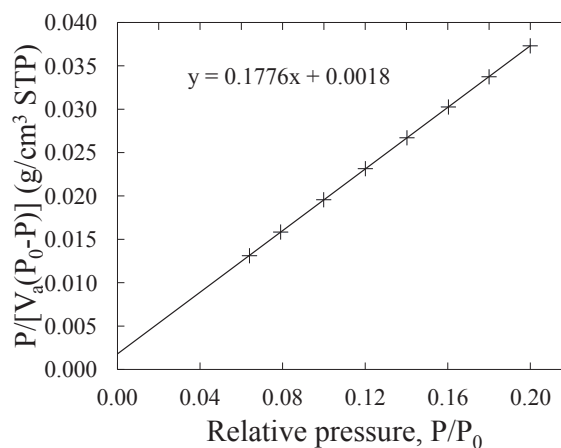
(e) BJH desorption  $dV/dD$  pore volume.

Figure A.5: Volumetric adsorption results for support S3 and catalyst C3.

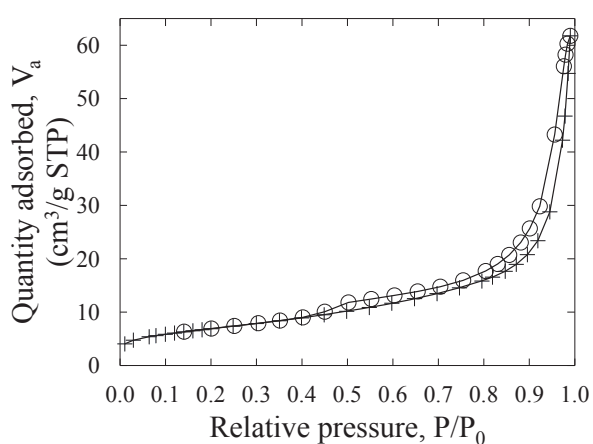




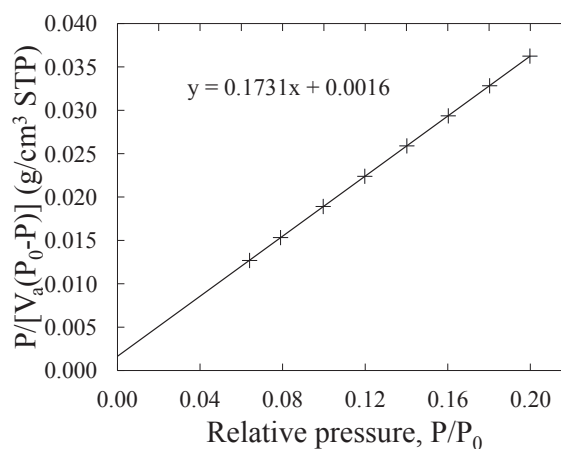
(a) Adsorption and desorption isotherm linear plot for C3.



(b) BET surface area plot for C3.

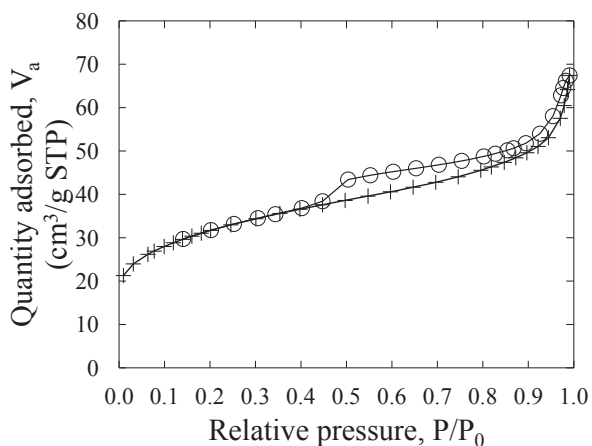


(c) Adsorption and desorption isotherm linear plot for C3.

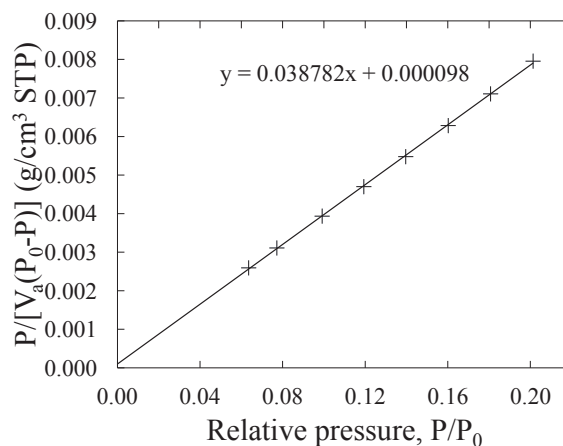


(d) BET surface area plot for C3.

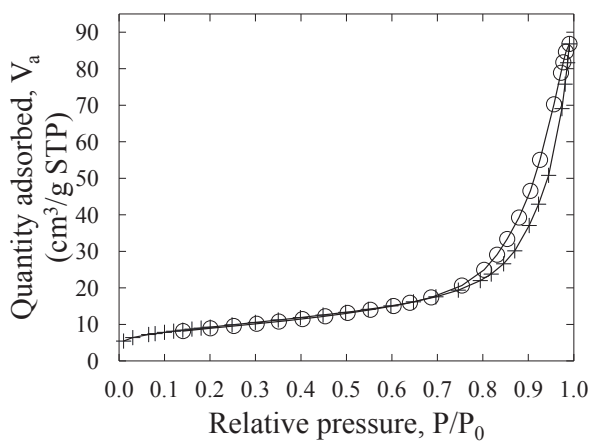
Figure A.6: Volumetric adsorption results for catalyst C3. Parallel runs.



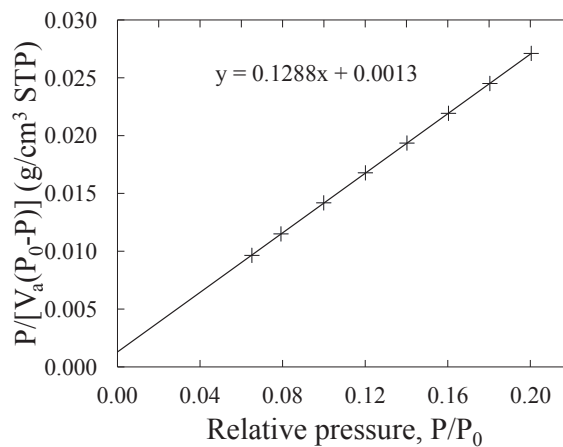
(a) Adsorption and desorption isotherm linear plot for S4.



(b) BET surface area plot for S4.



(c) Adsorption and desorption isotherm linear plot for C4.



(d) BET surface area plot for C4.

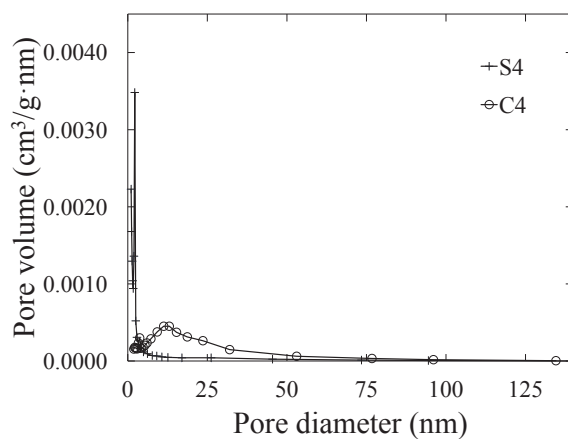
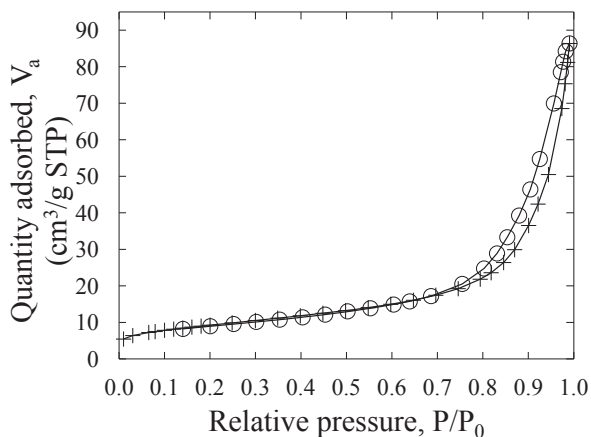
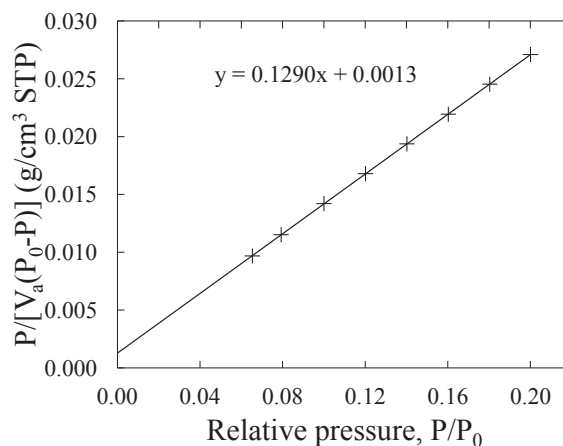
(e) BJH desorption  $dV/dD$  pore volume.

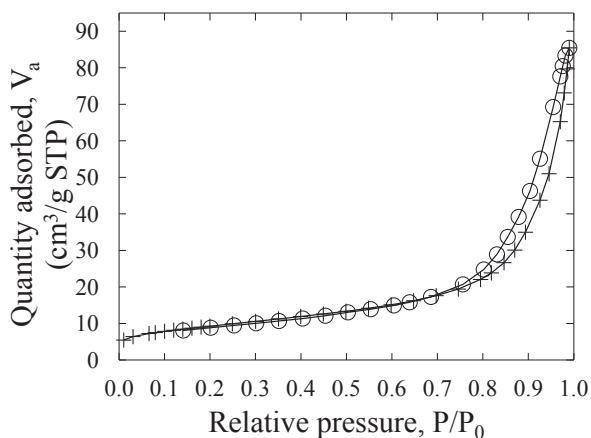
Figure A.7: Volumetric adsorption results for support S4 and catalyst C4.



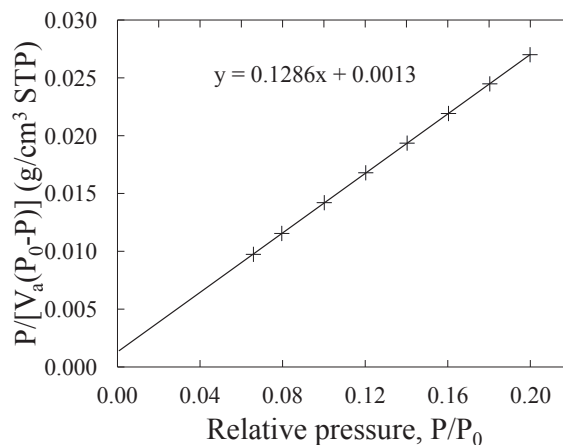
(a) Adsorption and desorption isotherm linear plot for C4.



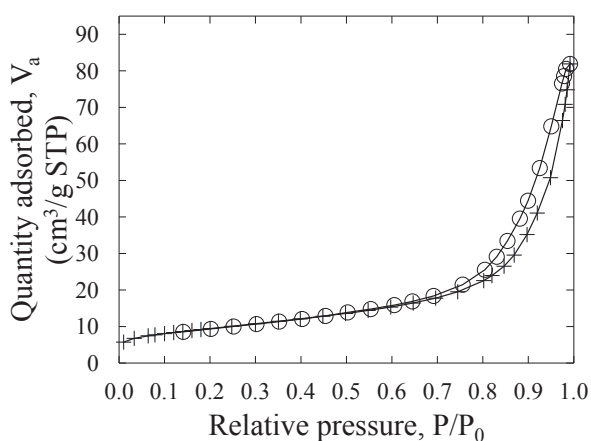
(b) BET surface area plot for C4.



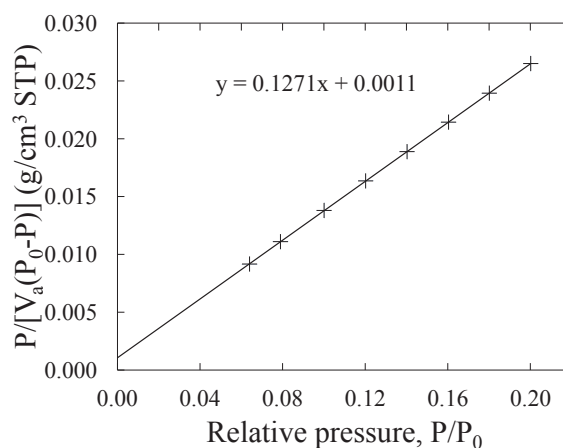
(c) Adsorption and desorption isotherm linear plot for C4.



(d) BET surface area plot for C4.

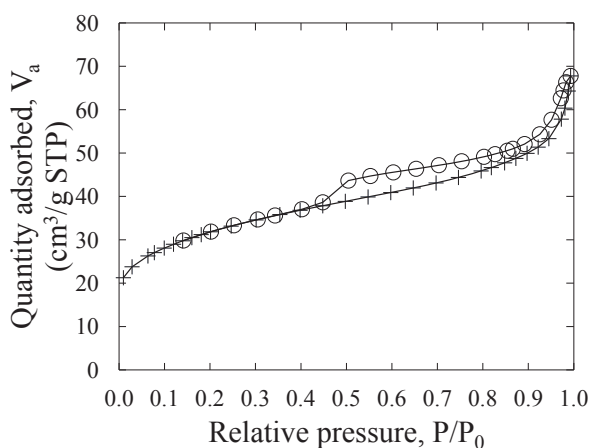


(e) Adsorption and desorption isotherm linear plot for C4.

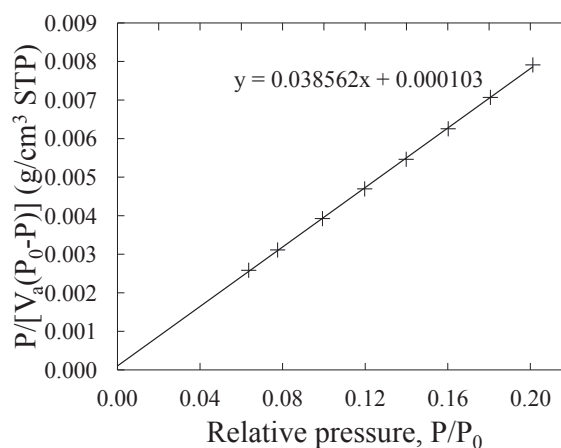


(f) BET surface area plot for C4.

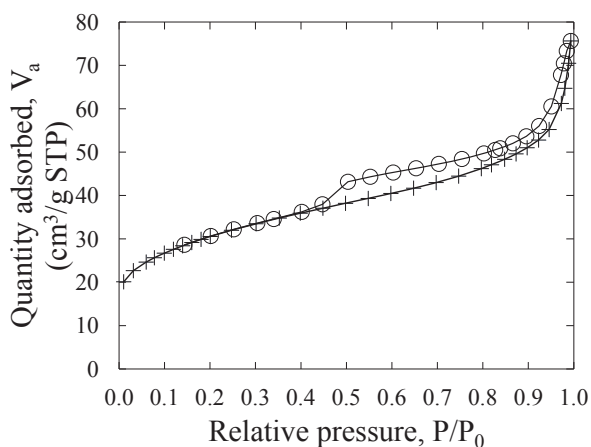
Figure A.8: Volumetric adsorption results for catalyst C4. Parallel runs.



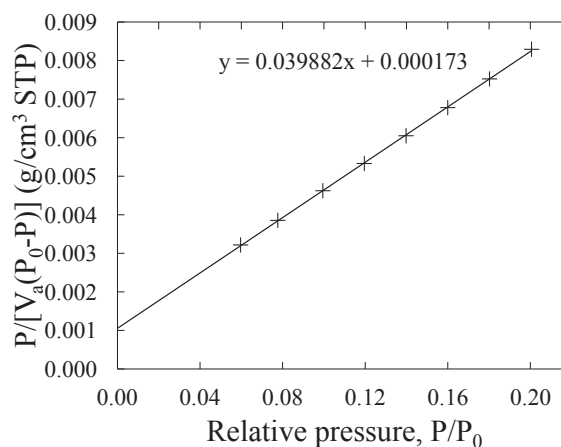
(a) Adsorption and desorption isotherm linear plot for S4. Only calcined.



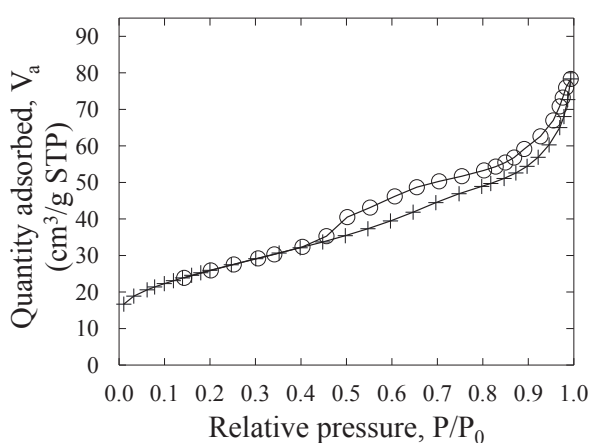
(b) BET surface area plot for S4. Only calcined.



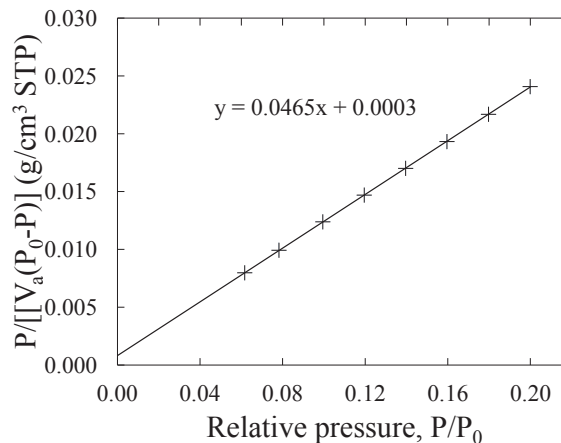
(c) Adsorption and desorption isotherm linear plot for S4. Wetted with water.



(d) BET surface area plot for S4. Wetted with water.

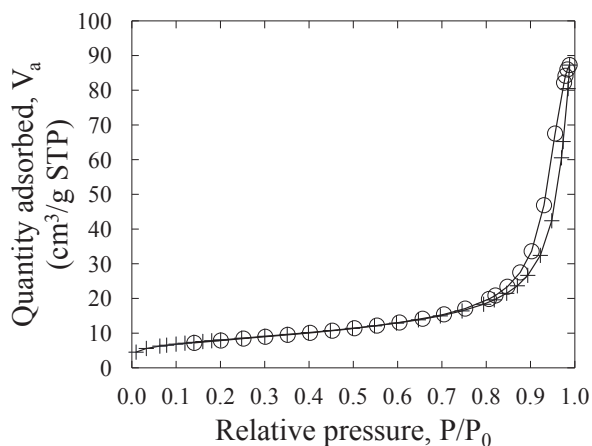


(e) Adsorption and desorption isotherm linear plot for C4. Prolonged drying.

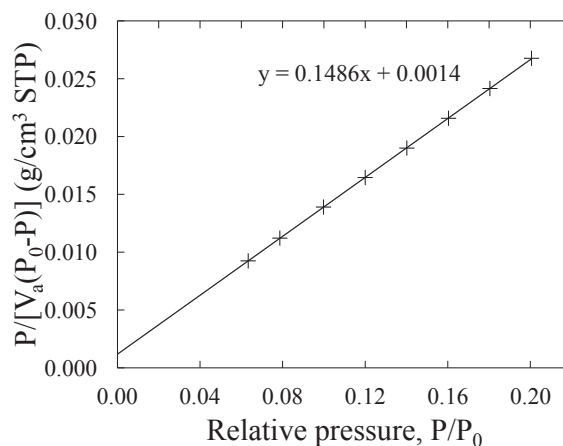


(f) BET surface area plot for C4. Prolonged drying.

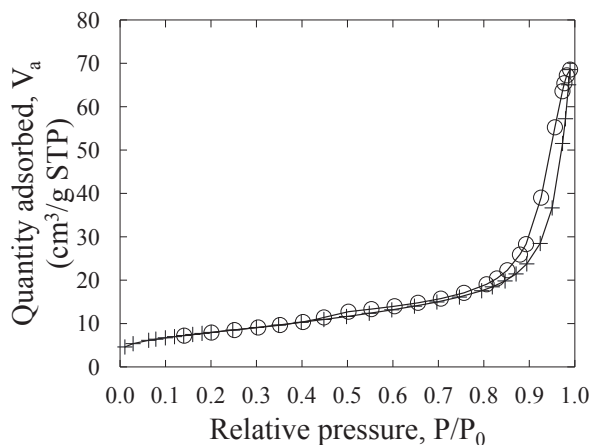
Figure A.9: Volumetric adsorption results for support S4 and catalyst C4. See table 4.2.



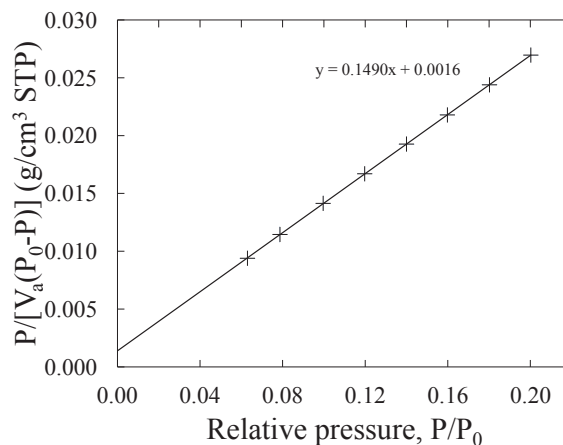
(a) Adsorption and desorption isotherm linear plot for S5.



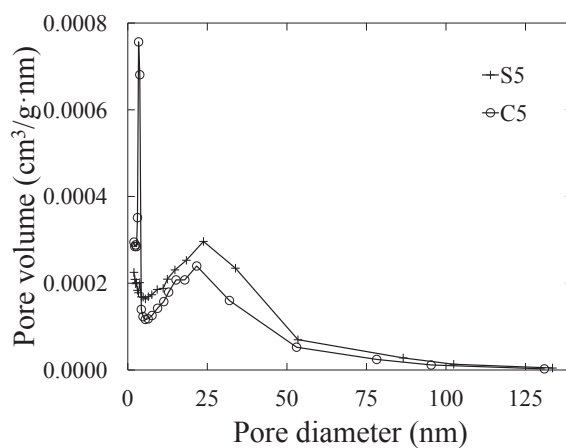
(b) BET surface area plot for S5.



(c) Adsorption and desorption isotherm linear plot for C5.

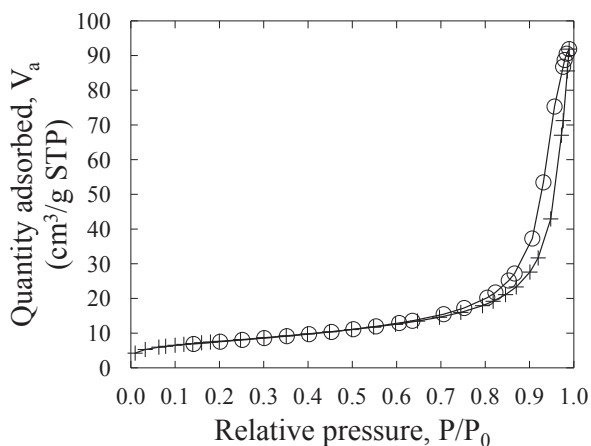


(d) BET surface area plot for C5.

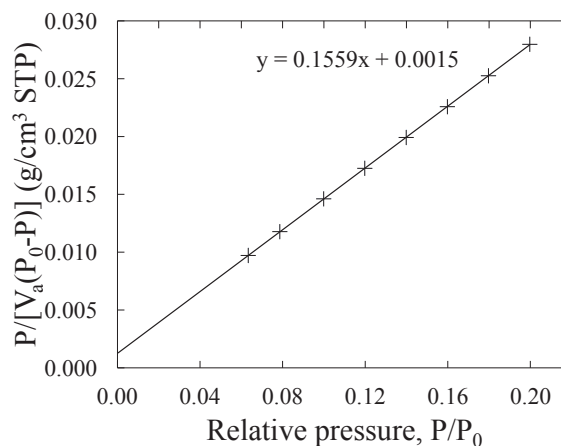


(e) BJH desorption  $dV/dD$  pore volume.

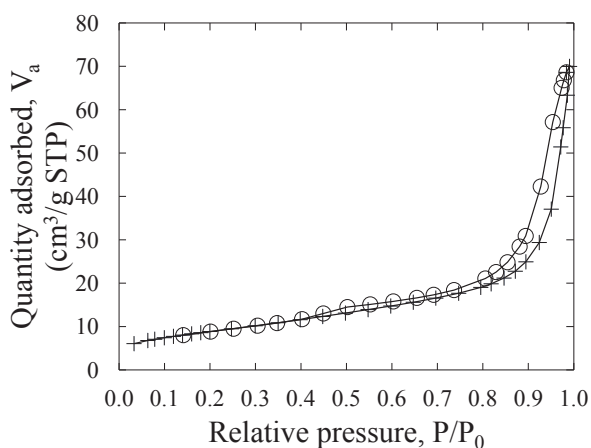
Figure A.10: Volumetric adsorption results for support S5 and catalyst C5.



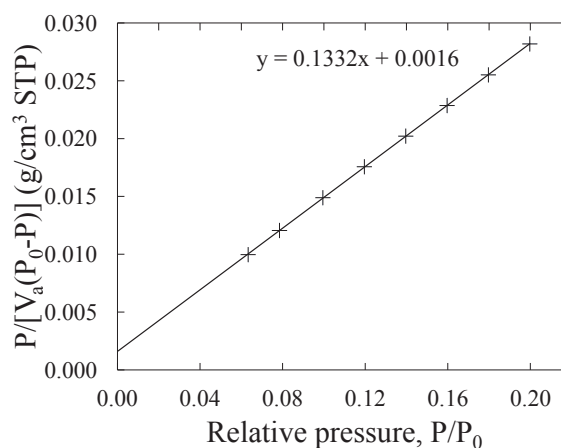
(a) Adsorption and desorption isotherm linear plot for S6.



(b) BET surface area plot for S6.



(c) Adsorption and desorption isotherm linear plot for C6.



(d) BET surface area plot for C6.

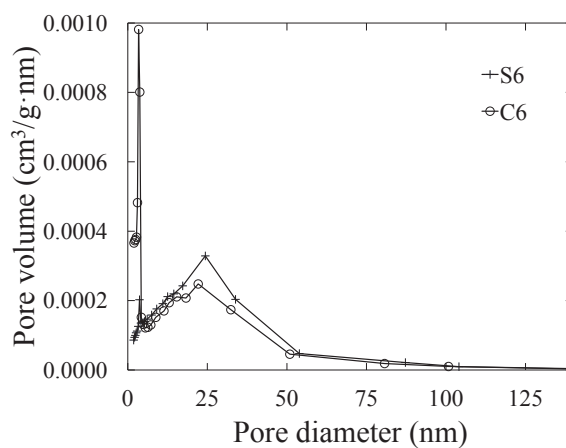
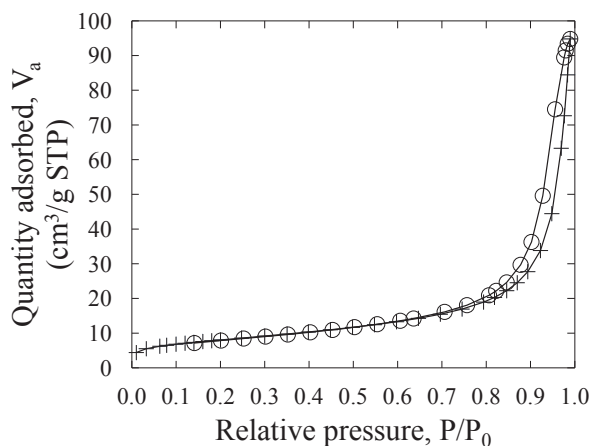
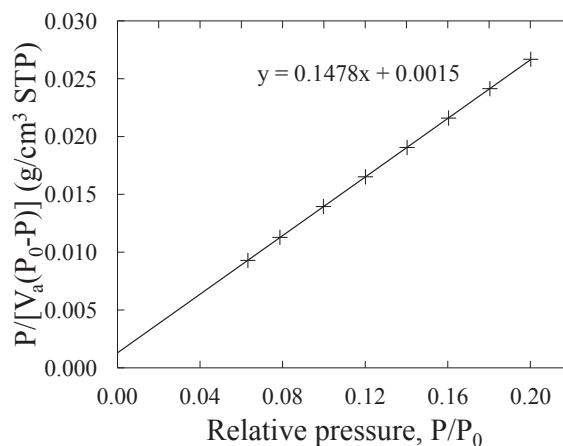
(e) BJH desorption  $dV/dD$  pore volume.

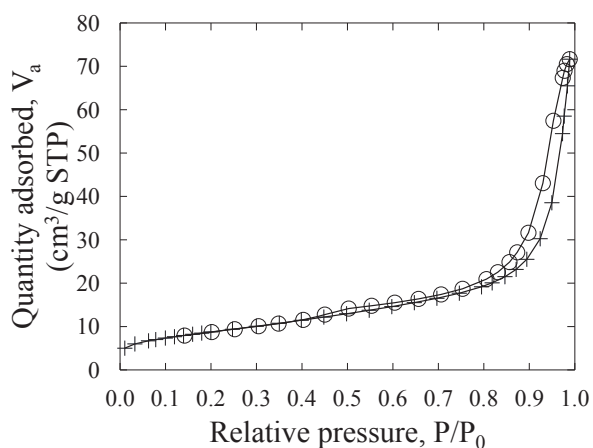
Figure A.11: Volumetric adsorption results for support S6 and catalyst C6.



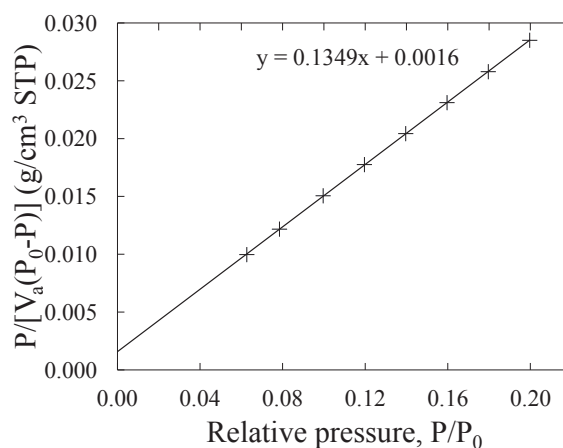
(a) Adsorption and desorption isotherm linear plot for S7.



(b) BET surface area plot for S7.



(c) Adsorption and desorption isotherm linear plot for C7.



(d) BET surface area plot for C7.

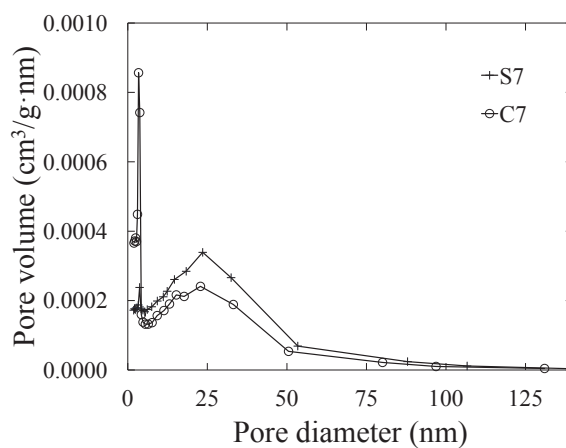
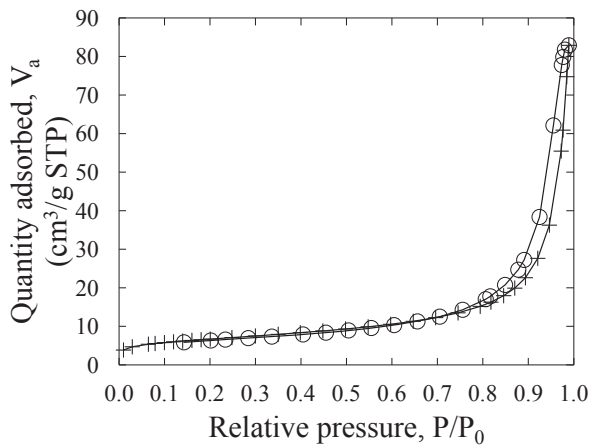
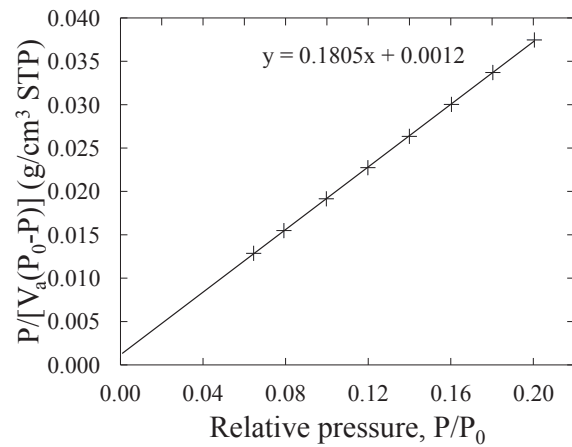
(e) BJH desorption  $dV/dD$  pore volume.

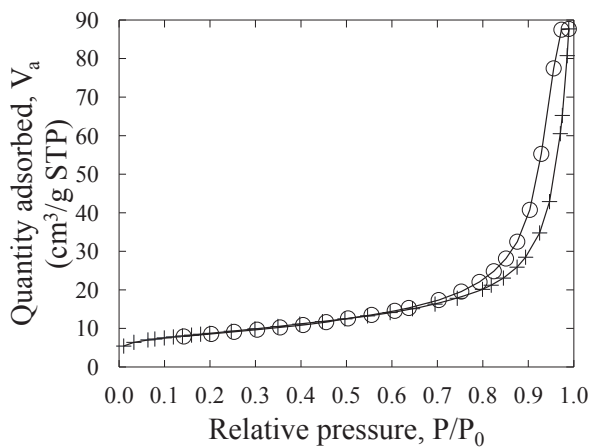
Figure A.12: Volumetric adsorption results for support S7 and catalyst C7.



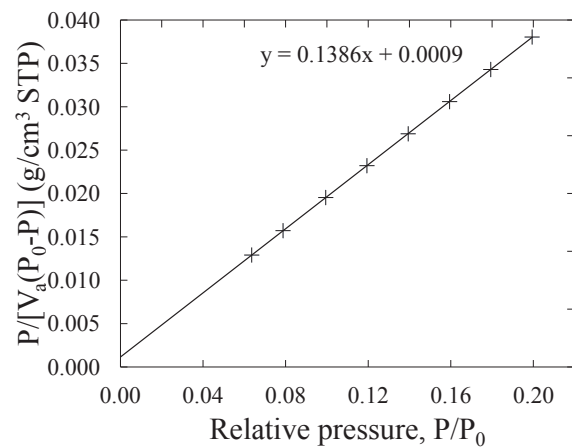
(a) Adsorption and desorption isotherm linear plot for S1.



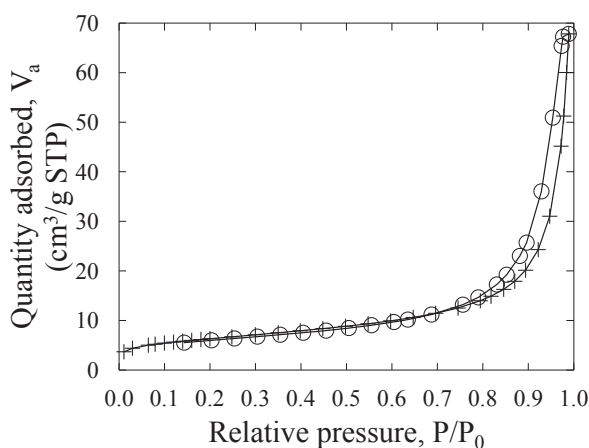
(b) BET surface area plot for S1.



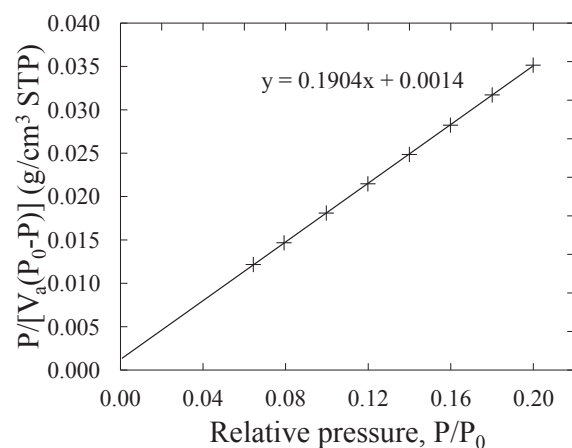
(c) Adsorption and desorption isotherm linear plot for S2.



(d) BET surface area plot for S2.



(e) Adsorption and desorption isotherm linear plot for S3.



(f) BET surface area plot for S3.

Figure A.13: Volumetric adsorption results for supports S1–S3, in extrudate form.



## A.4 Volumetric chemisorption

The collected isotherms from H<sub>2</sub>-chemisorption are presented in figures A.14 through A.17. These were used to calculate the cobalt metal dispersion which is presented in table 4.4.

Volumetric chemisorption experiments were performed with two different *ASAP 2020C* instruments. C1–C4 was analyzed on one, C5–C7 on the other. This is the reason to the difference in number of data point selected between the two groups. However, this should not be of any significance with regards to the experimental results obtained.

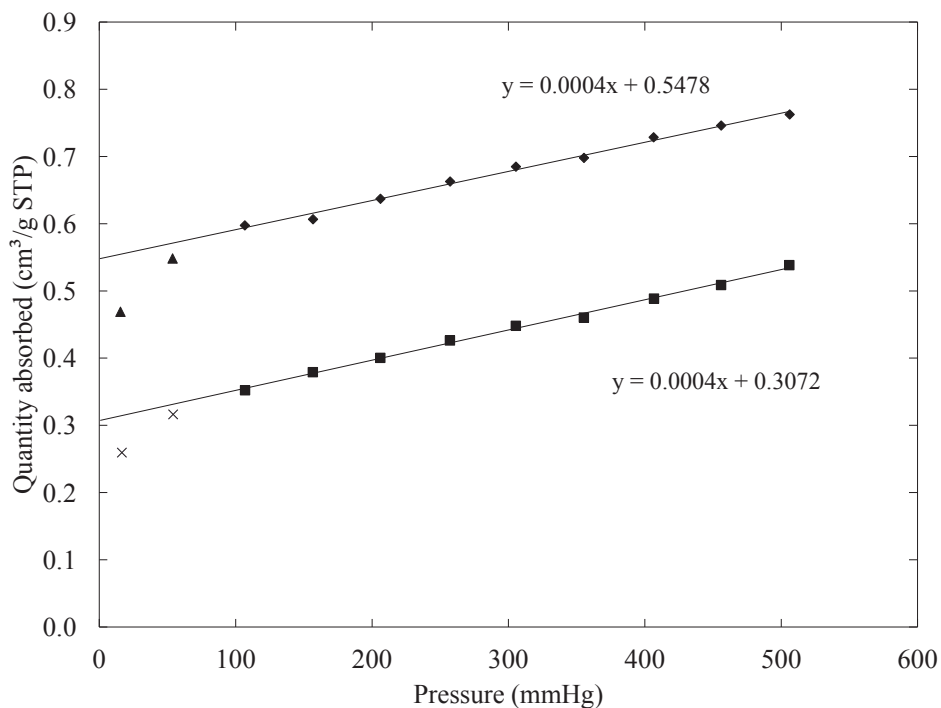
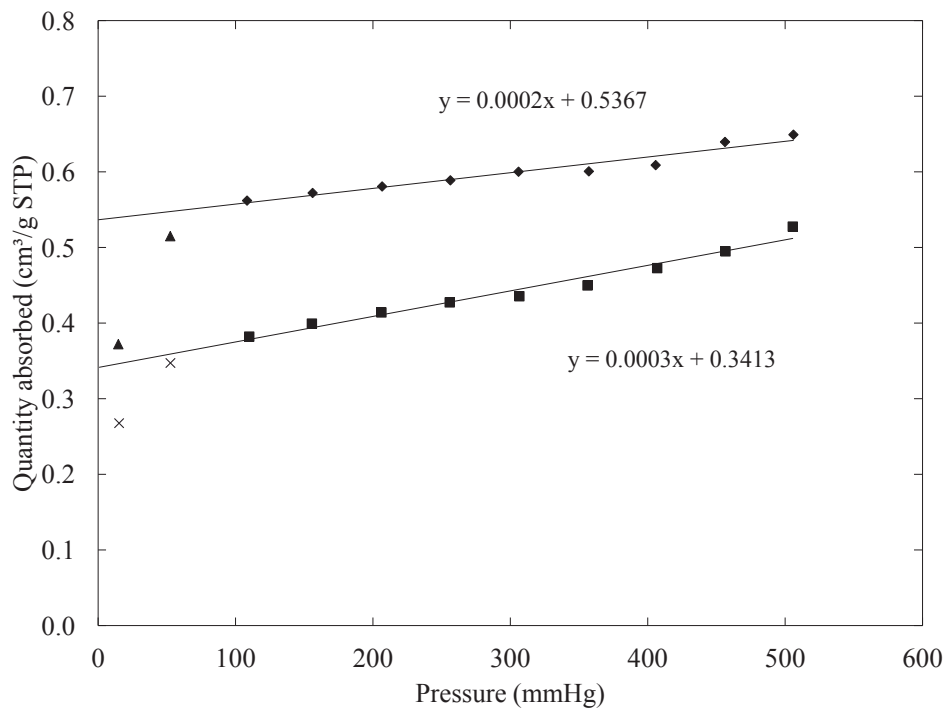
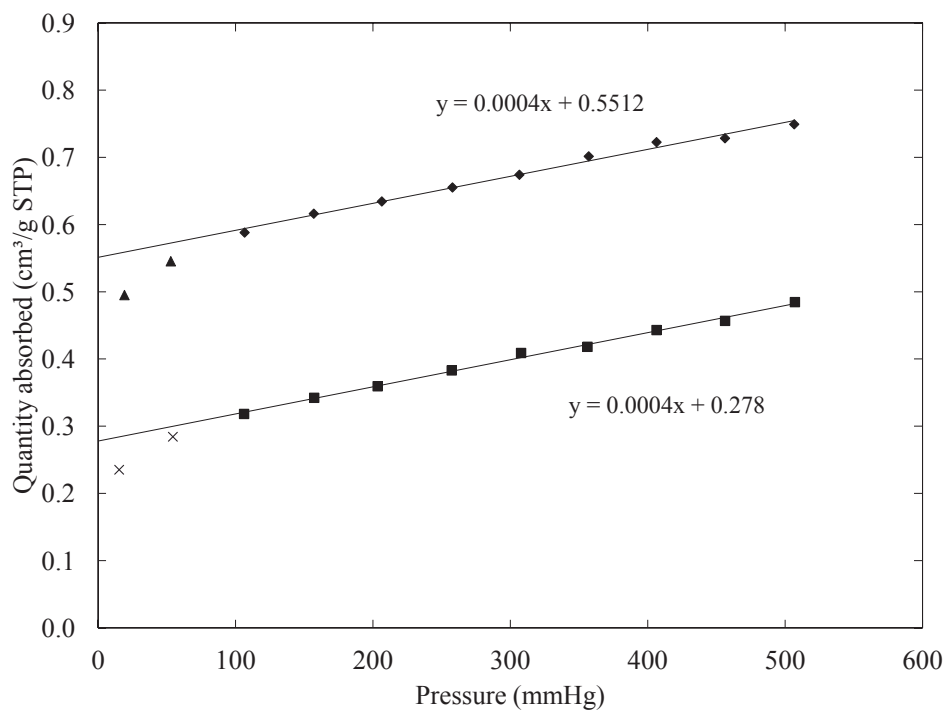


Figure A.14: Adsorption isotherms of catalyst C1. Chemisorption + physisorption (upper isotherm) and physisorption (lower isotherm). ◆■: Selected data points, ▲×: Non-selected data points.

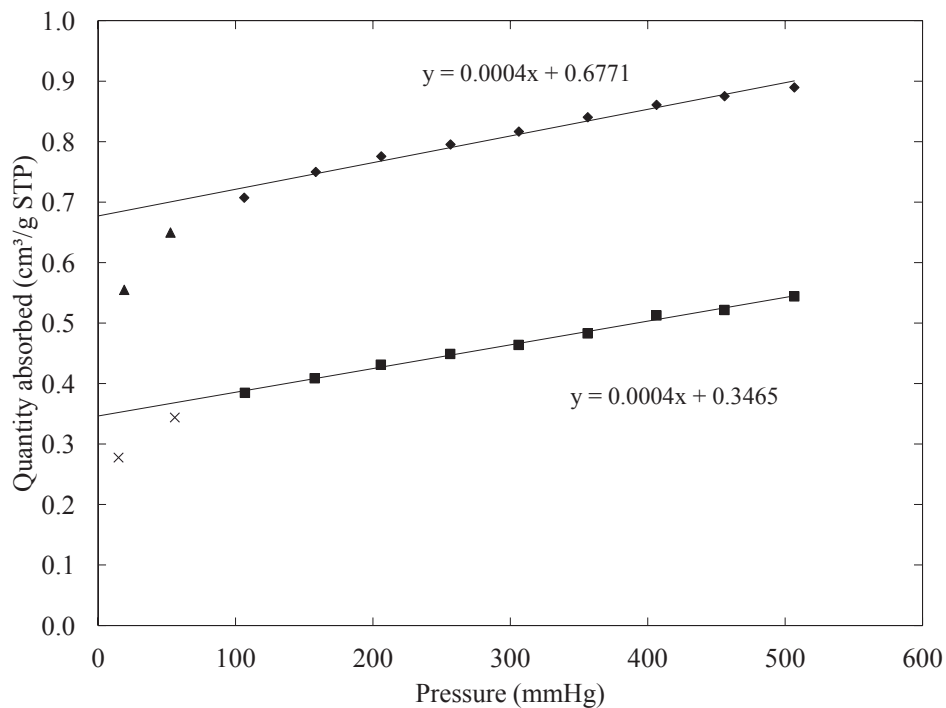


(a) Isotherm plot for C2.

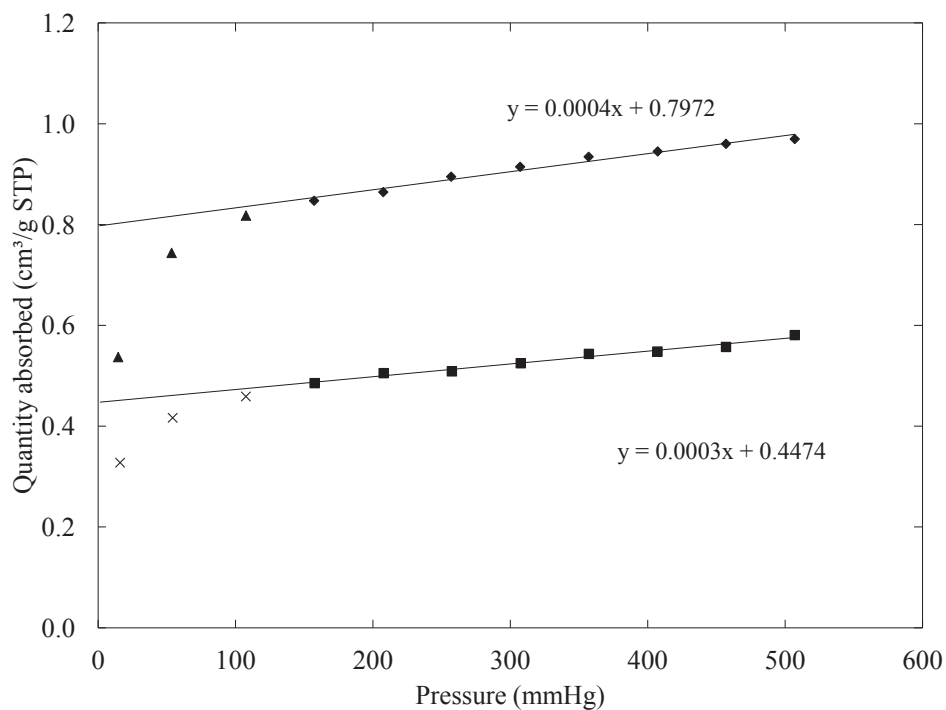


(b) Isotherm plot for C3.

Figure A.15: Adsorption isotherms for catalysts C2 and C3. Chemisorption + physisorption (upper isotherm) and physisorption (lower isotherm). ◆■: Selected data points, ▲×: Non-selected data points.

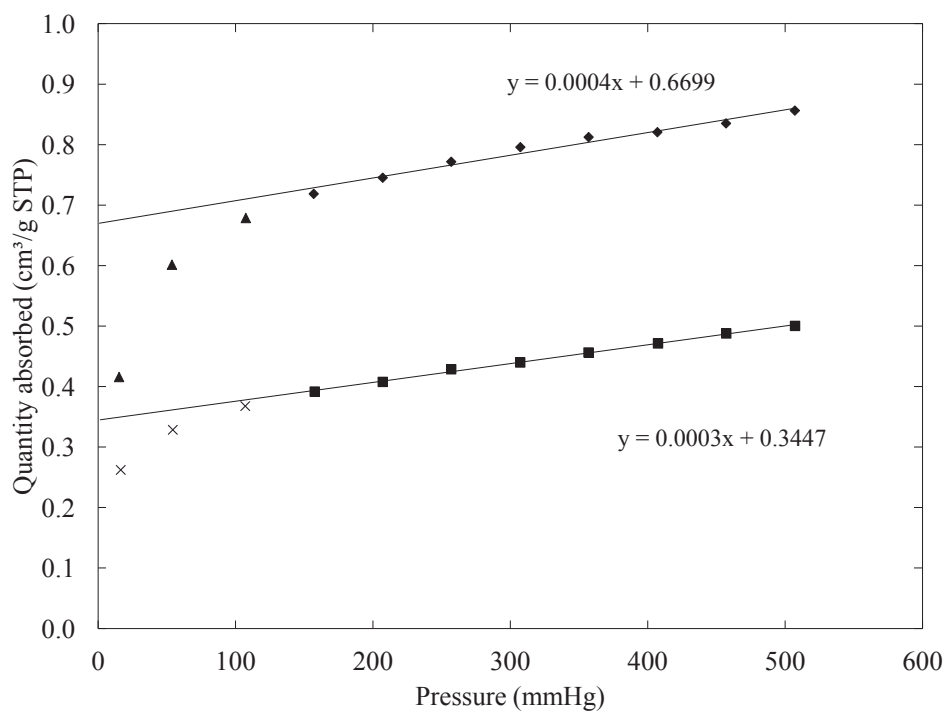


(a) Isotherm for plot C4.

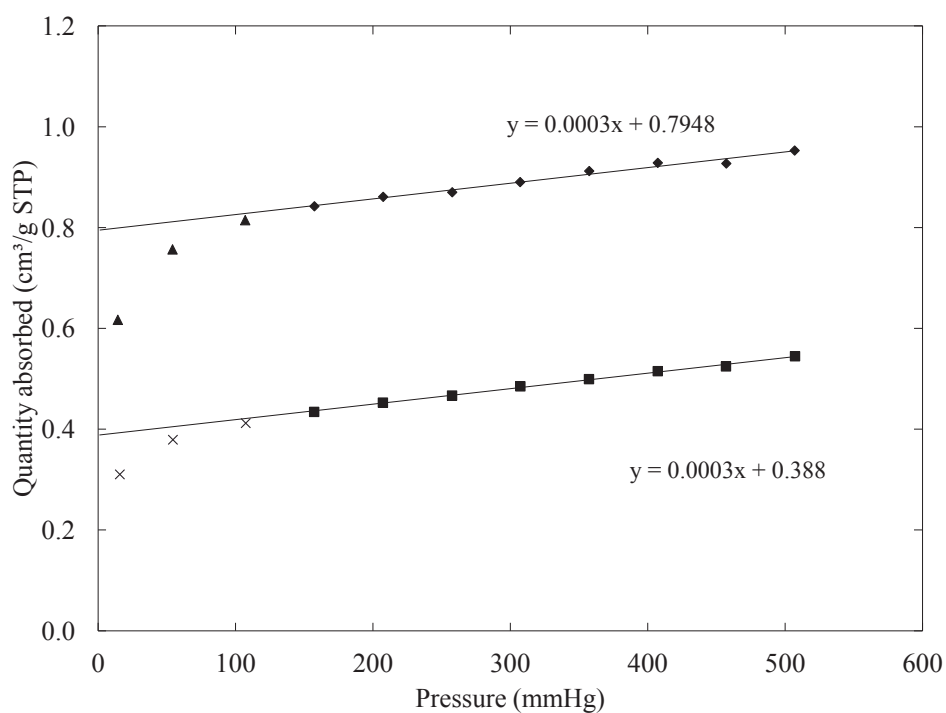


(b) Isotherm for plot C5.

Figure A.16: Adsorption isotherms for catalysts C4 and C5. Chemisorption + physisorption (upper isotherm) and physisorption (lower isotherm). ◆■: Selected data points, ▲×: Non-selected data points.



(a) Isotherm for plot C6.



(b) Isotherm for plot C7.

Figure A.17: Adsorption isotherms for catalysts C6 and C7. Chemisorption + physisorption (upper isotherm) and physisorption (lower isotherm). ◆■: Selected data points, ▲×: Non-selected data points.

# Appendix B

## Example of calculations

This appendix shows examples of how the results were processed and how different calculations were carried out. The full calculations were done in Microsoft Excel. Files can be found on the appended CD-ROM (if there is one). Or, go to <http://daim.idi.ntnu.no>, search for this thesis, and download the .rar file, which contains all excel files.

### B.1 Incipient wetness impregnation

None of the results from the preparation of the catalysts are shown in the report. However, an example of the calculations outlined in chapter 3 section 3.1.3, are given below.

#### Calculations for C1

$$IWP = \frac{m_{Water}}{m_{Support}} = \frac{5.0015g}{3.8562g} = 0.7710$$

$$m_{Support} = m_{Catalyst} \cdot (1 - x_{Co}) = 10.0g \cdot (1 - 0.125) = 8.75g$$

$$m_{Water} = IWP \cdot m_{Support} = 0.7710 \cdot 8.75g = 6.7463g$$

$$m_{Co} = 10.0g \cdot 0.125 = 1.25g$$

$$m_{Co(NO_3)_2 \cdot 6H_2O} = \frac{M_W(Co(NO_3)_2 \cdot 6H_2O)}{M_W(Co)} \cdot m_{Co} = \frac{291.03g/mol}{58.933g/mol} \cdot 1.2500g = 6.1729g$$

## B.2 Volumetric adsorption

The catalyst surface area results presented in chapter 4 table 4.1, were calculated as shown below. Calculations are shown for one of three analysis of C1.

### Calculations for C1

Data points, presented in table B.1, were collected from the report produced by the computer program *TriStar II 3020 V1.03*, and  $\frac{P}{P_0}$  was plotted against  $\frac{P}{V_a(P_0 - P)}$ . Resulting in figure B.1.

Table B.1: Reported values from *TriStar II 3020 V1.03* for calculation of surface area for C1.

Relative pressure, $P/P_0$	Quantity adsorbed, $V_a$ ( $\text{cm}^3/\text{g STP}$ )	$P/[V_a(P_0 - P)]$
0.064086079	5.4872	0.012479
0.078836022	5.7008	0.015013
0.099730735	5.9679	0.018563
0.119979220	6.2067	0.021966
0.140125920	6.4298	0.025345
0.160234004	6.6420	0.028727
0.180295596	6.8491	0.032114
0.200310963	7.0523	0.035518

The values of  $\alpha$  and  $\eta$  was extracted from the equation shown in the figure:  $y = \alpha x + \eta$ . Then these values were used to calculate  $V_0$  by equation 3.7.

$$V_0 = \frac{1}{\alpha + \eta} = \frac{1}{(0.1688 + 0.0017)g/cm^3 STP} = 5.8651cm^3/g STP$$

where  $V_0$  is the volume of adsorbed gas in the first monolayer,  $\alpha$  is the slope [ $g/cm^3 STP$ ] and  $\eta$  is the intersection of the slope with the Y-axis [ $g/cm^3 STP$ ].

Next, the number of molecule in the first monolayer,  $N_0$ , was calculated by equation 3.8.

$$\begin{aligned} N_0 &= \frac{P_{STP} \cdot V_0 \cdot 10^{-6}}{T_{STP} \cdot k_B} \\ &= \frac{101300Pa \cdot 5.8651cm^3/g STP \cdot 10^{-6}m^3/cm^3}{273.15K \cdot 1.38065 \cdot 10^{-23}J/K} = 1.5754 \cdot 10^{20}g^{-1} \end{aligned}$$

where  $N_0$  is the number of molecules adsorbed in the first monolayer,  $P_{STP}$  is the pressure at STP conditions,  $V_0$  is the volume of adsorbed gas in the first monolayer,  $10^{-6}$  is a correction for the volume unit,  $T_{STP}$  is the temperature at STP conditions and  $k_B$  [4] is the Boltzmann constant.

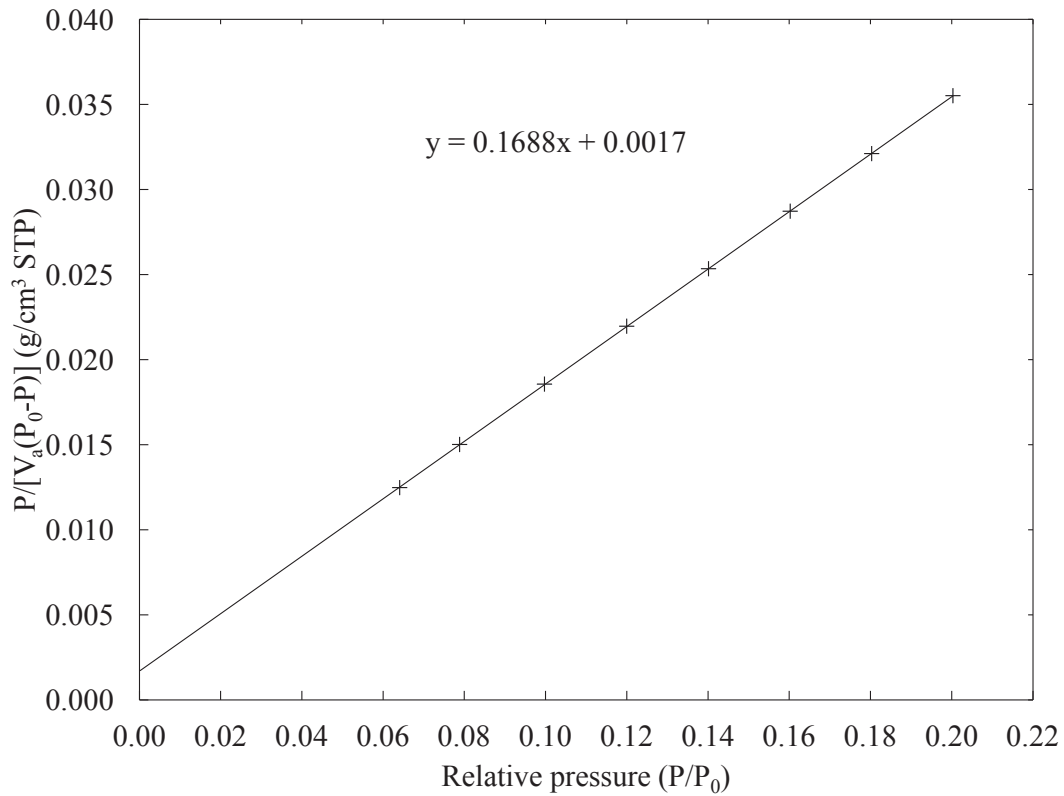


Figure B.1: BET surface area plot for C1.

Finally, the surface area was calculated by equation 3.9.

$$A_{BET} = N_0 \cdot A_0 = 1.5754 \cdot 10^{20} g^{-1} \cdot 16.2 \cdot 10^{-20} m^2 = 25 m^2$$

where  $A_{BET}$  is the BET surface area,  $N_0$  is the number of molecules adsorbed in the first monolayer and  $A_0$  is the surface area a nitrogen gas molecule occupies at the analysis conditions (77.15 K).

## Calculation of experimental uncertainty for C2

Three parallel analyses of C2 were used to calculate the experimental uncertainty of the BET surface area results. The calculations were performed as outlined below.

$$\bar{x} = \frac{x_1 + x_2 + x_3}{3} = \frac{(30.20 + 32.11 + 31.76)m^2/g}{3} = 31.36 m^2/g$$

where  $\bar{x}$  is the average surface area and  $x_i$  is the surface area from the different analyses.

Next, the deviation from the average value was calculated for each analysis. Calculation is shown for analysis nr. 1.

$$(x_1 - \bar{x}) = (30.20 - 31.36)m^2/g = -1.16 m^2/g$$

where  $\bar{x}$  is the average surface area and  $x_1$  is the surface area from analysis nr. 1.

The standard deviation was then calculated as follows.

$$\sigma = \sqrt{\frac{\sum (x_i - \bar{x})^2}{n - 1}} = \sqrt{\frac{((-1.16)^2 + 0.57^2 + 0.16^2)m^2/g}{3 - 1}} = 1.02m^2/g$$

where  $\sigma$  is the standard deviation,  $\bar{x}$  is the average surface area,  $x_i$  is the surface area from the different analyses and  $n$  is the number of analyses.

Finally, the experimental uncertainty was reported as two times standard deviation.

$$2\sigma = 2 \cdot 1.02m^2/g = 2.04 \approx 2m^2/g$$

where  $\sigma$  is the standard deviation.

### B.3 Volumetric chemisorption

The H<sub>2</sub>-chemisorption results presented in chapter 4 table 4.4, were calculated as outlined below.

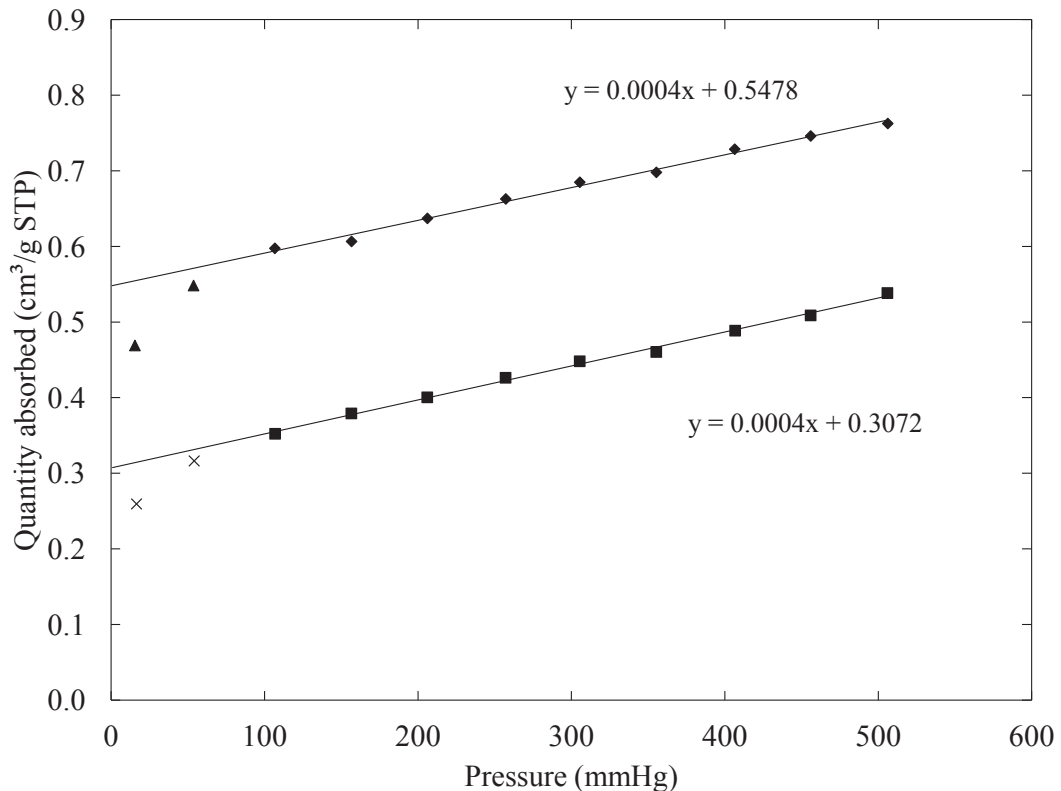


Figure B.2: Adsorption isotherms for catalyst C1. Chemisorption + physisorption (upper isotherm) and physisorption (lower isotherm). ◆■: Selected data points, ▲×: Non-selected data points.



## Metal dispersion for C1

Data points, presented in table B.2, were collected from the report produced by the computer program *ASAP 2020C v1.09*. The data points were plotted, resulting in figure B.2

Table B.2: Reported values from *ASAP 2020C v1.09* for calculation of dispersion from volumetric chemisorption for C1.

Pressure (mmHg)	Quantity adsorbed (cm <sup>3</sup> /g STP)	Pressure (mmHg)	Quantity adsorbed (cm <sup>3</sup> /g STP)
19.0110	0.5550	14.8532	0.2776
52.6659	0.6497	55.7995	0.3439
106.3453	0.7073	106.8201	0.3847
158.3979	0.7499	157.6105	0.4088
206.0546	0.7756	205.7348	0.4312
256.4439	0.7953	256.2096	0.4490
306.1768	0.8166	305.9677	0.4639
356.3365	0.8403	356.2463	0.4830
406.3944	0.8608	406.2924	0.5127
455.8957	0.8751	455.8354	0.5217
506.6933	0.8896	506.6207	0.5442

The selected data points (chosen by *ASAP 2020C v1.09*) were fitted with linear regression. Then the intersection of the slope with the Y-axis was found from the equations showing in the figure. The chemisorption + physisorption isotherm was used for the calculations.

The intersection with the Y-axis gives the adsorbed volume,  $v_{ads}$ , which had to be converted from cm<sup>3</sup>/g STP to mol/g STP.

$$\begin{aligned}
 v_{ads,mol} &= v_{ads,cm^3} \cdot \frac{P}{R \cdot T} \\
 &= 0.5478 \text{cm}^3/\text{g}[STP] \cdot \frac{10^5 \text{Pa}}{8.314 \text{J/K mol} \cdot 273.15 \text{K} \cdot 10^6 \text{cm}^3/\text{m}^3} = 2.4122 \cdot 10^{-5} \text{mol/g}[STP]
 \end{aligned}$$

where R = gas constant, P = pressure and T = temperature, the latter two at STP conditions.

Equation 3.10 was used to calculate the cobalt dispersion.

$$\begin{aligned}
 D_{H_2,ads} &= \frac{v_{ads} \cdot M_W(Co) \cdot F}{x_m} \\
 &= \frac{2.4122 \cdot 10^{-5} \text{mol/g}[STP] \cdot 58.933 \text{g/mol} \cdot 2}{0.125} = 0.02275 n_{surface}/n_{tot}
 \end{aligned}$$

where  $D_{H_2,ads}$  is the dispersion of cobalt on the support,  $v_{ads}$  is the adsorbed amount of H<sub>2</sub>,  $M_W(Co)$  is the molecular mass,  $F$  is the adsorption stoichiometry and  $x_m$  is the mass fraction.

## Average metal particle size for C1

Average metal particle size was calculated by equation 3.14, as follows.

$$\begin{aligned}
 d_{H_2,ads} &= \frac{f \cdot M_W}{\sigma \cdot \rho \cdot N_A \cdot D_{H_2,ads}} \\
 &= \frac{6 \cdot 58.933g/mol}{6.85cm^2 \cdot 8.9g/cm^3 \cdot 6.022 \cdot 10^{23}mol^{-1} \cdot 0.02275 \cdot 10^7nm/cm} \\
 &= 42.3nm
 \end{aligned}$$

where  $d_{H_2,ads}$  is the metal particle size,  $f$  is a factor describing the particle shape,  $\rho = 8,9[g/cm^3]$  is the density,  $\sigma$  is the average surface area occupied by a surface atom,  $N_A$  is Avogadro's number,  $M_W$  is the molecular mass and  $D_{H_2,ads}$  is the dispersion.

## B.4 X-ray diffraction

The XRD results presented in chapter 4 table 4.4, were calculated as outlined below.

### Average cobalt metal particle size for C1

Cobalt oxide average particle diameter was converted to cobalt metal average particle diameter by equation 3.15.

$$\begin{aligned}
 d_{XRD}(Co^0) &= 0.75 \cdot d_{XRD}(Co_3O_4) \\
 &= 0.75 \cdot 23.7nm \\
 &= 17.7nm
 \end{aligned}$$

where  $d_{XRD}(Co^0)$  is the average particle size of cobalt metal and  $d_{XRD}(Co_3O_4)$  is the average particle size of cobalt oxide.

From the cobalt metal average particle size, the cobalt metal dispersion was calculated by equation 3.17.

$$\begin{aligned}
 D_{XRD} &= \frac{99.66}{d_{XRD}(nm)} \\
 &= \frac{99.66}{17.7} \\
 &= 5.54\%
 \end{aligned}$$

where  $D_{XRD}$  is the cobalt dispersion and  $d_{XRD}(Co^0)$  is the average particle size of cobalt metal.

## B.5 Fischer-Tropsch synthesis

The use of the equations given in chapter 3 section 3.3, to calculate the FTS results, are outlined below. Since the full calculations would take up too much space here, only necessary calculations needed to show the use of each equation are showed.

### Calculations for C1

At first, the CO/N<sub>2</sub> ratio in the syngas feed bottle was calculated. The nine last analysis from the GC was calculated, and the average value of these was used.

$$\begin{aligned}
 R_{CO/N_2,in} &= \frac{1}{10} \cdot \sum_{i=1}^{10} \frac{A_{CO,i}}{A_{N_2,i}} \\
 &= \frac{\frac{86.4337}{9.2026} + \frac{86.4395}{9.1995} + \frac{86.4454}{9.1998} + \frac{86.4373}{9.2050} + \frac{86.4505}{9.1983} + \frac{86.2831}{9.1811} + \frac{86.4529}{9.1932} + \frac{86.4604}{9.1881} + \frac{86.4588}{9.1895}}{10} \\
 &= 9.3994
 \end{aligned}$$

where  $R_{CO/N_2,in}$  is the CO/N<sub>2</sub> feed ratio,  $A_{CO}$  and  $A_{N_2}$  are the peak area of the respective compound from the GC TCD signal, and  $i$  denotes one of the ten last GC analyses.

Next, the mole fractions of CO and H<sub>2</sub> in the syngas was calculated. The GC TCD response factors are shown in chapter 3 table 3.4.

$$\chi_{CO} = \chi_{N_2} \cdot R_{CO/N_2,in} \cdot \frac{f_{N_2}}{f_{CO}} = 0.0322 \cdot 9.3994 \cdot \frac{616.70}{619.38} = 0.3013$$

$$\chi_{H_2} = 1 - \chi_{CO} - \chi_{N_2} = 1 - 0.3013 - 0.0322 = 0.6665$$

where  $\chi_{CO}$ ,  $\chi_{N_2}$  and  $\chi_{H_2}$  are component mole fractions in the feed flow,  $f_{N_2}$  and  $f_{CO}$  are the response factors of the two components in the GC.

Feed flow rates of CO were calculated by equations 3.21 and 3.22.

$$\dot{V}_{CO,in} = \dot{V}_{tot,in} \cdot \chi_{CO} = 9000.0 \text{ ml/h} \cdot 0.3013 = 2711.7 \text{ ml/h}$$

$$\dot{F}_{CO,in} = \frac{\dot{V}_{CO,in}}{m_{cat} \cdot V_m^{i.g.}} = \frac{2711.7 \text{ ml/h}}{1.9939 \text{ g} \cdot 22414 \text{ ml/mol}} = 6.068 \cdot 10^{-2} \text{ mol/g}_{cat} \text{ h}$$

where  $\dot{V}_{CO,in}$  is the feed flow rate of CO,  $\dot{V}_{tot,in}$  is the total feed flow rate,  $\chi_{CO}$  is the CO mole fraction,  $\dot{F}_{CO,in}$  is the feed flow rate of CO,  $m_{cat}$  is the amount of catalyst used,  $V_m^{i.g.}$  is the molar volume of ideal gas at 273.15 K and 1 atm.

Feed flow rates of N<sub>2</sub> were equally calculated by equations 3.21 and 3.22.

$$\dot{V}_{N_2,in} = \dot{V}_{tot,in} \cdot \chi_{N_2} = 9000.0ml/h \cdot 0.0322 = 289.8ml/h$$

$$\dot{F}_{N_2,in} = \frac{\dot{V}_{N_2,in}}{m_{cat} \cdot V_m^{i.g.}} = \frac{289.8ml/h}{1.9939g \cdot 22414ml/mol} = 6.484 \cdot 10^{-3}mol/g_{cat}h$$

where  $\dot{V}_{N_2,in}$  is the feed flow rate of  $N_2$ ,  $\dot{V}_{tot,in}$  is the total feed flow rate,  $\chi_{N_2}$  is the  $N_2$  mole fraction,  $\dot{F}_{N_2,in}$  is the feed flow rate of  $N_2$ ,  $m_{cat}$  is the amount of catalyst used,  $V_m^{i.g.}$  is the molar volume of ideal gas at 273.15 K and 1 atm.

Exit flow rate of CO was calculated by equation 3.23, and represents the calculation for components detected in the TCD. Calculations are shown for analysis number five for C1 from now on, to give representative values.

$$\begin{aligned} \dot{F}_{CO,out} &= \dot{F}_{N_2,in} \cdot \frac{f_{N_2} \cdot A_{CO}}{f_{CO} \cdot A_{N_2}} \\ &= 6.484 \cdot 10^{-3}mol/g_{cat}h \cdot \frac{616.70 \cdot 14266.5}{619.38 \cdot 1655.6} = 5.563 \cdot 10^{-2}mol/g_{cat}h \end{aligned}$$

where  $\dot{F}_{CO,out}$  is the exit flow rate of CO,  $\dot{F}_{N_2,in}$  is the  $N_2$  feed flow rate,  $f$  is the GC TCD response factors and  $A$  is the GC TCD peak area.

Exit flow rate of  $CH_4$  was calculated by equation 3.23.

$$\begin{aligned} \dot{F}_{CH_4,out} &= \dot{F}_{N_2,in} \cdot \frac{f_{N_2} \cdot A_{CH_4}}{f_{CH_4} \cdot A_{N_2}} \\ &= 6.484 \cdot 10^{-3}mol/g_{cat}h \cdot \frac{616.70 \cdot 125.1}{469.50 \cdot 1655.6} = 6.436 \cdot 10^{-4}mol/g_{cat}h \end{aligned}$$

where  $\dot{F}_{CH_4,out}$  is the exit flow rate of  $CH_4$ ,  $\dot{F}_{N_2,in}$  is the  $N_2$  feed flow rate,  $f$  is the GC TCD response factors and  $A$  is the GC TCD peak area.

Exit flow rate of ethane was calculated by equation 3.24, and represents the calculation for components detected in the FID.

$$\begin{aligned} \dot{F}_{ethane,out} &= \dot{F}_{CH_4,out} \cdot \frac{A_{ethane}}{A_{CH_4} \cdot n_C} \\ &= 6.436 \cdot 10^{-4}mol/g_{cat}h \cdot \frac{50.0}{339.1 \cdot 2} = 4.745 \cdot 10^{-5}mol/g_{cat}h \end{aligned}$$

where  $\dot{F}_{ethane,out}$  is the exit flow rate of ethane,  $\dot{F}_{CH_4,out}$  is the methane exit flow,  $A$  is the GC FID peak area,  $n_C$  is the number of carbon atoms in the given component.

Conversion of CO was calculated by equation 3.25, as follows.

$$\begin{aligned}
 X_{CO} &= \frac{\dot{F}_{CO,in} - \dot{F}_{CO,out}}{\dot{F}_{CO,in}} \\
 &= \frac{6.068 \cdot 10^{-2} \text{mol/g}_{cat}h - 5.563 \cdot 10^{-2} \text{mol/g}_{cat}h}{6.068 \cdot 10^{-2} \text{mol/g}_{cat}h} = 0.08322
 \end{aligned}$$

where  $X_{CO}$  is the conversion of CO,  $\dot{F}_{CO,in}$  is the CO feed flow rate and  $\dot{F}_{CO,out}$  is the CO exit flow rate.

Selectivity to CH<sub>4</sub> and CO<sub>2</sub> were calculated by equation 3.26. These were the components detected in the TCD, calculation for CH<sub>4</sub> is shown below.

$$\begin{aligned}
 S_{CH_4} &= \frac{\dot{F}_{CH_4,out} \cdot m_{cat} \cdot V_m^{i.g.}}{\dot{V}_{CO,in} \cdot X_{CO}} \cdot 100 \\
 &= \frac{6.436 \cdot 10^{-4} \text{mol/g}_{cat}h \cdot 1.9939g \cdot 22414 \text{ml/mol}}{2711.7 \text{ml/h} \cdot 0.08322} \cdot 100 = 12.74\%
 \end{aligned}$$

where  $S_{CH_4}$  is the selectivity to CH<sub>4</sub>,  $\dot{F}_{CH_4,out}$  is the exit flow rate of CH<sub>4</sub>,  $m_{cat}$  is the amount of catalyst used,  $V_m^{i.g.}$  is the molar volume of ideal gas at 273.15 K and 1 atm,  $\dot{V}_{CO,in}$  is the feed flow of CO and  $X_{CO}$  is the conversion of CO.

Selectivity to ethane was calculated by equation 3.27, and represents the calculation for C<sub>2</sub>–C<sub>4</sub> components detected in the FID.

$$\begin{aligned}
 S_{ethane} &= \frac{\dot{F}_{ethane,out} \cdot m_{cat} \cdot V_m^{i.g.} \cdot n_C}{\dot{V}_{CO,in} \cdot X_{CO}} \cdot 100 \\
 &= \frac{4.745 \cdot 10^{-5} \text{mol/g}_{cat}h \cdot 1.9939g \cdot 22414 \text{ml/mol} \cdot 2}{2711.7 \text{ml/h} \cdot 0.08322} \cdot 100 = 1.88\%
 \end{aligned}$$

where  $S_{ethane}$  is the selectivity to ethane,  $\dot{F}_{ethane,out}$  is the exit flow rate of ethane,  $m_{cat}$  is the amount of catalyst used,  $V_m^{i.g.}$  is the molar volume of ideal gas at 273.15 K and 1 atm,  $n_C$  is the number of carbon atoms in ethane,  $\dot{V}_{CO,in}$  is the feed flow of CO and  $X_{CO}$  is the conversion of CO.

The calculation for the C<sub>5+</sub> selectivity by equation 3.28 is rather trivial, and will not be shown here.

Reaction rate of CO was calculated by equation 3.29, as follows.

$$\begin{aligned}
 -r_{CO} &= \frac{\dot{V}_{CO,in} \cdot X_{CO}}{m_{cat} \cdot V_m^{i.g.}} \\
 &= \frac{2711.7 \text{ml/h} \cdot 0.08322}{1.9939g \cdot 22414 \text{ml/mol}} = 5.049 \cdot 10^{-3} \text{molCO/g}_{cat}h
 \end{aligned}$$

where  $-r_{CO}$  is the reaction rate of CO being consumed,  $\dot{V}_{CO,in}$  is the feed flow of CO,  $X_{CO}$  is the conversion of CO,  $m_{cat}$  is the amount of catalyst used and  $V_m^{i.g.}$  is the molar volume of ideal gas at 273.15 K and 1 atm.

Turnover frequency (TOF) was calculated by equation 3.30 [41], as follows.

$$\begin{aligned} TOF &= \frac{-r_{CO} \cdot M_W(Co)}{D_{H_2,ads} \cdot X_{CO} \cdot 3600} \\ &= \frac{5.049 \cdot 10^{-3} \text{ molCO}/g_{cat}h \cdot 58.933g/mol}{0.023 \cdot 0.08322 \cdot 3600s/h} = 0.029s^{-1} \end{aligned}$$

where  $TOF$  is the turnover frequency,  $-r_{CO}$  is the reaction rate of CO,  $M_W(Co)$  is the molecular weight of cobalt,  $D_{H_2,ads}$  is the cobalt dispersion calculated in section B.3,  $X_{CO}$  is the conversion of CO and 3600 converts hours to seconds.

The GC analyzed the exit flow of gas components from each of the two parallel reactors every 1.7 hours. Thus, equations 3.23–3.30 were repeated for all analyses from the GC.

# Appendix C

## Poster presentation

Results from the work of this thesis was presented on the 15<sup>th</sup> *Nordic Symposium on Catalysis* by *Andreas H. Lillebø* [53]. The conference was held in Mariehamn, Åland, from June 10<sup>th</sup> to June 12<sup>th</sup> 2012.

The poster, made by *Andreas H. Lillebø*, is appended on the following page.





# SiC as support material for Co-based Fischer-Tropsch catalysts



A. H. Lillebø<sup>1,\*</sup>, Sindre Håvik<sup>1</sup>, E. A. Blekkan<sup>1</sup>, A. Holmen<sup>1</sup>

<sup>1</sup> Department of Chemical Engineering, Norwegian University of Science and Technology (NTNU), NO-7491 Trondheim, Norway

\* Contact e-mail: [andreli@chemeng.ntnu.no](mailto:andreli@chemeng.ntnu.no)

## INTRODUCTION

Porous  $\beta$ -SiC has been proposed as a catalyst support [1], and due to favorable properties (mechanical strength, heat conductivity, weak interaction with the active metal) it has also been tried as a support for Fischer-Tropsch catalysts. Recent studies have reported high  $C_{5+}$  selectivities (above 90%) and superior activity compared to other supports [1-3]. In this paper we present new results comparing porous SiC with  $\gamma$ -Al<sub>2</sub>O<sub>3</sub> as a support for cobalt FTS catalysts.

Table 1

Sample		C1-Catalyst	C1-support
Parameter	Unit	KA-065294	KA-065295
Ca	%	<0.05	<0.05
Fe	%	0.19	0.24
Na	%	<0.010	<0.010
P	%	0.011	0.015
S	%	<0.02	<0.02

Table 1: This table displays the results from ICP elemental analysis.

## Experimental

Seven types of SiC support with different surface area, pore volume and preparation procedure were provided in pellet form by SICAT [4]. The samples were crushed and sieved to a particle range of 53-90  $\mu$ m before impregnation with Co(NO<sub>3</sub>)<sub>2</sub>·6H<sub>2</sub>O by incipient wetness impregnation to achieve 12.5 wt% Co loading. The catalyst samples were dried in air at 383 K and calcined in flowing air at 573 K. H<sub>2</sub>-chemisorption was done at 313 K after reduction at 623K for 16 h before analysis. TPR was performed with 7% H<sub>2</sub> in Ar and ramp rate of 10 K/min. FT-synthesis was performed in a fixed bed reactor at 483 K, 20 bar, 2,1 H<sub>2</sub>/CO ratio and at a flow rate of 150 NmL/min. The catalyst (2g) was diluted with 15g SiC (75 – 150  $\mu$ m) in order to improve the heat distribution and reduced in flowing H<sub>2</sub> for 16 h at 623 K before FT-synthesis. Only 0.2 g of the reference catalyst (20 wt% Co on  $\gamma$ -alumina) were loaded in order to obtain comparable CO conversion.

## Results/Discussion

Activities for the SiC samples compared to the reference sample, both in terms of reaction rate per g Co and site time yields (TOF) are considerably lower. However, the  $C_{5+}$  selectivities are higher when comparing with the conventional support. The rather low  $C_{5+}$  selectivities found here are linked with the low CO conversion and should not be compared to results obtained at higher conversions. These results differ from previous reports and are surprising, but we propose that the difference can be linked with the presence of impurities in the support material.

We have previously reported the loss of activity due to ppm levels of impurities (e.g. Na and Ca) on Co catalysts [5]. The data on the effect of sodium and calcium in figure 1 is from our previous work, which have been done on the same catalyst as the reference catalyst in this study. Assuming that the TOF of a uncontaminated SiC catalyst and our reference catalyst would be the same, we plotted catalyst C1, C2, C4 and C5 into Figure 1 to estimate how much sodium is needed to cause an equal lowering of TOF as in our reference sample. From table 1 we can see that there is less than 100 ppm sodium and 500 ppm Ca in catalyst C1. Considering the much lower Co surface area per gram of catalyst in our SiC samples it is not unreasonable that these amounts of alkali and earth alkali elements could be responsible for the much lower catalytic activity observed in the SiC samples. An effect on activity caused by alkali natively present in  $\gamma$ -alumina support have been reported earlier [6]. The support used for our reference sample is alkali free.

Table 2

Sample	Note	Surface area (m <sup>2</sup> /g)	Pore diameter (nm)	Co loading [wt %]	Dispersion (H: Co) [%]	TPR peak 1 [K]	TPR peak 2 [K]	CO conv. [%]	Selectivities		
									S(CH <sub>4</sub> ) [%]	S(C <sub>5</sub> <sup>+</sup> ) [%]	TOF [s <sup>-1</sup> ]
Ref	$\gamma$ -alumina support			20.0	7.8	650	875	7.0	14.1	71.8	0.048
C1		27	14.2	12.5	2.3	603	668	7.4	12.3	74.9	0.026
C2		31	12.8	12.5	2.2	609	677	9.1	13.5	74.2	0.032
C3		24	13.3	12.5	2.3	607	660	7.0	13.4	74.5	0.024
C4	SiC/TiO <sub>2</sub>	34	14.9	12.5	2.8	594	642	11.1	13.1	76.9	0.031
C5	Washed	29	13.5	12.5	3.3	603	705	15.4	11.7	78.8	0.036
C6	Low alkali precursors	32	12.2	12.5	2.8	610	706	5.3	16.8	68.8	0.015
C7	Intermediate grade	32	12.7	12.5	3.3	597	677	9.3	10.4	81.2	0.022

Table 2: X(CO), S(CH<sub>4</sub>), S(C<sub>5</sub><sup>+</sup>), TOF and TOS denotes CO conversion, methane selectivity, C<sub>5</sub><sup>+</sup> selectivity and TOF (turnover frequency based on chemisorption values) respectively. Activity and selectivity results reported are after 27 hours on stream. Table 2 contains information on the sample compositions.

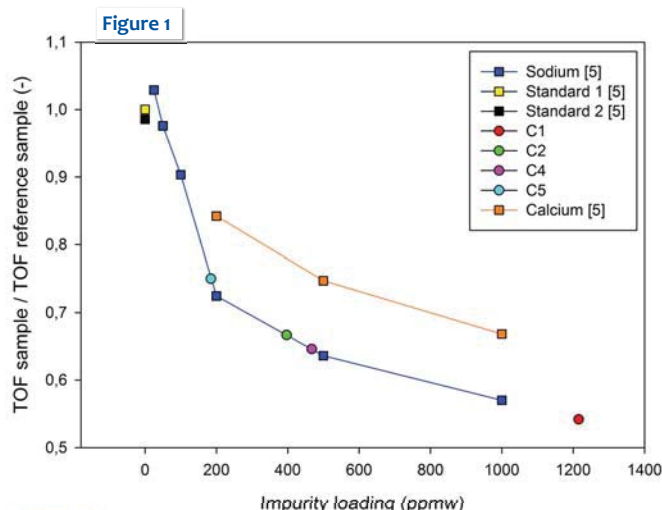


Figure 1: (In this figure, ■ denotes alumina support and ● denotes SiC support.) This figure displays activity data for sodium and calcium samples from Balonek et al. [4]. Sample C1, C2, C4 and C5 have been plotted into this graph to display how much sodium is required to cause an equal drop in turn over frequency for the reference catalyst. Be mindful of the difference in Co loading and dispersion between the SiC samples and alumina supported samples when interpreting the figure.

## Conclusion

Results from this study clearly show the importance of proper control with alkali contaminants present in catalyst support materials. For future work it is desired to investigate the properties of alkali and earth alkali free SiC support materials.

## References

- [1] P. Nguyen, C. Pham, Applied Catalysis A: General 391 (2011) 443–454.
- [2] A. Osa, R. A. Lucas, L. Sanches-Silva, J. Diaz-Maroto, J. Valverde, P. Sanchez, Fuel (2012) 95:587-598
- [3] A.Osa, A. Lucas, J. Valverde, P. Sanchez, Catalysis Today 176 (2011) 298– 302.
- [4] www.sicatcatalyst.com/
- [5] C. Balonek, A. Lillebø, S. Rane, E. Rytter, S. Rane, L. Schmidt, A. Holmen, Catalysis Letters (2010) 138:8-13
- [6] Ø. Borg, S. Eri, E. A. Blekkan, S. Storsæter, H. Wigum, E. Rytter, A. Holmen, Journal of Catalysis (2007) 248:89-100

## Acknowledgements

We gratefully acknowledge the financial support from the Norwegian Research Council, Statoil, SINTEF and NTNU through the NRC project 190763 Biomass to liquid fuels. Statoil and Sicat is acknowledged for providing the standard/reference catalyst and SiC support, respectively.





# Appendix D

## Communication

### D.1 Information on support material from manufacturer SICAT

Two e-mails were sent to Prof. Anders Holmen [42] regarding the SiC-based support materials used in the work of this thesis. Different information in this e-mail was used in the report, including pore volume and pore diameter values measured by SICAT.

Willstätt, August 17<sup>th</sup>, 2011

To: Pr. Anders Holmen  
 From: Patrick Nguyen  
 CC:  
 Date: August 17, 2011

Dear Professor Holmen,

Following our recent discussion, we will ship to your attention early next week samples of porous beta-SiC based catalyst carriers for trials in catalysis.

Code	Phase	Shape	M (g)	BET (m <sup>2</sup> /g)	Pore vol. (Hg)	Comment
SB0689A	SiC	Ø: 1 mm Ex.	100	25-35	0.55 cc/g	UHP3
SB0677P4	SiC	Ø: 3 mm Ex.	100	25-35	0.6 cc/g	UHP3+BP1100 Bimodal
SB0700G	SiC	Ø: 3 mm Ex.	100	25-35	0.6 cc/g	UHP3+D, bimodal large Pores
SB0700C	SiC	Ø: 3 mm Sp.	100	25-35	0.85 cc/g	UHP3+K, High Pore Volume

Code	Phase	Shape	M (g)	BET (m <sup>2</sup> /g)	Pore vol. (Hg)	Comment
SB0723B	TiC-SiC	Ø: 3 mm Ex.	50	62	0.3 cc/g	TiC phase
DA0558B	TiO <sub>2</sub> -SiC	Ø: 1 mm Ex.	50	100	0.3 cc/g	TiO <sub>2</sub> phase

Code	Phase	Shape	M (g)	BET (m <sup>2</sup> /g)	Pore vol. (Hg)	Comment
SD0019A	TiC-SiC	µ Spheres	50	Not meas.	0.52 cc/g	TiC-SiC, spray dried
SD0019B	SiC	µ Spheres	50	Not meas.	0.45 cc/g	SiC spray dried

#### I. Different SiC products (beta SiC phase):

I have selected various samples of regular (pure) beta SiC extrudates differing in the total pore volume and mean pore diameter. The surface chemistry of the four samples is the same. The specific surface area measured by N<sub>2</sub> adsorption should be roughly the same for the four samples.

The pore size distribution (measured by mercury porosimetry) is represented in the figure 1.

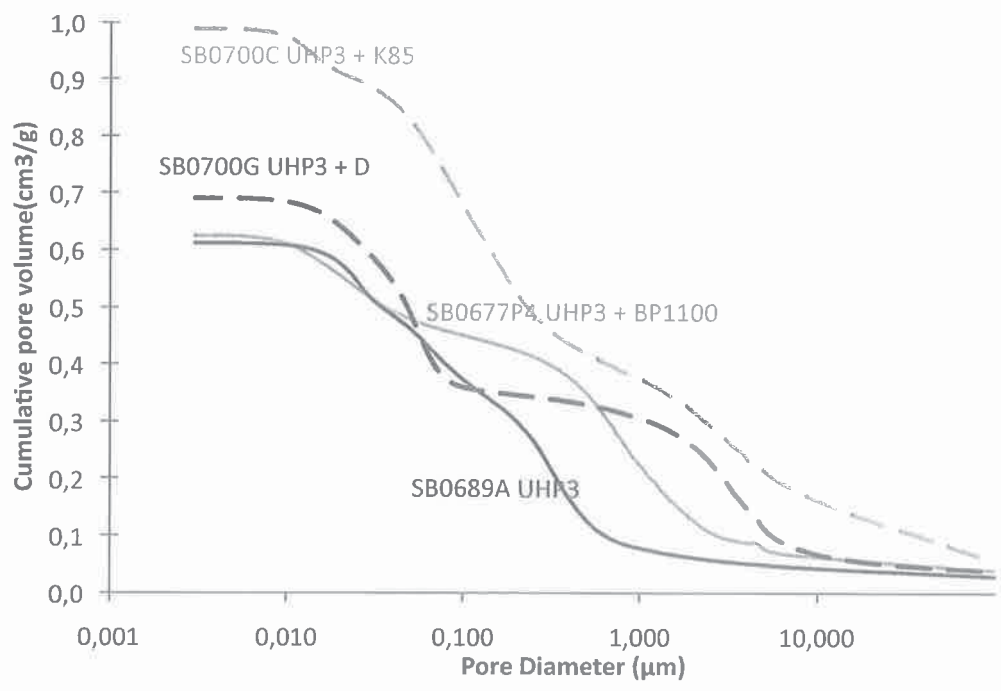


Figure 1. Pore size distribution of pure beta SiC samples

II. TiC-SiC and TiO<sub>2</sub>-SiC samples

Sample SB0723B is a mixed carbide made of TiC encapsulated in a SiC lattice. The composite has a BET surface area of 62 m<sup>2</sup>/g and a pore volume of 0.3cc/g (Hg porosimetry).

The TiC included in the material can be oxidized into TiO<sub>2</sub> leading to an increase in surface area. Sample DA0558B was a TiC-SiC composite oxidized at 400°C during 8 hours in order to convert the TiC into TiO<sub>2</sub> (anatase). At higher oxidation temperature, the TiO<sub>2</sub> is converted in the rutile phase leading to a decrease in surface area and an increase in the pore diameter.

The amount of Ti in the composite can be tailored regarding the needs of each application. TiC-SiC and TiO<sub>2</sub>-SiC material have been developed to bring a solution to the lack of mechanical resistance of TiO<sub>2</sub> catalyst carrier.

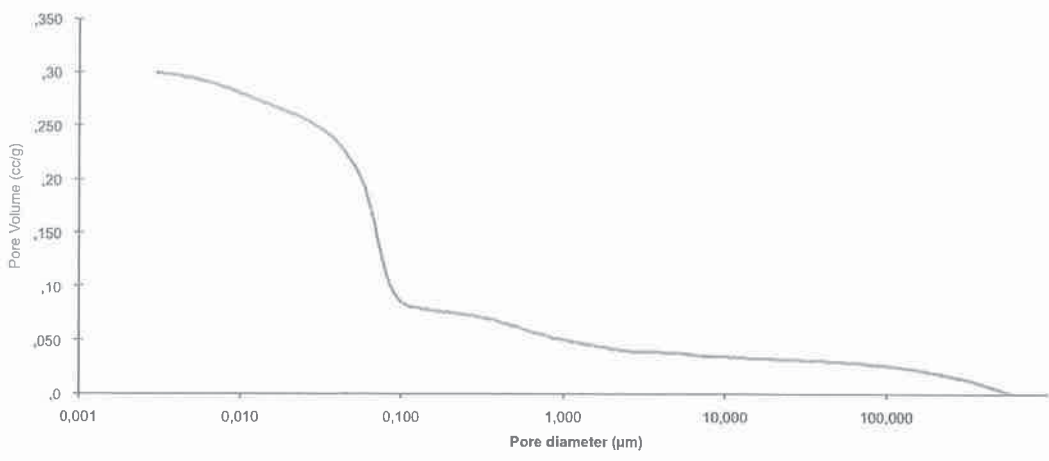


Figure 2. Pore size distribution of sample SB0723B

### III. Spray dried TiC-SiC and SiC material:

We have recently produced various grades of spray dried pure SiC and TiC-SiC microspheres for fluidized and slurry bed reactors. The material is under development and is not fully characterized. The attrition resistance of the material should be higher compared to competitor's carriers.

PS: the table below lists the typical amount of impurities in the SiC (coming from the silicon used as raw material). Impurities can be washed out by an acidic treatment if needed.

Element	Metallurgical Si typical values	Metallurgical SiC typical values
Al	0,13%	0,09%
Si		
P	26 ppm	18 ppm
S	< 30 ppm	0,03% *
Cl	NA	NA
K	NA	NA
Ca	0,09%	0,06%
Ti	NA	NA
V	30 ppm	21 ppm
Cr	96 ppm	67 ppm
Mn	0,01%	0,01%
Fe	0,44%	0,31%
Co	4 ppm	3 ppm
Ni	26 ppm	18 ppm
Cu	31 ppm	22 ppm
Zn	5 ppm	4 ppm
Sr	3 ppm	2 ppm
Zr	14 ppm	10 ppm

We use to develop jointly catalyst supports regarding the specification of the application (pore size distribution, pore volume, surface area, promoters...).

I look forward to the material evaluation,

Patrick



SICAT R&D  
20 place des Halles  
67000 – STRASBOURG, FRANCE  
☎ 0033 (3) 88 52 26 69  
[www.sicatcatalyst.com](http://www.sicatcatalyst.com)  
[pnguyen@sicatcatalyst.com](mailto:pnguyen@sicatcatalyst.com)



Strasbourg, March 27 2011

To: Pr. Anders Holmen  
From: Patrick Nguyen  
CC:  
Date: March 27 2012

Dear Professor Holmen,

Following our recent discussion about the potential detrimental effect of alkali and alkaline earth elements on the FTS activity, we will ship to your attention new samples of porous beta-SiC with lower impurities.

Code	Phase	Shape	M (g)	BET (m <sup>2</sup> /g)	Pore vol. (Hg)	Comment
C5 DI0234	SiC	< 500 μm	90	27	0.55 cc/g	Regular UHP3 SD0024A washed
C6 SD0035B <sub>2D</sub>	SiC	Ø: 2 mm Ex.	20	24	N.A	New UHP3' Purer S.M, no additives
C7 SD0037F <sub>G</sub>	SiC	Ø: 1 mm Ex.	20	N.A	N.A	New UHP3 Purer Si

Sample description:

Sample **DI0234** was washed in order to remove the impurities; this material has the same properties as sample SB0689A sent to your attention last year. In this material, the level of Na, Ca, K, and Fe should be lower than in the material that you have tested. As the SiC is not soluble in any media, it is not possible to perform ICP to analyze the level of contamination. We have started oxidizing several samples into SiO<sub>2</sub> in order to do ICP. The washing process has not affected on the surface area and pore size distribution.

Sample **SD0035B<sub>2D</sub>** was manufactured with a purer starting material and without additives suspected to add alkali to the final SiC material. The theoretical level of impurities calculated with the typical values of the raw materials is the following:

S: <50 ppm  
Fe<91ppm  
Ca: 27 ppm  
Na<<240 ppm  
K<<63ppm  
Al: 41ppm

Sample **SD0037FG** is an intermediate grade, its level of impurities is:

S: <50 ppm  
Fe<91ppm

Ca: 27 ppm  
Na<242 ppm  
K<63ppm  
Al: 41ppm

We are still working on the improvement of the material for the FTS. For fixed bed reactor, one partner has demonstrated superior productivity for a SiC based catalyst compared to the incumbent catalyst. The porous network and the higher thermal conductivity of the SiC seemed to be the key parameters. Regarding slurry phase reactors we are focusing our work on the manufacturing of highly attrition resistant catalyst carriers.

We also planed to produce ultra pure SiC with ultra high purity starting material; we hope that the first samples would be available this summer.

With my best regards,


Patrick

A handwritten signature in black ink, appearing to read 'Patrick', enclosed within a large, light-colored oval scribble.



## D.2 Molab AS

The original report received from *Molab AS*, regarding the elemental analysis of support S1 and catalyst C1 are appended on the next page. Contact information to *Molab AS* and reference number to this requisition can be found here.

		<b>Molab as, 8607 Mo i Rana</b> Telefon: 75 13 63 50 Besøksadr. Mo i Rana: Mo Industripark Besøksadr. Oslo: Kjelsåsveien 174 Besøksadr. Glomfjord: Ørnesveien 3 Besøksadr. Porsgrunn: Herøya Forskningspark B92 Organisasjonsnr.: NO 953 018 144 MVA	
Kunde: NTNU Att: Andreas H Lillebø Institutt for kjemisk prosess teknologi  7491 TRONDHEIM		<b>RAPPORT</b>  <b>Analyse av Co-SiC katalysatorer.</b>	
		Ordre nr.: 45598	Antall sider + bilag: 1
		Rapport referanse: KR-14748	Dato: 06.03.2012
Rev. nr. 0	Kundens bestillingsnr./ ref.: N12110150	Utført: Stein Hanssen	Ansvarlig signatur:

Prøver mottatt dato: 29.02.2012

## RESULTATER

Prøve merket:			C1- Catalyst	C1- support
Parameter	Enhet	Ana. dato	KA-065294	KA-065295
Ca	%	06.03.12	<0,05	<0,05
Fe	%	06.03.12	0,19	0,24
Na	%	06.03.12	<0,010	<0,010
P	%	06.03.12	0,011	0,015
S	%	06.03.12	<0,02	<0,02

## ANALYSEINFORMASJON

Parameter	Metode/Analyseteknikk
Ca+Fe+Na+P	ICP
S	Forbrenning



# Appendix E

## Risk assessment

On the following pages the risk assessments of possibly hazardous tasks, carried out during the experimental work in the laboratories, are appended.

Identified hazardous tasks were:

- Crushing of catalyst support pellets
- Incipient wetness impregnation
- Handling of Co-catalysts
- Calcination
- Temperature programmed reduction
- Fischer-Tropsch synthesis

NTNU	<b>Hazardous activity identification process</b>				Risikovurdering	Nummer	Dato
					HMS-avd.	HMSRV2601	
HMS					Godkjent av	Side	Erstatter
							

Unit:

*Kjemisk prosess teknologi*

Date: 12.09.2011

Line manager:

*Øyvind Gregersen*



Participants in the identification process (including their function):

Sindre Håvik, Master student

Short description of the main activity/main process:

Preparation and characterization of Co-catalysts

ID no.	Activity/process	Responsible person	Laws, regulations etc.	Existing documentation	Existing safety measures	Comment
1	Crushing of catalyst support	SH		Safety data sheet	Provide appropriate protection from	Avoid inhalation of fines
2					use fume hood	
3	Incipient wetness impregnation	SH		Safety data sheet	Lab coat, glasses, gloves, use in fume hood	Avoid skin contact and ingestion
4						
5	Handling of Co-catalyst	SH		Safety data sheet	Glasses, gloves	Avoid skin contact and ingestion
6	Calsination	SH			Glasses	Avoid touching hot surfaces
7	TPR	SH		Safety sheet on apparatus	Glasses, gloves	Avoid skin contact with CO <sub>2</sub> (s), avoid inhalation of 2-propanol,
8						avoid touching hot surfaces

NTNU	<b>Risk assessment</b>				Utarbeidet av	Nummer	Dato
					HMS-avd.	HMSRV2603	04.02.2011
HMS /KS					Godkjent av	Side	Erstatter
							

**Unit:** Kjemisk prosess teknologi      **Date:** 12.09.2011

**Line manager:** Øyvind Gregersen

**Participants in the identification process (including their function):** Sindre Håvik, Master student

**Signatures:** SH

ID no.	Activity from the identification process form	Potential undesirable incident/strain	Likelihood: Likelihood (1-5)	Consequence:				Risk value	Comments/status Suggested measures
				Human (A-E)	Environment (A-E)	Economy/material (A-E)	Reputation (A-E)		
1	Crushing of catalyst support	Inhalation of fines	2	A	A	A	A	Human 2A	
2									
3	Incipient wetness impregnation	Skin contact inhalation/ingestion of cobalt nitrate	1	B	A	A	A	Human 1B	
4									
5	Handling of Co-catalyst	Skin contact or ingestion	1	A	A	A	A	Human 1A	
6	Calsination	Burns	1	A	A	A	A	Human 1A	
7	TPR	Contact with CO2(s), inhalation of 2-propanol,	1	A	A	A	A	Human 1A	
8		burns							

 NTNU  HMS	<h2 style="margin: 0;">Hazardous activity identification process</h2>	Risikovurdering Nummer HMS-avd. Godkjent av Dato Erstatte	
		Nummer: HMSRV2601 Side: _____ Dato: _____ Erstatte: _____	

Unit: Kjemisk prosesssteknologi Date: 19.01.2012  
 Line manager: Oyvind Gregersen  
 Participants in the identification process (including their function):  
Anders Holmen (Supervisor), Andreas Lillebø (co-superv.)  
Sindre Høvik (Master student)

Short description of the main activity/main process: Catalyst testing in Fischer-Tropsch synthesis

ID no.	Activity/process	Responsible person	Laws, regulations etc.	Existing documentation	Existing safety measures	Comment
1	Fischer-Tropsch synthesis	AH	The working environment act	Apparatus card	Vents and gas detectors/alarms	Leave area if alarms go off.
2	"	"	"	"	Emergency stop button	
3	"	"	"	"	Heat resistant gloves	
4	"	"	"	"	Pressure gauges	Be sure whether equipment is pressurized
5						
6						
7						
8						



**Operating Instructions**

**Instrument/Apparatus:** Fischer-Tropsch synthes is  
**Serial Number:** — **Placement:** Chemistry hall D  
**Original Manual:** —

**Log book with signature for training & maintenance:** —

**Risk Evaluation**  
**Date:** 17.01.2012  
**Archived:** 19.01.2012

Compulsory Protection Equipment:		Hazards:	
Safety Goggles	<input checked="" type="checkbox"/>	Fire	
Gloves		Chemicals/Gasses	<input checked="" type="checkbox"/>
Hearing Protection		Electricity/Power	<input checked="" type="checkbox"/>
Protective Clothing	<input checked="" type="checkbox"/>	Temperature/Pressure	<input checked="" type="checkbox"/>
Breathing Protection		Cutting/Crushing	
Shielding		Rotating Equipment	
Other		Hazardous Waste	
None		Out of normal working hours	
		Others	
		None	

**Operating Instructions**  
 (Fill In or Attach Seperate Instructions)  
 Operate under supervision of co-supervisor  
 Andreas Lillebø.

**Emergency Procedure**  
 (Emergency Stop Procedure, Image of Switches/Stop Procedure):  
 Close all gas bottles and clear the area until  
 hazardous gases have been ventilated

**Maintenance Routines**  
**Frequency:** When something breaks  
**Service Agreements:**  
**Maintenance Contact:** Andreas Lillebø  
**Maintenance Described In Seperate Attachment**

<b>Person Responsible:</b>	<b>Deputy:</b>
Name: Anders Holmen	Name: Andreas Lillebø
Telephone:	Telephone: 40032484
Mobile: 91847164	Mobile:
Signature: Anders Holmen	Signature: Anders Lillebø

**Controlled & Updated:**

Date:	Date:	Date:
Date:	Date:	Date:



**Potential undesirable incident/strain**

Identify possible incidents and conditions that may lead to situations that pose a hazard to people, the environment and any materiel/equipment involved.

**Criteria for the assessment of likelihood and consequence in relation to fieldwork**

Each activity is assessed according to a worst-case scenario. Likelihood and consequence are to be assessed separately for each potential undesirable incident. Before starting on the quantification, the participants should agree what they understand by the assessment criteria:

Minimal 1 Once every 50 years or less	Low 2 Once every 10 years or less	Medium 3 Once a year or less	High 4 Once a month or less	Very high 5 Once a week
<b>Grading</b>	<b>Human</b>	<b>Environment</b>	<b>Financial/material</b>	
<b>E Very critical</b>	May produce fatality/ies	Very prolonged, non-reversible damage	Shutdown of work >1 year.	
<b>D Critical</b>	Permanent injury, may produce serious health damage/sickness	Prolonged damage. Long recovery time.	Shutdown of work 0.5-1 year.	
<b>C Dangerous</b>	Serious personal injury	Minor damage. Long recovery time	Shutdown of work < 1 month	
<b>B Relatively safe</b>	Injury that requires medical treatment	Minor damage. Short recovery time	Shutdown of work < 1week	
<b>A Safe</b>	Injury that requires first aid	Insignificant damage. Short recovery time	Shutdown of work < 1day	

**Likelihood**

**Consequence**

The unit makes its own decision as to whether opting to fill in or not consequences for economy/materiel, for example if the unit is going to use particularly valuable equipment

It is up to the individual unit to choose the assessment criteria for this column.

**Risk = Likelihood x Consequence**

Please calculate the risk value for "Human", "Environment" and, if chosen, "Economy/materiel", separately.

**About the column "Comments/status, suggested preventative and corrective measures":** Measures can impact on likelihood and consequences. Prioritise measures:

both that can prevent the incident from occurring; in other words, likelihood-reducing measures are to be prioritised above greater emergency preparedness,

i.e. consequence-reducing measures.